



*Pacific Gas and
Electric Company*

Diablo Canyon Power Plant
P.O. Box 56
Avila Beach, CA 93424

805.545.6000

February 2, 2005

PG&E Letter No. DCL-05-002

U.S. Nuclear Regulatory Commission
ATTN: Document Control Desk
Washington, DC 20555-0001

Docket No. 50-275, OL-DPR-80
Docket No. 50-323, OL-DPR-82
Diablo Canyon Units 1 and 2
Final Report: San Simeon Earthquake of December 22, 2003

Dear Commissioners and Staff:

On December 22, 2003, at 1116 PST, with Diablo Canyon Power Plant (DCPP) Unit 1 and Unit 2 operating at 100 percent power, a 6.5 magnitude earthquake occurred approximately 50 km NNW of San Simeon, California. Plant seismic instruments measured about 0.04 g at the plant site. Therefore, operators declared an Unusual Event (Reference NRC Event Notification Number 40408).

Pacific Gas & Electric Company (PG&E) has issued three reports on the San Simeon earthquake. In subsequent discussions with the NRC, PG&E agreed to submit a final report. Enclosure 1 constitutes the final PG&E report on the San Simeon Earthquake of December 22, 2003. This enclosure also includes specific references to previous reports.

Enclosure 2 is the engineering analysis update to the Special Report 03-04, Supplemental Report Dated March 29, 2004.

Sincerely,

Donna Jacobs
Vice President Nuclear Services

swh/A0600470 AE03
Enclosures

A-025



Document Control Desk
February 2, 2005
Page 2

PG&E Letter DCL-05-002

cc: Bruce S. Mallett, Region IV
David L. Proulx, Resident
Girija S. Shukla, NRR
Diablo Distribution

EVALUATION OF THE DECEMBER 22, 2003 M_w 6.5 SAN SIMEON EARTHQUAKE

Final Report to the U.S. Nuclear Regulatory Commission
December 2004

1.0 INTRODUCTION

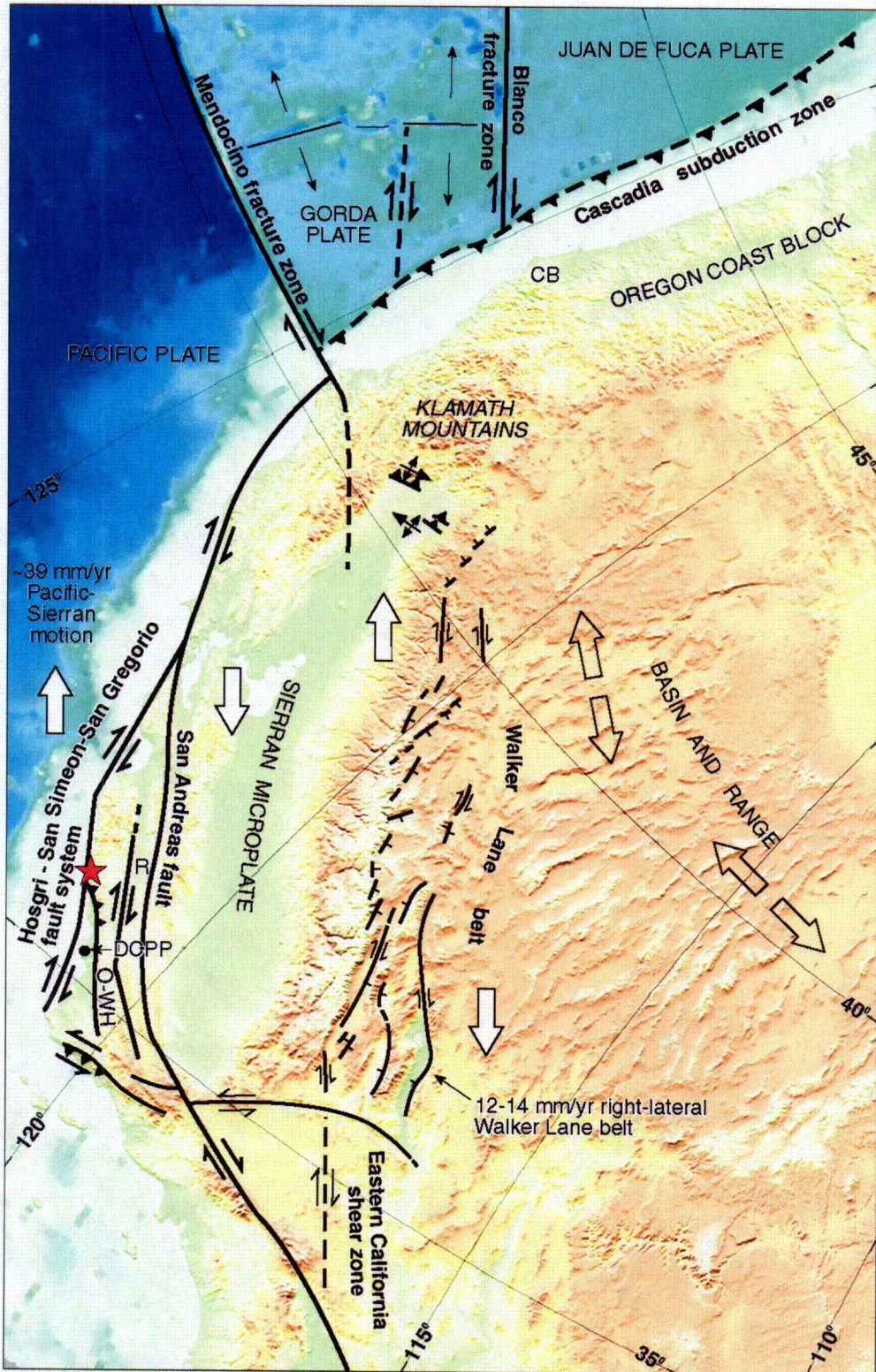
This report responds to a request from the Nuclear Regulatory Commission (NRC) to provide a final evaluation of the relevance of the December 22, 2003 M_w 6.5 San Simeon earthquake to the seismotectonic interpretations of the south-central coastal California region performed for the Long Term Seismic Program (LTSP) for the Diablo Canyon Power Plant (PG&E, 1988). This report updates information presented on the San Simeon earthquake in three previous PG&E reports to the NRC. The first was on January 5, 2004, *Special Report 03-04: San Simeon Earthquake of December 22, 2003*, (PG&E Letter DCL-03-184). This report was superseded on March 29, 2004, by *Supplement to Special Report 03-04: San Simeon earthquake of December 22, 2003* (PG&E Letter DCL-04-031). A third report was issued on June 7, 2004, *Update to the Seismicity Evaluation of the December 22, 2003 San Simeon Earthquake* (PG&E Letter DCL-04-071). We also present new information on the depth of the San Simeon earthquake, the tectonic setting and geology, and the earthquake ground motions.

2.0 TECTONIC FRAMEWORK

The December 22, 2003 M_w 6.5 San Simeon earthquake occurred in the southern Coast Ranges of south-central California, 11 kilometers northeast of San Simeon, in a region of transpressional deformation associated with the boundary between the Pacific Plate and the Sierran microplate (Figure 2-1). Our characterization of the tectonic setting of the region is based upon extensive geologic mapping and analyses of seismicity performed over the past 18 years (for example, PG&E, 1988, 1991; Hanson and others, 1994, 2004; McLaren and Savage, 2001; Lettis and others, 2004) and two reconnaissance field surveys in the region following the earthquake. The first survey was performed on January 15 and 16, 2004, and included aerial and field reconnaissance of the epicentral region to document ground deformation associated with the earthquake and to evaluate whether or not surface fault rupture had occurred along mapped bedrock faults in the region (including the Oceanic-West Huasna, Nacimiento, and San Simeon fault zones). The second survey, on October 27-30, 2004, focused on identifying active Quaternary deformation along the southwestern margin of the southern Coast Ranges, particularly in the epicentral and aftershock region, the association of any Quaternary deformation with the Oceanic-West Huasna fault zone, and the style and rate of Quaternary deformation occurring in the Santa Lucia Mountains and nearby areas.

2.1 Tectonic Model

The San Simeon region lies within a broad area of active deformation driven primarily by distributed motion between the Pacific Plate on the west and the Sierran microplate (also called



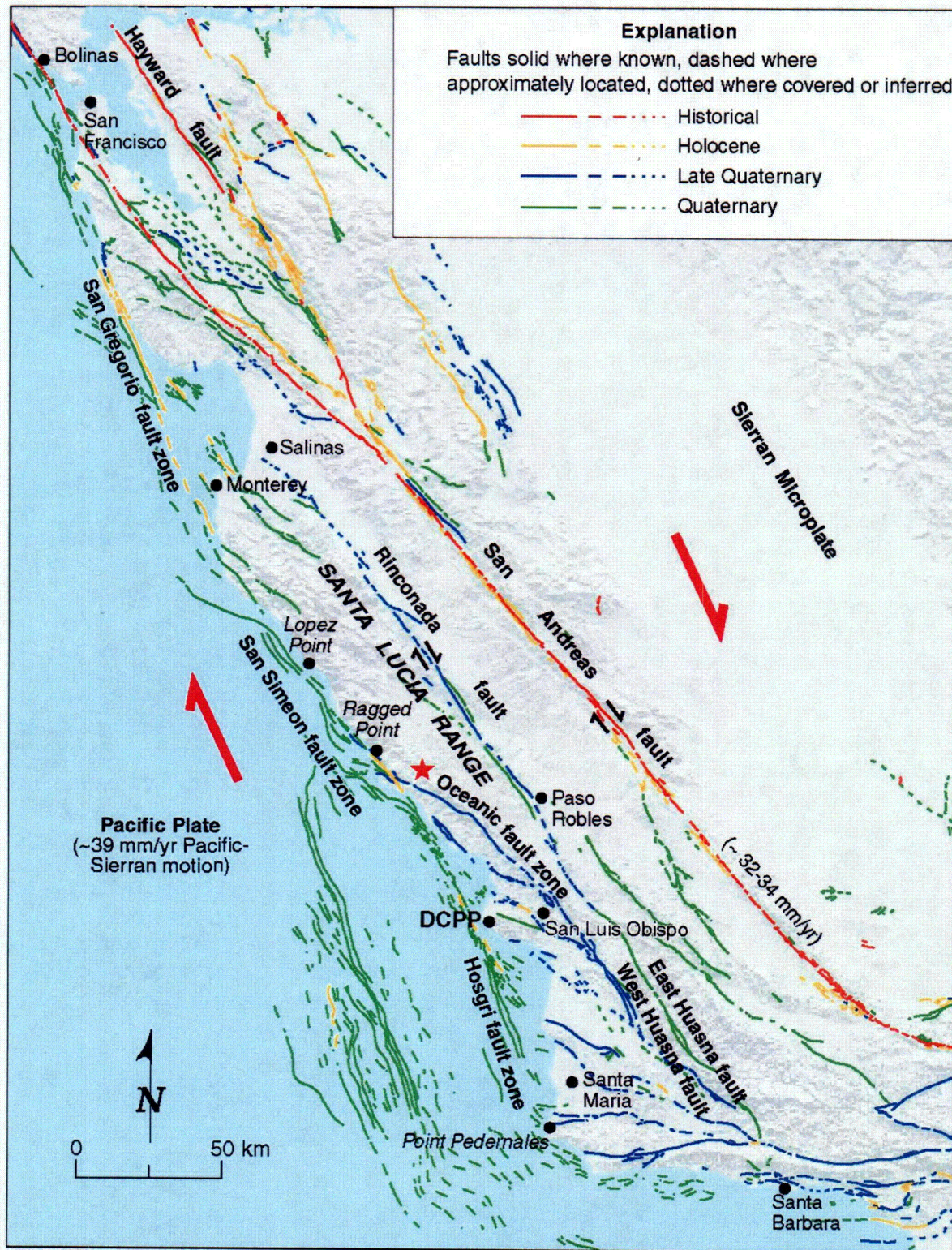
Note: R = Rinconda fault; O-WH = Oceanic-West Huasna fault zone; DCP = Diablo Canyon Power Plant. Red star shows location of the December 2003 San Simeon earthquake.

Figure 2-1. Regional tectonic setting of the San Simeon earthquake.

the Sierra Nevada-Central Valley block) on the east (Figure 2-1). Space-based geodetic observations indicate that the average motion across the Pacific-Sierran plate boundary is characterized by about 39 millimeters per year of right-lateral shear directed N32°W (Argus and Gordon, 2001). The San Andreas transform fault is the major structure within the plate boundary and accommodates about 32 millimeters per year of right-lateral motion at the latitude of south-central California. However, the San Andreas fault strikes about N40°W in this region, which is about 8 degrees counterclockwise of the average plate motion vector (Figure 2-2). The slight misfit between the strike of the San Andreas fault here and the plate motion vector results in a small component of crustal shortening being resolved across the plate boundary. This shortening, together with the remaining 7 millimeters per year of right shear, is accommodated by secondary strike-slip faults, thrust/reverse faults, and folds in the crust adjoining the San Andreas fault over a zone up to 100 miles wide. Examples of secondary right-slip faults within the plate boundary in the south-central coastal region include the Hosgri-San Simeon-San Gregorio fault system and the Rinconada fault (Figure 2-2). Examples of secondary thrust/reverse faults and folds include those along the western margin of the Central Valley, such as the Coalinga and Kettleman Hills anticlines and related thrust faults; those within the southern Coast Ranges, such as Oceanic fault zone; and those offshore of California, such as the Queenie structure and Piedras Blancas anticlinorium. The 1927 M_w 7.0 Lompoc earthquake within the southwestern structural margin of southern offshore Santa Maria basin (PG&E, 1991; Satake and Somerville, 1992) and the 1983 M_w 6.5 Coalinga earthquake beneath the Coalinga anticline indicate that these secondary structures are seismogenic.

South-central coastal California, which includes the San Simeon region, can be divided into four tectonic domains characterized by distinct styles of Quaternary deformation (PG&E, 1988; Hanson and others, 2004; Lettis and others, 2004). These domains include the Los Osos domain; the Southern Coast Ranges domain (including the Santa Lucia Range); the Western Transverse Ranges domain; and the offshore Santa Maria domain (Figure 2-3). The Los Osos domain is a triangular region separated on the west from the offshore Santa Maria domain by the right-slip Hosgri-San Simeon fault zone; from the Southern Coast Ranges domain on the northeast by reverse and reverse-right oblique-slip faulting along the northeast-dipping Oceanic-West Huasna fault zone; and from the Western Transverse Ranges domain on the south by reverse-left-oblique-slip faulting along the Santa Ynez River fault. The 2003 San Simeon earthquake occurred along the northeastern border of the Los Osos domain (Figure 2-3).

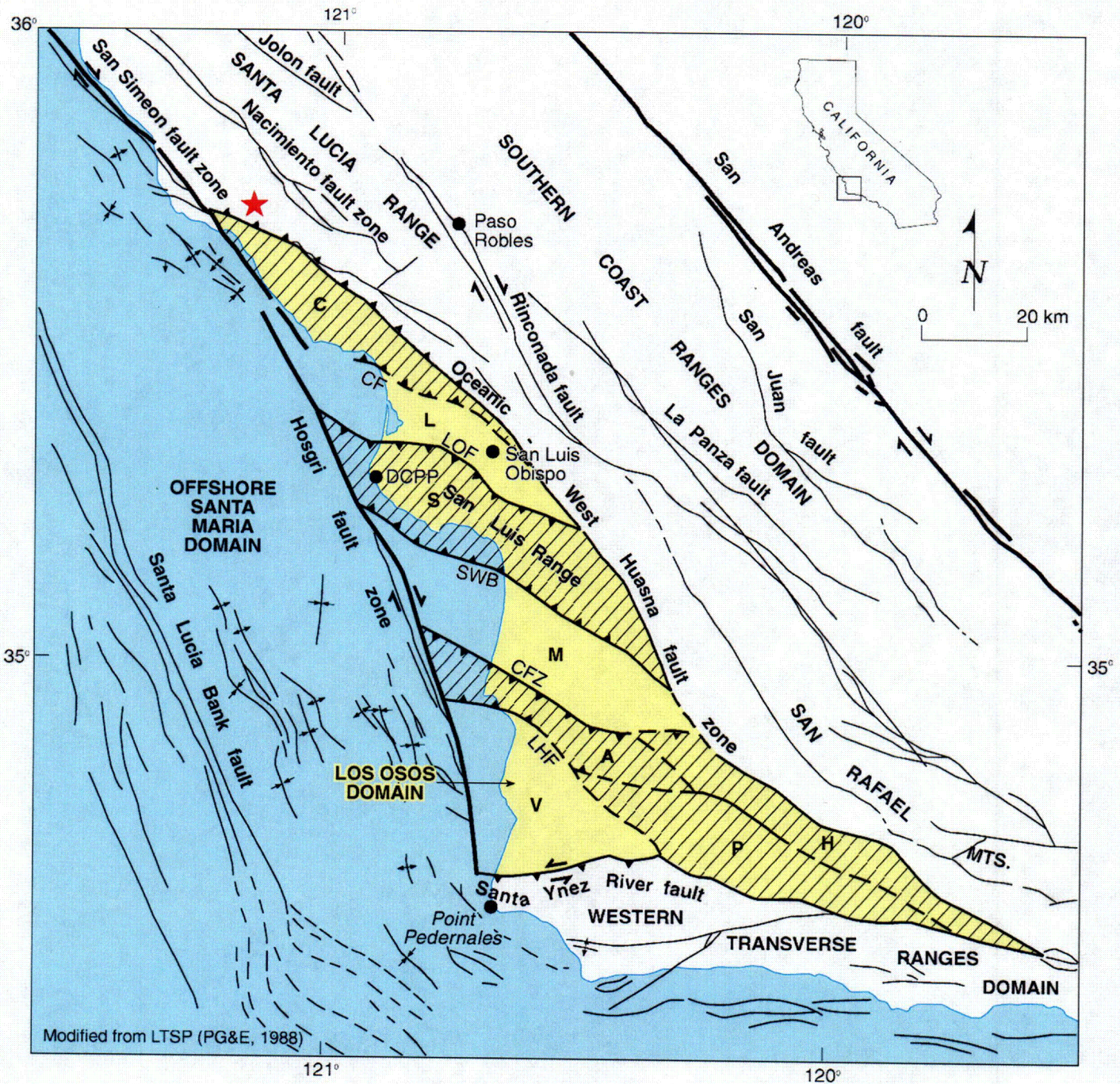
Several models have been proposed to explain patterns of strike-slip faulting and crustal shortening within and adjacent to the Los Osos domain (PG&E, 1988, 1991; Lettis and others, 2004; Lettis and Hanson, 2004). One model postulates that clockwise rotation of the Transverse Ranges drives the southern margin of the Los Osos domain northward, causing north-northeast-directed crustal shortening and reverse faulting on a series of northwest-striking reverse faults within the domain (Figures 2-3 and 2-4). Crustal shortening along the northeastern margin of the Los Osos domain and within the Southern Coast Ranges domain also may be driven, in part, by a left-restraining transfer of slip between prominent strike-slip faults in the region (Figure 2-5). A possible example of this process is transfer of right slip from the northwest-striking Rinconada fault to the San Simeon fault zone across the west-northwest-striking Oceanic-West Huasna fault zone along the northeastern boundary of the Los Osos domain. Crustal shortening and uplift of



Note: Faults from Jennings (1994). DCP = Diablo Canyon Power Plant. Red star shows location of the December 2003 San Simeon earthquake.

Figure 2-2. Active faults in the southern Coast Ranges area.

CO2



Note: Los Osos domain (incorporating areas that are hachured and colored yellow) is bounded by the Hosgri fault zone, Oceanic-West Huasna fault zone, and the Santa Ynez River fault. The Los Osos domain is divided into distinct structural blocks, including: C-Cambria, L-Los Osos Valley, S-San Luis/Pismo, M-Santa Maria Valley, A-Casmalia, H-Solomon Hills, V-Vandenberg/Lompoc, P-Purisima. Hachured areas show location of Quaternary uplift within the Los Osos domain. Bedrock and Quaternary faults shown as light lines; domain boundary faults shown as bold lines. CF = Cayucos fault, LOF = Los Osos fault, SWB = Southwest Boundary zone; CFZ = Casmalia fault zone; LHF = Lion's Head fault. DCP = Diablo Canyon Power Plant. Red star shows location of the December 2003 San Simeon earthquake.

Figure 2-3. Major kinematic domains in west-central California.

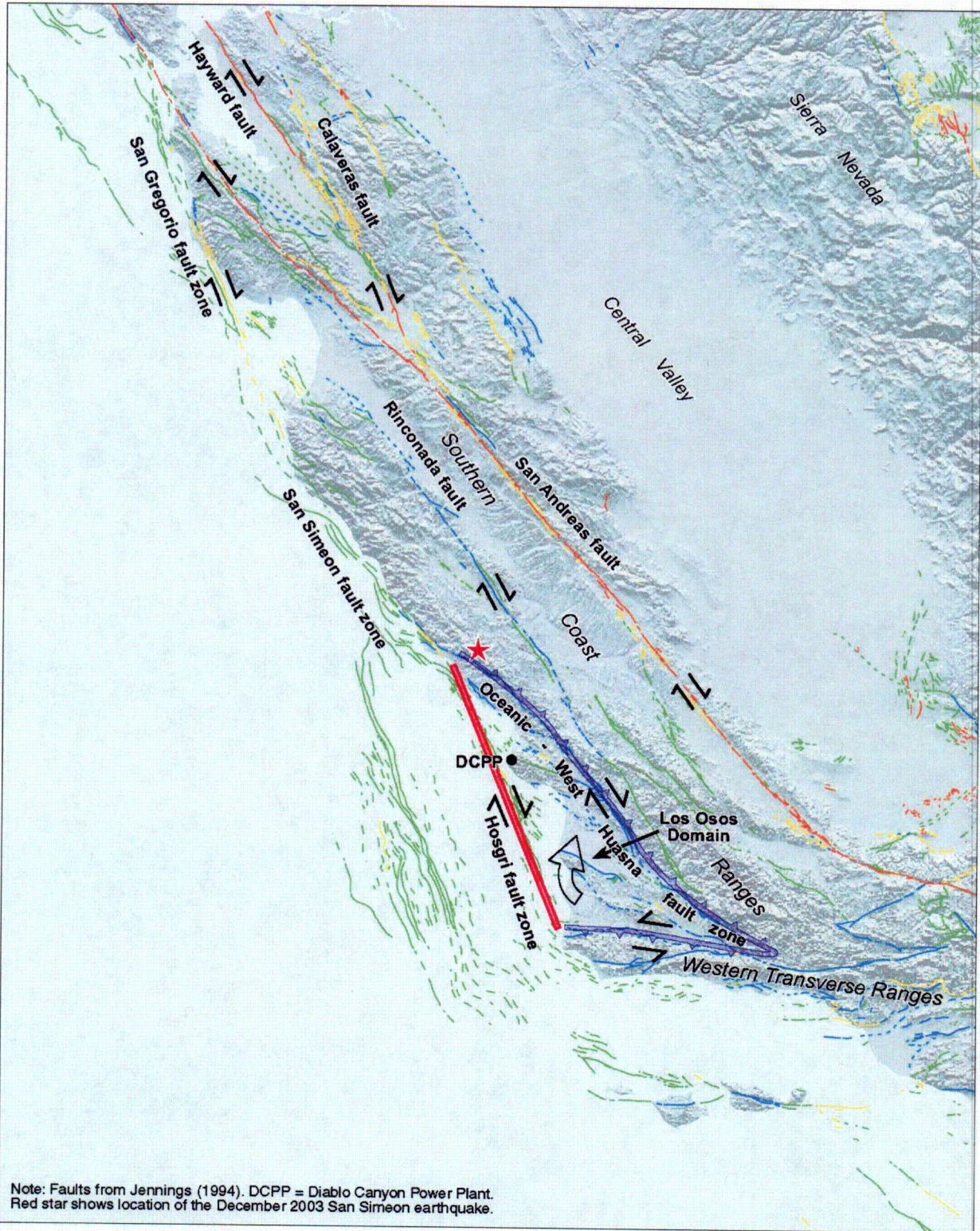


Figure 2-4. Model for crustal shortening in the Los Osos domain driven by clockwise rotation of the western Transverse Ranges.

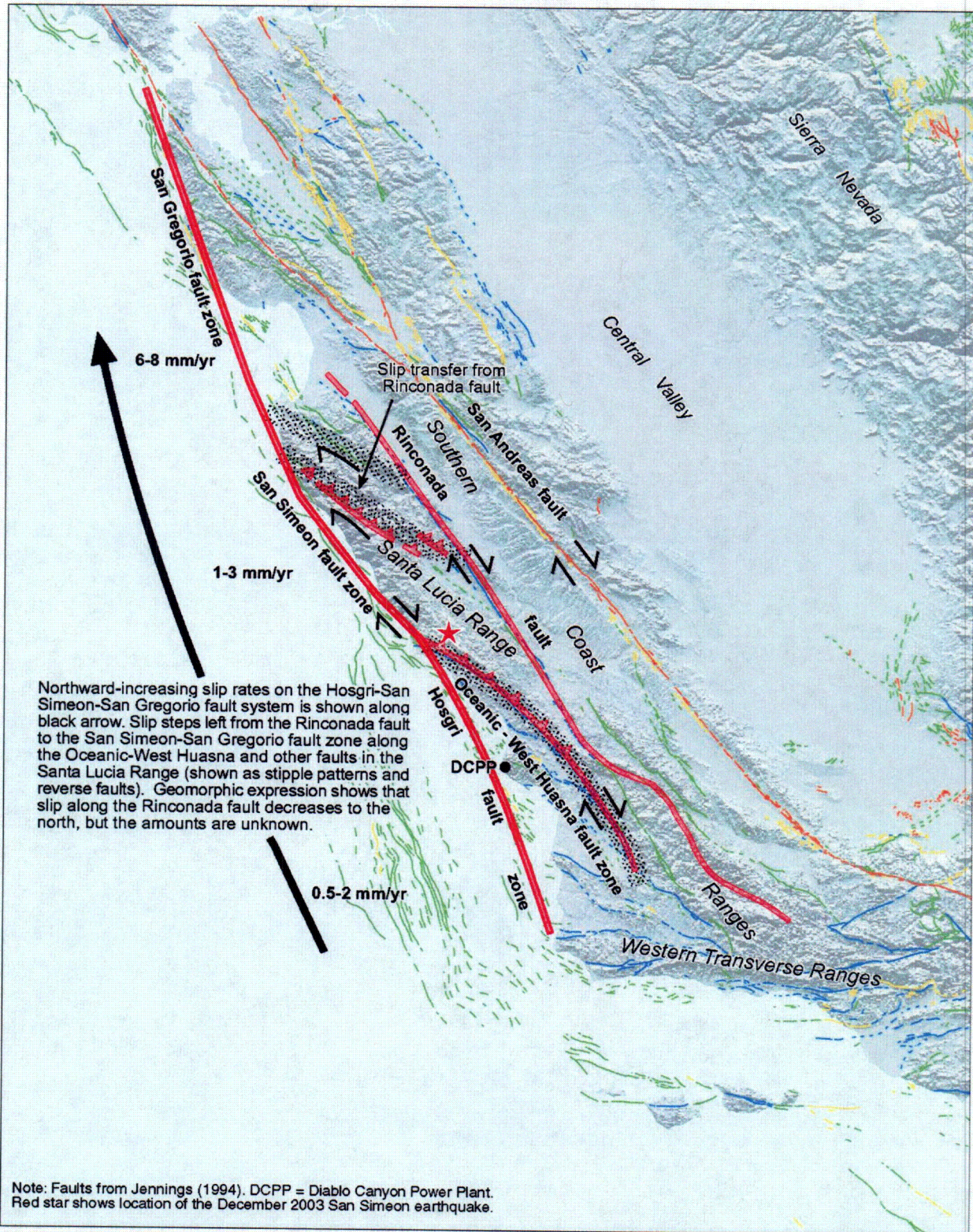


Figure 2-5. Model for crustal shortening in the San Simeon region driven by a left-restraining transfer of right slip from the Oceanic-West Huasna fault zone to the San Simeon fault zone.

the Santa Lucia Range and the offshore Piedras Blancas anticlinorium in the San Simeon region also appears to be generated by a broad left-restraining bend in the Hosgri-San Simeon-San Gregorio fault system, centered on the San Simeon fault zone (Figure 2-6). The scale of this restraining bend is comparable to the restraining bend along the San Andreas fault in the Santa Cruz Mountains area, which has produced uplift and crustal shortening in the southwestern San Francisco Bay area. Quaternary deformation within the Los Osos domain and bordering Southern Coast Ranges domain likely results from a combination of these three processes.

2.2 San Simeon Region in the Southern Coast Ranges Domain

The Southern Coast Ranges domain is about 300 kilometers long, 60 to 75 kilometers wide, and extends from the Monterey embayment south to the western Transverse Ranges (Figure 2-2). Individual ranges within the Southern Coast Ranges domain generally are about 120 kilometers to 300 kilometers long, 10 to 50 kilometers wide, and attain crestral elevations ranging from about 400 meters to 1200 meters (Page and others, 1998). Several ranges, including the Santa Lucia Range east of San Simeon, have remnants of low-relief upland surfaces that are hundreds of feet above the modern stream base level and are being incised by headward-eroding canyons. Page and others (1998) interpret these and other structural, stratigraphic, and tectonic-geomorphic relations as evidence that the southern Coast Ranges have been uplifted in the past 3.5 million years, possibly due to a change in relative motion between the Pacific Plate and Sierran microplate.

In addition to regional uplift, the Southern Coast Ranges domain has been deformed internally in late Cenozoic time by strike-slip faulting and crustal shortening. Page and others (1998) report that the San Andreas fault is generally parallel to rather than oblique to the ranges in the domain, and they interpreted this as evidence that regional crustal shortening is not driven by wrench tectonics. At the latitude of San Simeon, however, mapping by Dibblee (1971; 1976) clearly documents that the axes of folds within the southern Coast Ranges trend about 30 degrees to 45 degrees more westerly than the Rinconada and San Simeon faults, both of which are more indicative of the direction of right shear in this region than the more distant San Andreas fault to the east. In addition to being oblique to the local strike-slip faults, the folds commonly have well-defined, right-stepping en echelon patterns. The trend and geometry of these folds are consistent with regional right-slip wrench tectonics. Page and others (1998) cite stratigraphic and structural evidence for the onset of major folding in the southern Coast Ranges during the past 3.5 million years. Wrench-style folding, therefore, likely accommodates some of the regional shortening associated with the misfit between the strike of the San Andreas fault and the plate motion vector (Section 2.1).

The epicentral region of the 2003 San Simeon earthquake straddles the physiographic and tectonic boundary between the Southern Coast Ranges domain on the northeast and the Los Osos domain on the southwest (Figure 2-3). The principal late Cenozoic structure along this boundary is the northwest-striking Oceanic-West Huasna fault zone, which has evidence for right-oblique reverse displacement (Section 2.2.2).

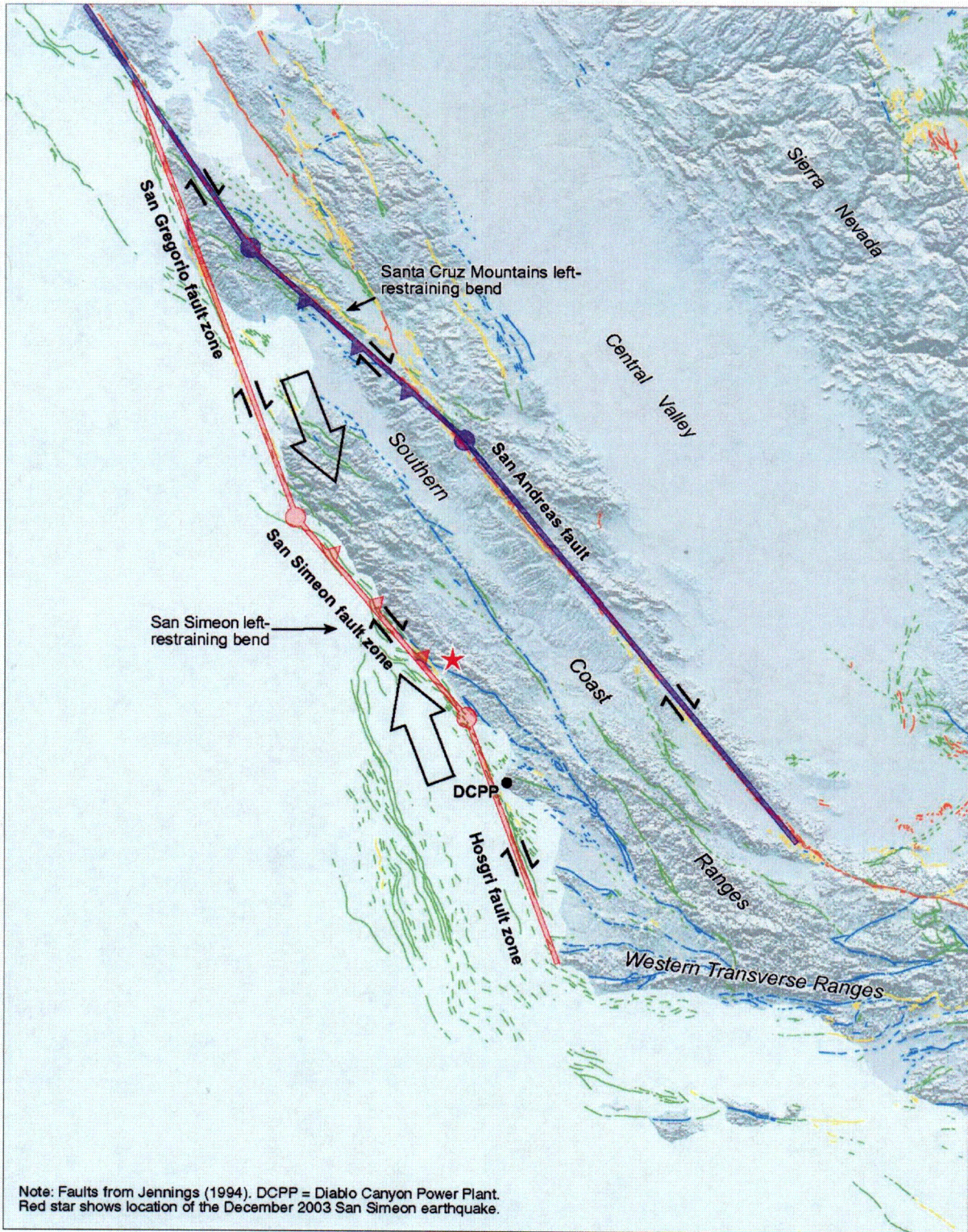


Figure 2-6. Model for regional shortening and uplift in the southern Coast Ranges at the latitude of San Simeon due to the presence of a left-restraining bend in the Hosgri-San Simeon-San Gregorio fault system.

2.2.1 Stratigraphy

The geology of the San Simeon region was compiled at 1:250,000 scale by Jennings (1958) and we use his map as a base to show the stratigraphy and structure (Figure 2-7). Field mapping and paleontological study by Thomas Dibblee, Clarence Hall, and many others have refined the interpretation of the major stratigraphic units in the region; however, the basic relationships generally remain as depicted by Jennings (1958), with some changes noted below. These units, discussed in the following sections, include

- Mesozoic to Tertiary Franciscan complex, which contains highly deformed marine sandstone, shale and volcanic rock that accumulated in an accretionary prism above an east-dipping subduction zone. This unit includes the Mesozoic to Tertiary mélange and ophiolitic rock shown on Figure 2-7.
- Late Cretaceous to Paleogene marine strata, consisting of well-lithified, interbedded sandstone and shale. These rocks are represented by the Mesozoic-Tertiary marine deposits shown on Figure 2-7.
- Miocene Monterey and Vaqueros formations, typically consisting of well-bedded marine sandstone and shale. The Monterey Formation is characterized by thin-bedded chert and siliceous shale. The Monterey and Vaqueros formations coincide with the Miocene marine deposits shown on Figure 2-7.
- Pliocene-Pleistocene fluvial deposits and basin fills, and erosion surfaces. With the exception of the erosion surfaces, these units correspond to the Pliocene-Quaternary continental and marine terrace deposits shown on Figure 2-7.
- Quaternary marine and fluvial terraces and alluvial fan deposits. These units correspond to the Pliocene-Quaternary continental and marine terrace deposits shown on Figure 2-7.

One of the best-developed and preserved sequences of marine terraces along the entire California coastline occurs in the San Simeon region between Ragged Point on the north and Morro Bay on the south. This marine terrace sequence has been mapped in detail (Weber, 1983; PG&E, 1988; Hanson and others, 1994) and provides an excellent sequence of Quaternary surfaces from which to identify the location, style, and rate of Quaternary deformation. From youngest to oldest, the mapped sequence of terraces includes the San Simeon Point, San Simeon, Tripod, Oso, and La Cruz terraces (Weber, 1983; Hanson and others, 1994) (terraces Q₁ to Q₅, Figure 2-8). These five terraces are correlated with marine oxygen isotope stages 3 or 5a, 5a or 5c, 5e, 7, and 9 based on (1) a comparison of relative terrace spacing to a global paleo sea-level curve, (2) the relative degree of preservation and soil-profile development, and (3) lateral correlation of the third-highest terrace to the dated substage 5e marine terrace near Cayucos (Weber, 1983). Additional higher (older) marine terraces are present in the region, but were not mapped in detail during these earlier studies. Therefore, a primary focus of our field surveys following the 2003 San Simeon earthquake was to map these older terraces where they are crossed by the Oceanic fault zone as mapped by Hall (1976). In these field surveys, we mapped the terraces associated with marine oxygen isotope stages 11 to 21 (terraces Q₆ to Q₁₁, Figures 2-8, 2-9). These older terraces provide an excellent Quaternary strain gauge from which to document the presence or absence of Quaternary activity along the Oceanic fault zone.

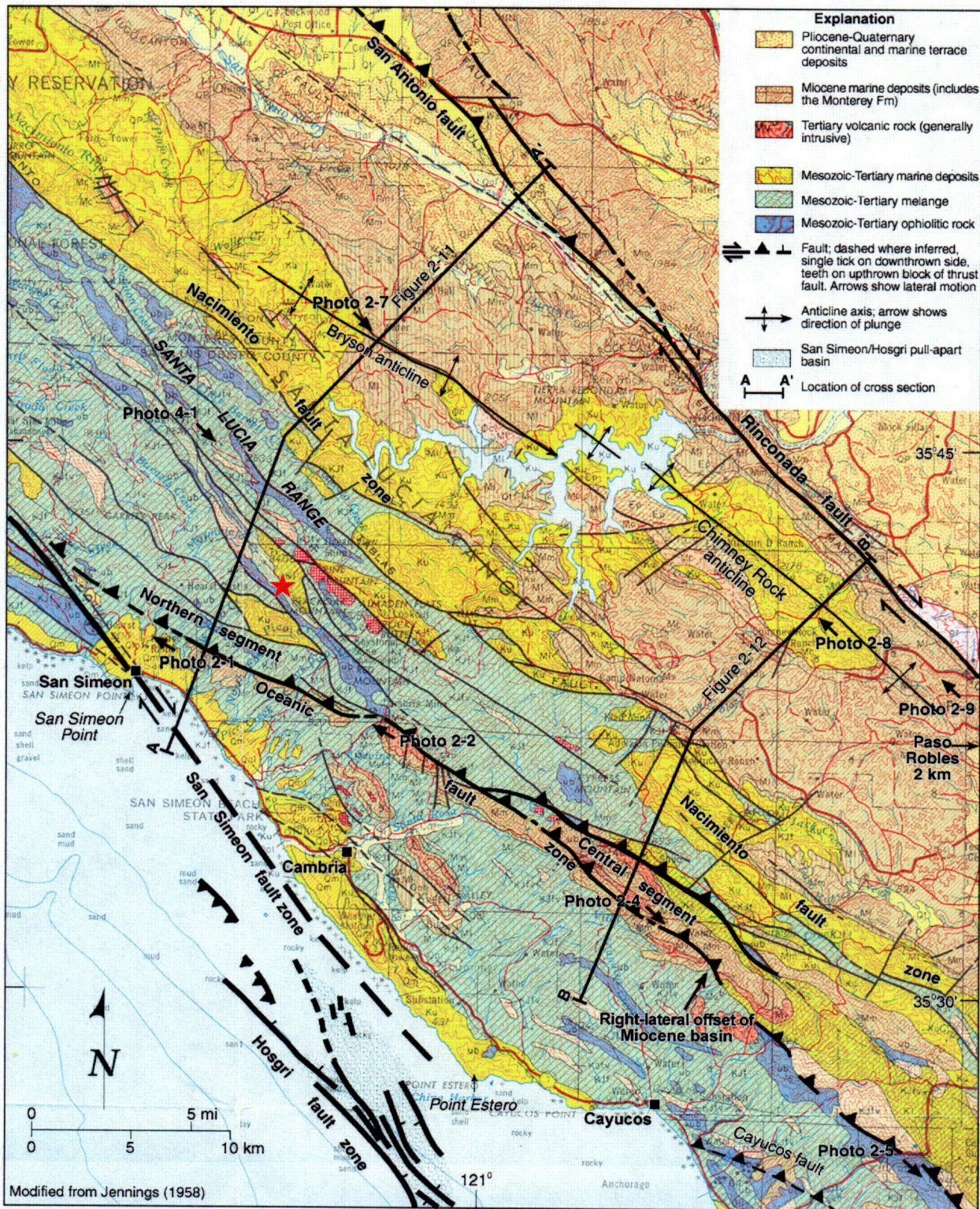
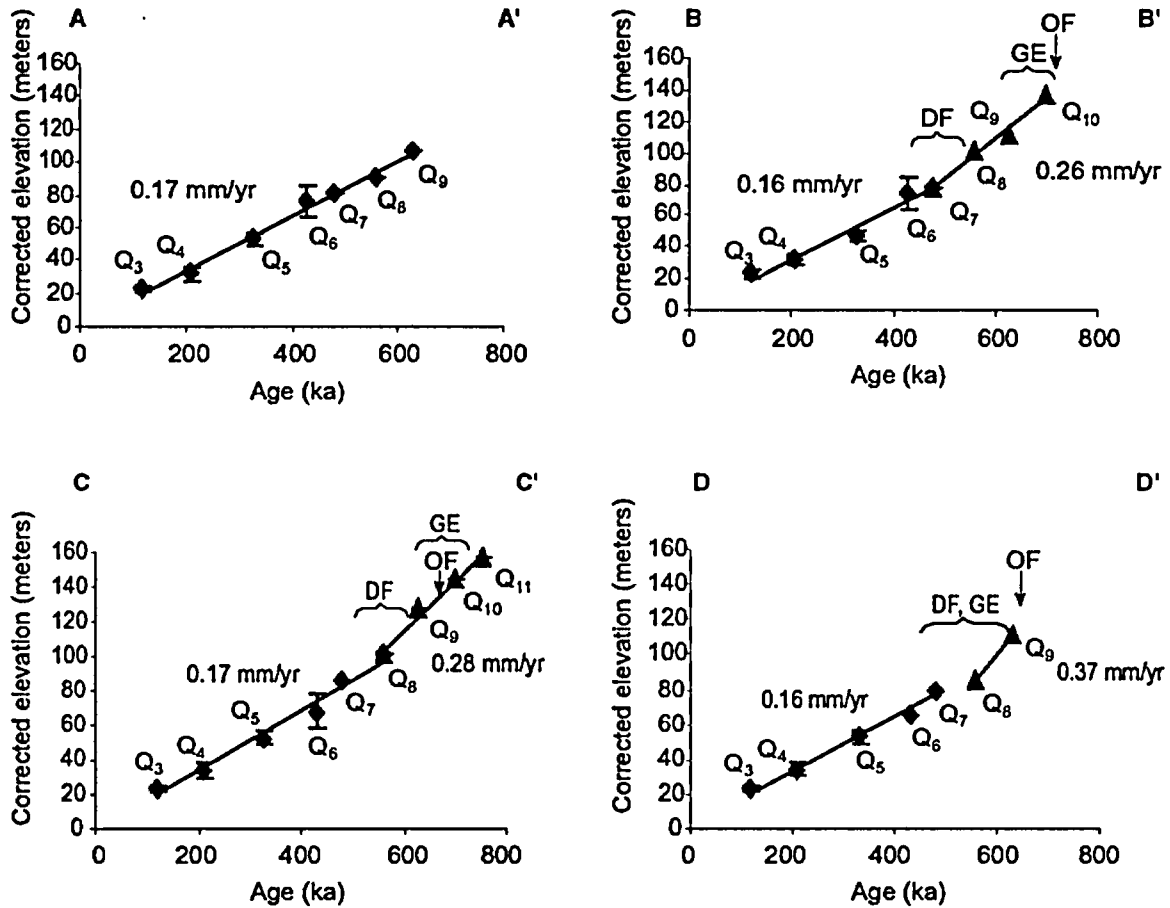


Figure 2-7. Geologic map of the San Simeon earthquake region.



Note: Terrace altitudinal spacing indicates a change in uplift rate from 0.16 m/kyr up to 0.37 m/kyr along a deformation front (DF) paralleling the Oceanic fault zone (OF) mapped by Hall (1976). Geomorphic expression (GE) of active deformation (scarps, tilted marine terraces, warped slopes) confirms changes in uplift rates along a deformation front in close vicinity of the Oceanic fault zone. Elevations were corrected for paleosea level at a time based on Hanson and others (1994). Profile A-A', located farthest from the Oceanic fault zone and deformation front, shows a constant uplift rate of 0.17 mm/yr over the past 700 ka, suggesting that the correlation of marine terraces to eustatic sea level curves is valid and that uplift rates of the coastal plain have remained constant. Topographic profiles A-A', B-B', C-C', and D-D' were traced transverse to the Oceanic fault zone and perpendicular to the coastline. Location of profiles is indicated on Figure 2-8.

Figure 2-9. Graphs of inferred uplift rate, Hearst Ranch study area.

2.2.2 Structure

The structural setting of western California reflects the culmination of repeated episodes of tectonic deformation beginning in the Late Jurassic and continuing to the present. These episodes of deformation produced a complex series of faults and folds in the San Simeon region. Many of these structures were overprinted on and deform older structures, whereas some structures were reactivated during succeeding episodes of deformation. Consequently, the identification and characterization of Quaternary deformation requires distinguishing younger deformation from older, inherited deformation. Some major Cretaceous and Tertiary structures, such as the Sur fault and the Nacimiento fault zone, formed in earlier tectonic regimes and show little evidence of Quaternary deformation. Quaternary structures significant to the understanding

of the tectonics in the San Simeon region include the San Simeon and Oceanic-West Huasna fault zones, as well as the Rinconada fault and other faults and folds (for example, the Bryson and Chimney Rock anticlines) within the southern Coast Ranges to the east of the Los Osos domain (Figure 2-7).

San Simeon Fault Zone

The San Simeon fault zone is part of the San Gregorio-San Simeon-Hosgri fault system, a system of kinematically linked right-slip faults that is subparallel to the central California coastline (Figure 2-2). As described by PG&E (1988), the fault system diverges from the San Andreas fault near Bolinas north of San Francisco (Jennings, 1994; Zoback and others, 1999) and extends approximately 410 kilometers to the southeast. The fault system appears to die out near Point Pedernales southwest of Santa Maria (Cummings and others, 1987) (Figure 2-2).

It should be noted that the San Simeon earthquake did not occur on the San Simeon fault zone. The earthquake was so named because it occurred 11 kilometers northeast of the town of San Simeon (Figure 2-7).

The San Simeon fault zone strikes northwest and extends from near Lopez Point south to Point Estero (Figures 2-2, 2-7). The fault is exposed onshore from San Simeon Point to north of Ragged Point, a distance of 20 kilometers. The total length of the fault is 87 kilometers, including the offshore and onshore portions of the fault. The northern termination of the San Simeon fault zone lies offshore north of Lopez Point, and is manifest as either a right step or a right bend into the San Gregorio fault zone. To the southeast, the San Simeon fault zone dies out west of Point Estero at a 3- to 5-kilometer-wide right stepover to the northern end of the Hosgri fault zone (PG&E, 1988) (Figure 2-7). Within the stepover, a series of en echelon, right-stepping normal or transtensional faults have produced a distinct basin, called the Hosgri-San Simeon pull-apart basin (Hanson and others, 2004; PG&E, 1991 [the Cambria stepover in PG&E, 1988]). The pull-apart basin is filled with post-late Wisconsinan sediment, indicating late Pleistocene and Holocene subsidence within an extensional releasing step along this right-lateral fault zone.

North of the pull-apart basin, the San Simeon fault zone extends onshore at San Simeon Bay, where it is constrained to a zone about 120 meters wide (Figure 2-8). North of San Simeon Bay, the fault forms a primary zone extending N35°W along Arroyo Laguna. The dominant sense of displacement along the primary trace of the San Simeon fault zone is right-slip; there is a minor component of west-side-up vertical displacement (Hanson and Lettis, 1994; Hall and others, 1994). Secondary faults within the zone splay northward with a more westerly trend, and have a primary component of dip-slip, east-side-up reverse displacement.

As described by Hanson and Lettis (1994) and PG&E (1988, 1991) the marine terrace sequence at San Simeon is clearly disrupted by the San Simeon fault zone. The terrace sequence southwest of the fault zone is elevated relative to the terrace sequence northeast of the fault zone, indicating vertical displacement has occurred on the fault. The ratio of lateral to vertical separation of the marine terrace sequence is about 10:1. Analysis of the displaced marine

terraces, deflected drainage channels across the fault, and the stratigraphic and structural relationships observed in trenches shows that the lateral slip rate on the San Simeon fault zone ranges between about 0.5 to 6.0 millimeters per year. The preferred range is 1.0 to 3.0 millimeters per year, which encompasses the minimum slip rate for displacement of the San Simeon marine terrace and the maximum slip rate for displacement of the Oso marine terrace. These terraces provide the best-constrained values of stratigraphic offset.

Oceanic-West Huasna Fault Zone

The Oceanic-West Huasna fault zone extends 120 kilometers southeast from the San Simeon area to near Santa Maria (Figure 2-3). The zone is divided into three distinct structural segments based on differences in strike: the northern and central segments comprise the Oceanic fault zone, and the southern segment is the West Huasna fault. The northern segment is about 20 kilometers long and strikes about N60° to 65°W. The central segment is about 50 kilometers long and strikes N45° to 55°W. The southern segment, or West Huasna fault, is 50 kilometers long and strikes about N30°W. Analysis of the San Simeon earthquake main shock and the distribution of aftershocks, described in Section 3, strongly suggests the northern and central segments of the Oceanic fault zone ruptured at depth. Thus, we focus our discussion on the Oceanic fault zone.

Oceanic Fault Zone - The Oceanic fault zone extends from its intersection with the San Simeon fault zone near Ragged Point (Photo 2-1) south-southeast along the southwestern margin of the

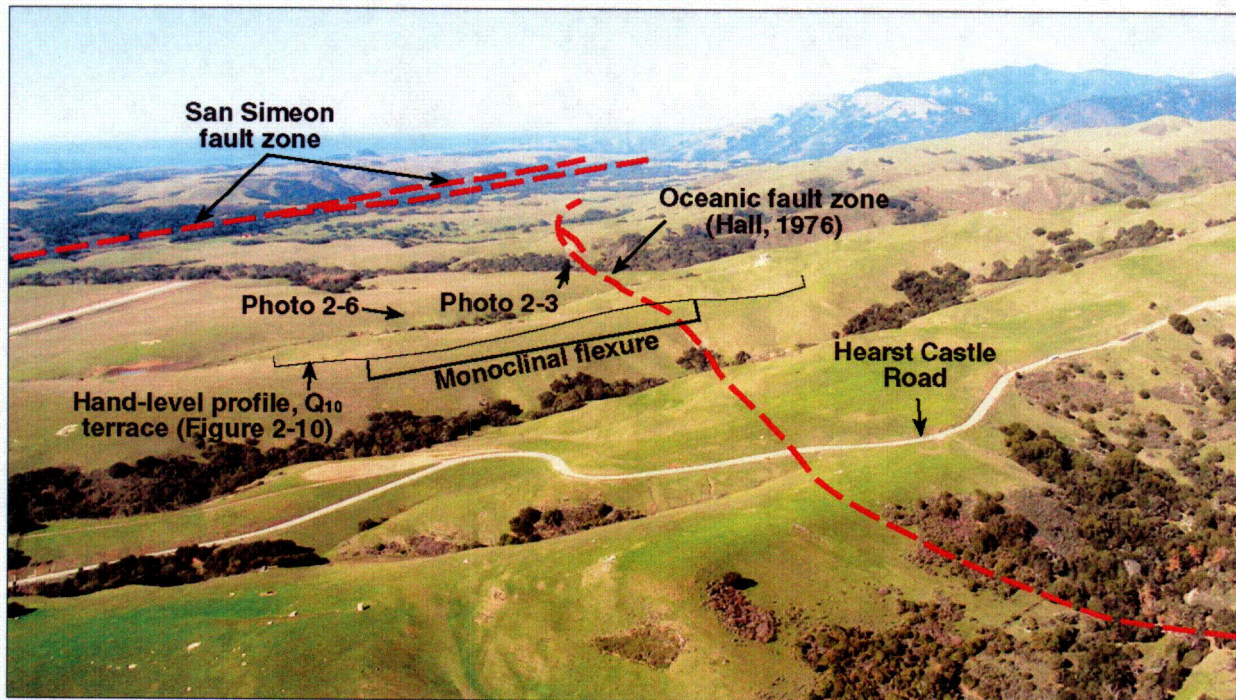


Photo 2-1. Aerial view to the northwest of the northern segment of the Oceanic fault zone across the Hearst Ranch site (Figure 2-7). The Oceanic fault zone coincides with the Quaternary deformation front and is associated with monoclinial folding of marine terraces and fault scarps.

CO9

Santa Lucia Range to where it merges into the West Huasna fault east of San Luis Obispo (Figures 2-2 and 2-3). In describing the Oceanic fault zone, it is important to make a clear distinction between (1) the bedrock traces of the fault zone mapped at the surface as the Oceanic fault zone by Hall (1974, 1976, 1991) and Hall and Prior (1975), (2) the zone of active range-front deformation along the western margin of the Santa Lucia Range that only locally coincides with the mapped bedrock fault (Photos 2-1, 2-2), and (3) the seismogenic fault that ruptured at depth during the 2003 San Simeon earthquake and projects to the surface generally coincident with the zone of range-front deformation and, locally, coincident with or within 1 to 3 kilometers west of the mapped bedrock traces of the Oceanic fault zone.

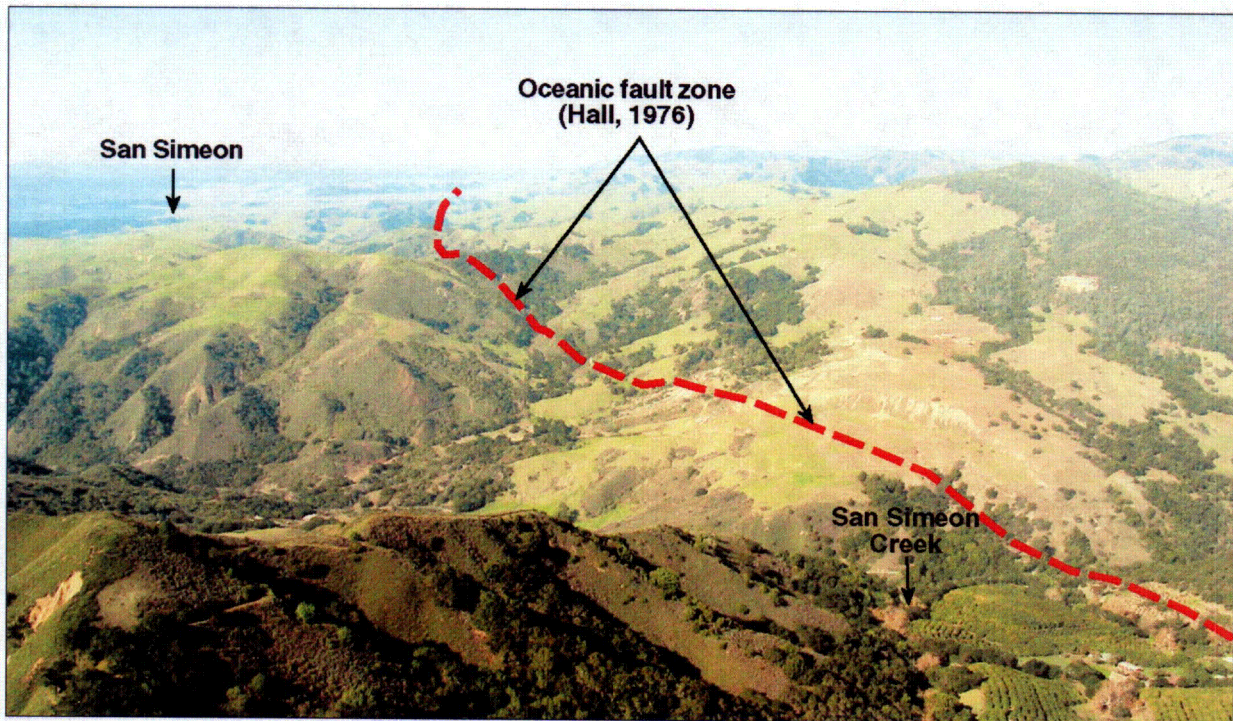


Photo 2-2. Aerial view to northwest of northern segment of the Oceanic fault zone from San Simeon Creek (Figure 2-7). The topographic front lies about 5 kilometers southwest of the fault zone mapped by Hall (1976) near San Simeon Creek, but coincides with the Oceanic fault zone near San Simeon (in the distance).

Hall Trace of the Oceanic Fault Zone - In this report, we refer to the bedrock traces of the Oceanic fault zone mapped at the surface by Hall (1974, 1976, 1991) and Hall and Prior (1975) as the "Hall trace." The Hall trace of the fault zone is mapped as a complex system of anastomosing and branching faults, commonly marked by distinct tabular bodies of serpentinite (Photo 2-3) that generally juxtaposes Franciscan complex rocks on the northeast against Cretaceous and Tertiary sedimentary and volcanic rock on the southwest. Many branches of the Hall trace of the fault zone also juxtapose various units of the Cretaceous and Tertiary rock. The trace of the Oceanic fault zone shown on Figure 2-7, originally mapped by Jennings (1958), generally coincides with the primary bedrock trace of the Oceanic fault zone later mapped in detail by Hall (1974, 1976, 1991) and Hall and Prior (1975).

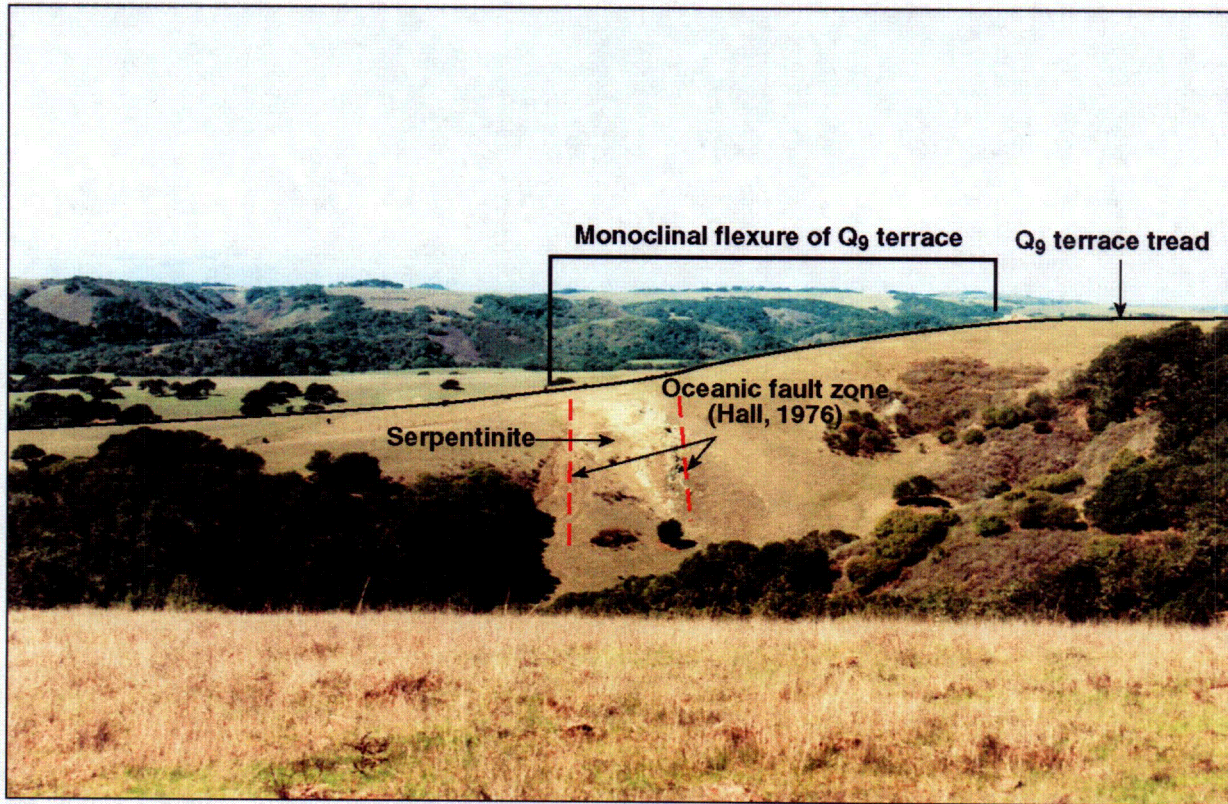
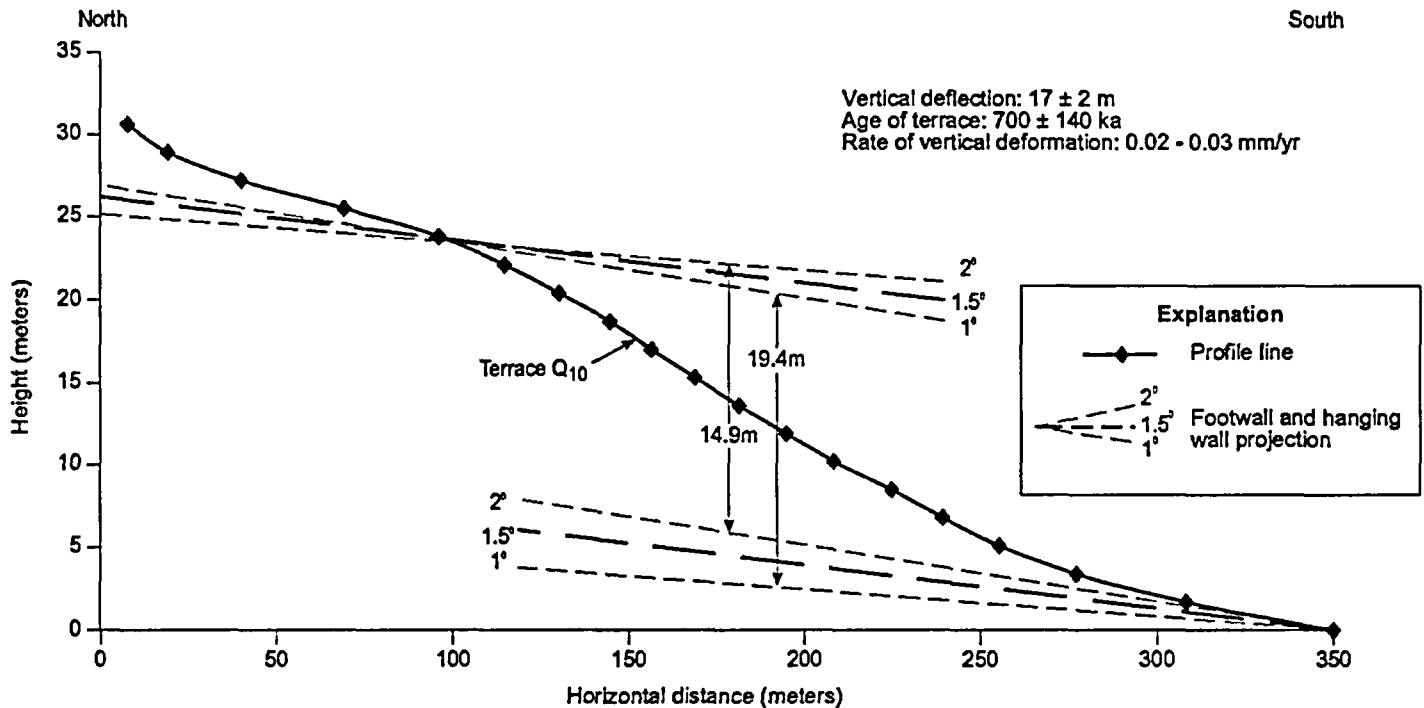


Photo 2-3. View to north of the Oceanic fault zone (Hall, 1976) as defined by a serpentinite outcrop. The Q₉ (630,000 years old) marine terrace surface is deformed in a southwest-facing monoclinical flexure over the fault zone. Figure 2-8 and Photo 2-1 show the location of this photo.

The dip of the Hall trace of the Oceanic fault zone is poorly known. Published cross sections show the fault zone to be subvertical (Hall, 1974, 1976, 1991; Hall and Prior, 1975). The map pattern of the Hall trace suggests it dips steeply to the northeast. Interpretation of the tectonic setting also suggests the fault zone dips to the northeast (Lettis and others, 2004). We did not directly observe exposures of Hall's primary fault plane during our field reconnaissance to verify this interpretation; however, small faults in the Monterey Formation exposed in a road cut along Santa Rosa Creek within the fault zone dip about 70°NE, have reverse motion with a right-slip component, and are associated with tight folds. The outcrop pattern of elongate serpentine bodies that locally define the Hall fault zone (Photo 2-3) have an approximately straight trace through steep topography, indicating the fault dips steeply (70 degrees or more) to the northeast.

Zone of Active Range-Front Deformation - Based on a preliminary analysis of a digital elevation model, there is a zone of active range-front deformation along the northern and central segments of the Oceanic fault zone. The zone of range-front deformation is well-defined where it crosses a flight of marine terraces on the Hearst Ranch north of San Simeon (Figures 2-8, 2-9, 2-10). At this location, the zone closely coincides with the Hall trace of the fault zone (Photos 2-1, 2-3). To the south, the active range front is less clear, but it probably coincides with the relatively broad rise in topography west of the crestal region of the Santa Lucia Range. In



Note: Hand-level profile is located at northern end of profile B-B' (see Figure 2-8 and Photos 2-1 and 2-6). Rounded fine gravel at the surface along the profile line indicates that a single terrace has been warped into a south-facing monocline. Assuming an original wave-cut platform angle of $1.5 \pm 0.5^\circ$, the monoclinical folding shows about 17 ± 2 m of vertical deformation. A 700 ± 140 ka age of the terrace yields an average vertical deformation rate of 0.02 - 0.03 mm/yr, substantially less than the approximately 0.1 to 0.2 mm/yr change in vertical uplift rate as suggested by profile B-B' and vertical uplift rate graphs farther northwest (Figure 2-9).

Figure 2-10. Hand-level profile of folded Q₁₀ marine terrace.

this area, the Hall trace of the fault zone diverges from the zone of range-front deformation and becomes an intra-range fault (Photos 2-2, 2-4, 2-5). The separation between the Hall fault zone and the approximate zone of active range-front deformation is particularly apparent along the central segment of the Oceanic fault.

Seismogenic Fault - The 2003 San Simeon earthquake defines the seismogenic fault. The location and geometry of this fault are inferred from dynamic rupture models of the main shock rupture and three-dimensional visualization of the aftershock sequence. On the northern segment of the Oceanic fault zone, the updip projection of the seismogenic fault closely corresponds to the Hall trace of the Oceanic fault zone and to the zone of active range-front deformation in the Hearst Ranch area (Figure 2-11). On the central segment of the Oceanic fault, the updip projection of the seismogenic fault corresponds generally to the zone of active range-front deformation, but is 1 to 3 kilometers west of the Hall trace of the Oceanic fault (Figure 2-12).

As reported by Hardebeck and others (2004) and PG&E (2004b), there was no surface rupture of the Oceanic fault zone during the San Simeon event, or on any other potentially causative faults within the Santa Lucia Range. There was no evidence of sympathetic movement on nearby regional faults, including the San Simeon, Los Osos, or Southwest Boundary zone faults. Fault rupture associated with the earthquake was not large enough to propagate to the ground surface.

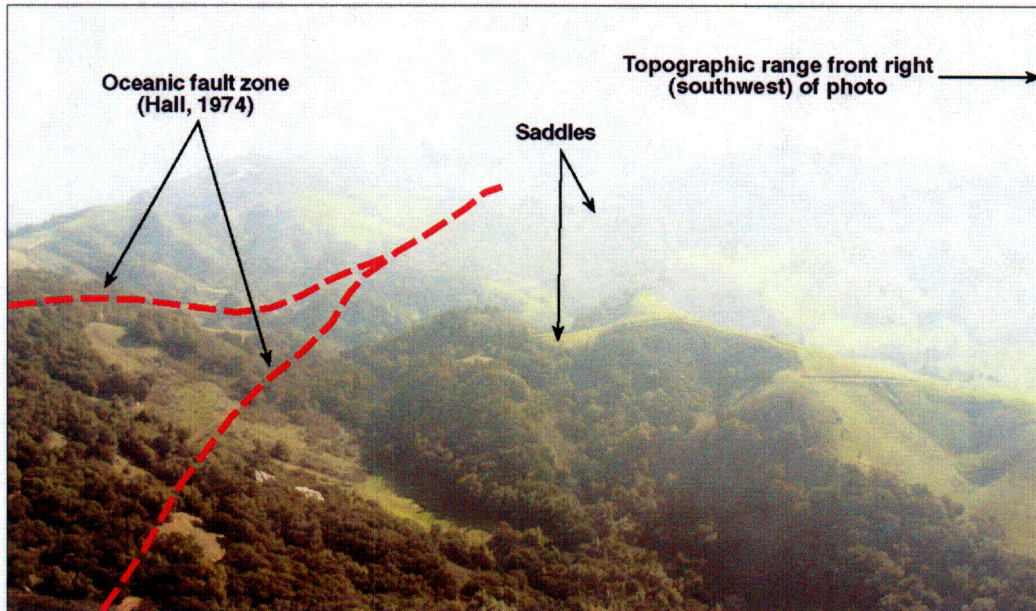


Photo 2-4. Aerial view to southeast of the central segment of the Oceanic fault zone directly south of Highway 46 (Figure 2-7). Note how the fault zone mapped by Hall (1974) does not coincide with the prominent topographic lineament locally defined by aligned saddles. The topographic front lies at least 8 kilometers southwest of the fault zone.

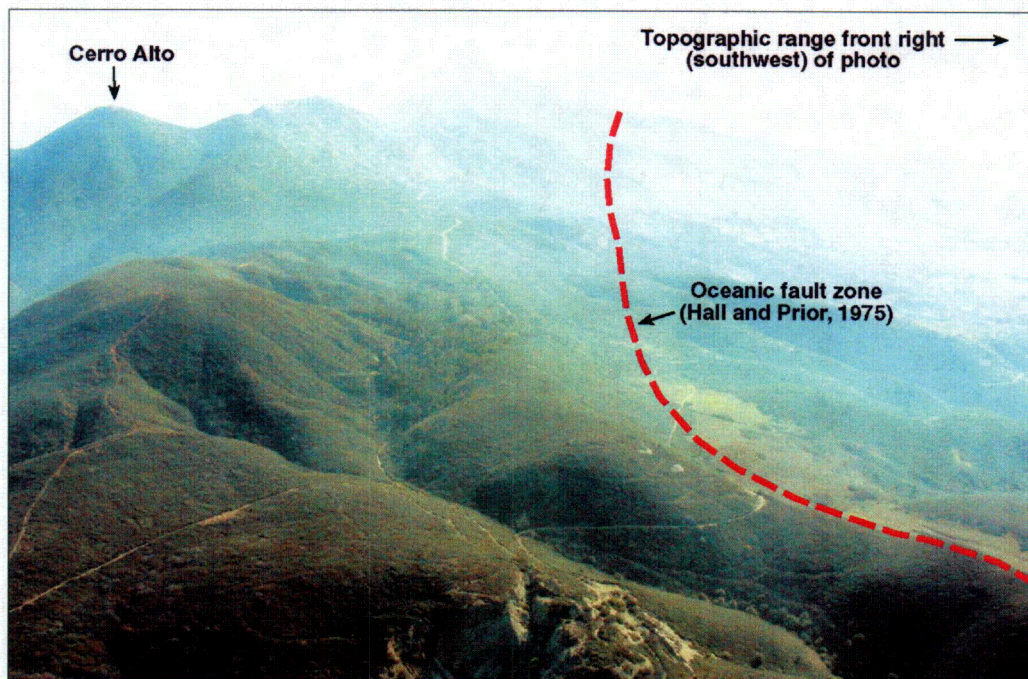


Photo 2-5. Aerial view to southeast of the central segment of the Oceanic fault zone (Hall and Prior, 1975) 0.5 kilometer south of Highway 41 (Figure 2-7). The topographic range front lies 8 to 10 kilometers southwest of the fault trace.

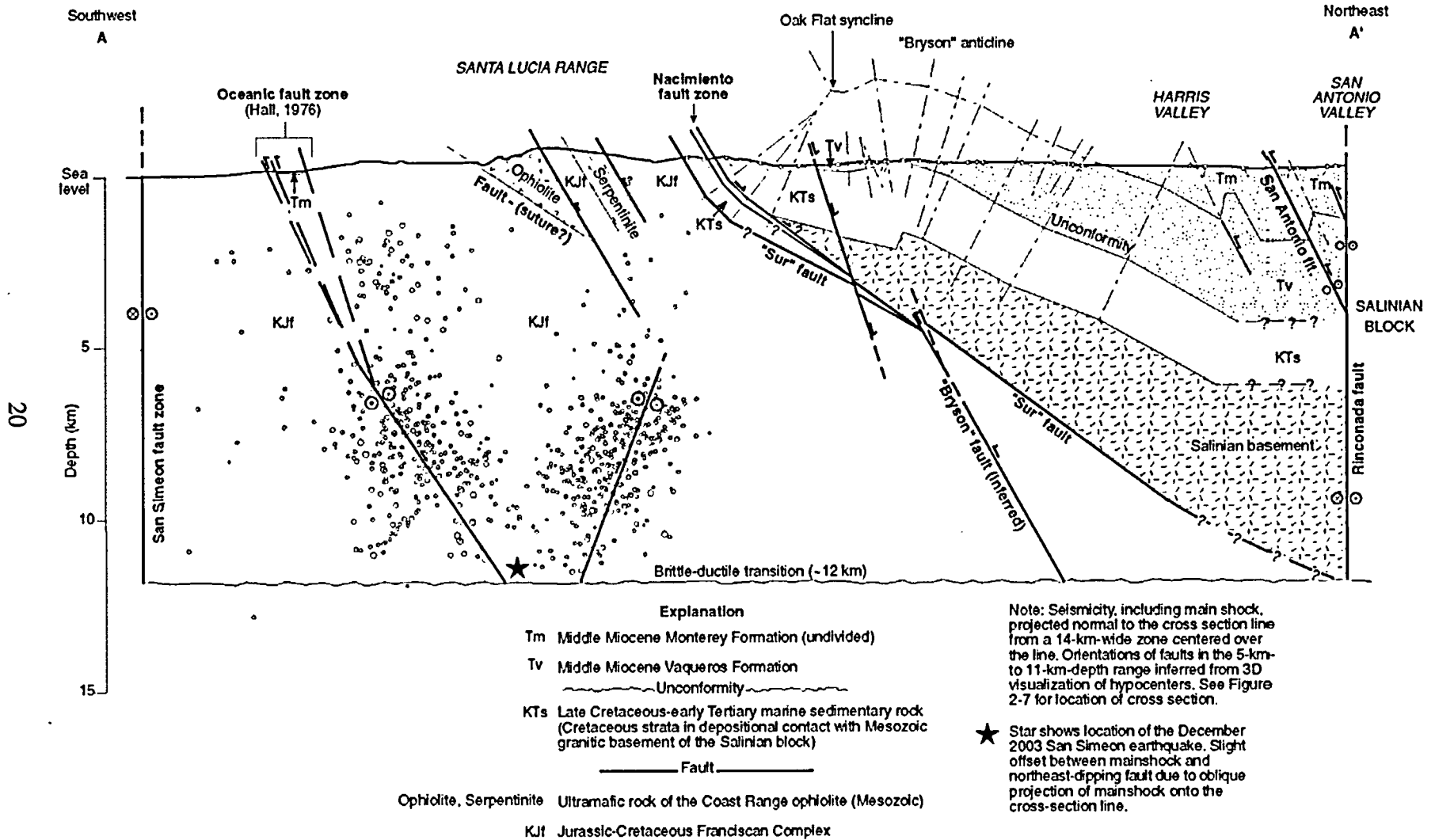


Figure 2-11. Cross Section A-A'.

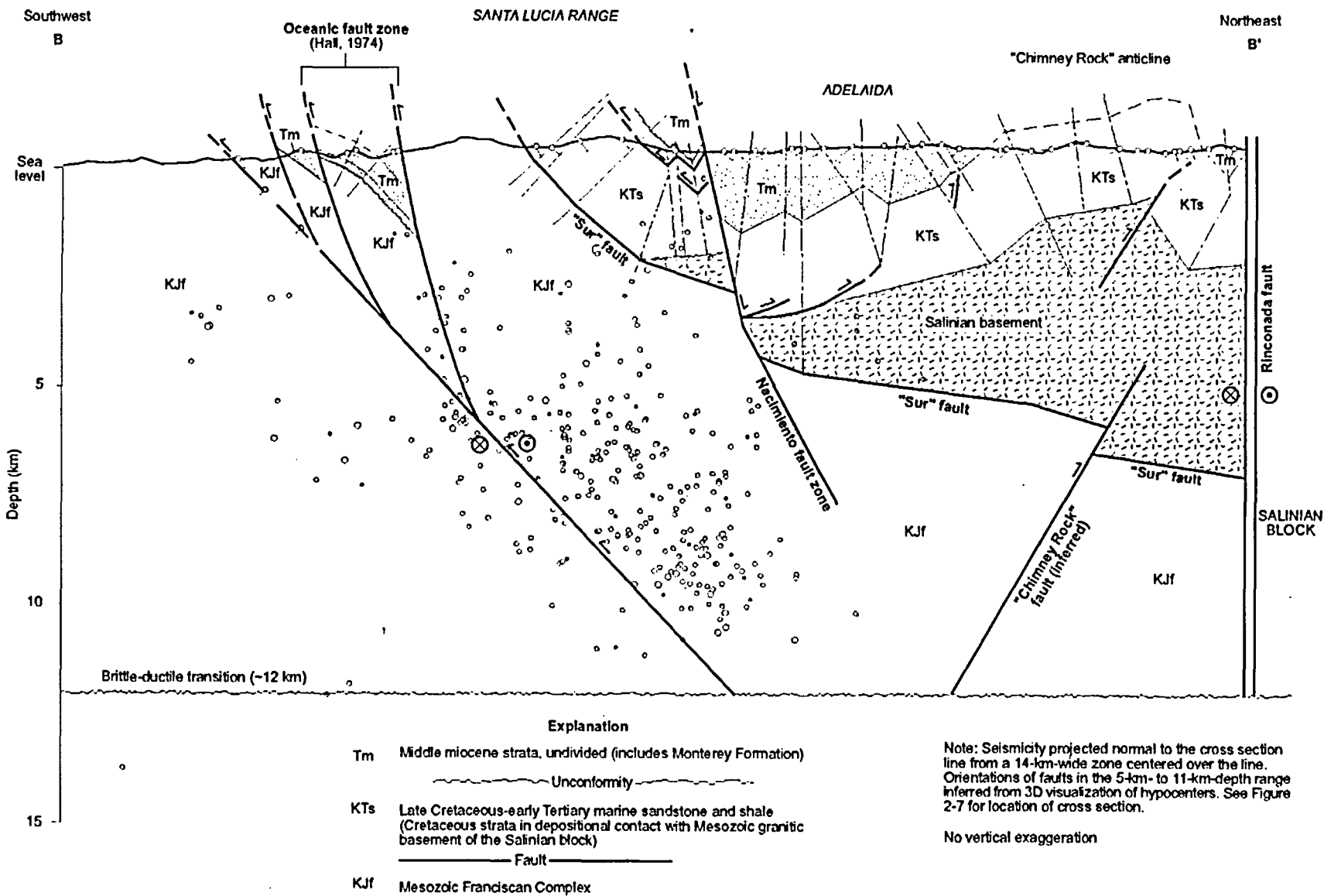


Figure 2-12. Cross Section B-B'.

Activity of the Oceanic Fault Zone - The Oceanic fault zone has clear evidence of post-middle Miocene activity and, locally, evidence of late Quaternary activity. Because the Hall trace of the Oceanic fault zone juxtaposes rocks of the Franciscan complex up on the east against middle Miocene Monterey Formation on the west (for example, Hall, 1974), it provides direct stratigraphic evidence for post-middle Miocene east-side-up displacement on the fault zone. In addition, a small middle Miocene basin is displaced laterally about 1 to 2 kilometers across the Hall trace of the central segment of the Oceanic fault zone (Figure 2-7; Hall, 1974). If we assume the displacement occurred since the middle Miocene (about 15 million years ago), then the minimum long-term average rate of right-slip displacement is about 0.1 millimeter per year. Assuming the displacement occurred entirely in the past 3.5 million years, coeval with onset of late Cenozoic uplift of the southern Coast Ranges (Page and others, 1998; Section 2.2), then the long-term average rate of right slip is about 0.3 to 0.6 millimeter per year. These low rates of slip are consistent with the geomorphic expression of the Hall trace. The trace is poorly defined geomorphically and stream channels are not obviously deflected across it, suggesting that if the Hall trace is active, the slip rate is probably only a few tenths of a millimeter per year or less. Variations in erosion rates by rock type (for example, between Franciscan *mélange*, serpentinite, and Tertiary and Cretaceous marine strata) appear locally to control changes in elevation across the Hall trace, suggesting that erosion rates are comparable to or greater than the rate of tectonic deformation along the fault zone.

As described earlier, the Hall trace of the Oceanic fault zone generally coincides with the base of the Santa Lucia Range front north of San Simeon, but lies within the range front to the south-southeast. For example, the distance between the Hall trace and the active range front ranges from near zero on the Hearst Ranch north of San Simeon along the northern segment of the fault (Figure 2-8; Photo 2-1) to several kilometers east of the range front at the latitude of Cambria and Cayucos along the central segment (Photos 2-4, 2-5). Because the Hall trace of the fault zone generally is not a true range-front fault to the southeast within the central segment, it cannot be the only fault driving uplift of the Santa Lucia Range, and probably is not even the major fault responsible for uplift. Other faults must be active west of and structurally below the Hall trace to produce the uplift along the physiographic range front.

North of San Simeon, a well-developed sequence of Pleistocene marine terraces is preserved across the Hall trace of the Oceanic fault zone and is beveled into the southwestern base of the Santa Lucia Range (Figure 2-8). These terraces are especially well preserved on the Hearst Ranch north of San Simeon. Geomorphic mapping of the marine terraces on the Hearst Ranch documents a zone of active deformation locally coincident with the Hall trace of the Oceanic fault zone at its northern end (Figure 2-8; Photos 2-1, 2-3, 2-6). The zone of deformation is expressed by a series of scarps, steps, and monoclinical flexures across the Q_9 and Q_{10} marine terraces (Figure 2-8; Photos 2-3, 2-6). The deformed terraces correlate to marine oxygen isotope stages 17 and 19 (terraces Q_9 and Q_{10} , 630,000 and 700,000 years old, respectively). Three profiles (B-B', C-C', and D-D', Figure 2-9) across the marine terraces and orthogonal to the range front show an abrupt change in altitudinal spacing of the marine terraces, indicating a change in uplift rate coincident with the range front. The estimated uplift rate changes from 0.16 millimeter per year southwest of the range front to between 0.26 to 0.37 millimeter per year east of the range front along a deformation zone that coincides with the Hall trace of the Oceanic



Photo 2-6. View to southeast of the Oceanic fault zone (Hall, 1976) crossing marine terraces near the deformation front of the Santa Lucia Range. The Q_{10} (700,000 years old) marine terrace surface at the right side of the photo is deformed in a southwest-facing monoclinal flexure over the fault zone. Figure 2-10 shows a hand-level profile across the monoclinal flexure. Figure 2-8 and Photo 2-1 show the location of this photo.

fault zone, but more commonly lies 100 meters to 850 meters southwest of the Hall trace. The differential rate of uplift across the zone of deformation is about 0.1 to 0.2 millimeter per year. A hand-level profile of a folded stage 19 (700,000 years old) terrace directly west of the Hall trace of the Oceanic fault zone indicates a local vertical separation rate of 0.02 to 0.03 millimeter per year (Figure 2-10). This uplift rate is only a portion of the change in uplift rate noted across the profile of the entire flight of terraces, indicating that total deformation is not localized on a single, near-surface fault trace. To the south, profile A-A' (Figure 2-9) drawn across a flight of similar-age marine terraces that do not cross the range front or the Hall trace of the Oceanic fault zone shows a negligible change in uplift rate, from 0.16 millimeter per year to 0.17 millimeter per year. This profile indicates that the "background" coastal uplift rate has remained relatively constant since marine oxygen isotope stage 19 (terrace Q_{10} , 700,000 years old).

The style and geometry of deformation along the range front and the Hall trace of the Oceanic fault zone is complex and not well constrained. The available marine terrace data provide clear evidence that a zone of Quaternary deformation is present along the southwestern range front of Santa Lucia Range and locally coincides with the bedrock trace of the Oceanic fault zone. However, field mapping did not identify prominent geomorphic expression of the surface trace

of an active fault. Rather, deformation primarily is expressed by tilting and warping (monoclinical folding) in a zone up to 1 kilometer wide. The nature of surface deformation suggests the active range front fault is non-emergent, but the relatively narrow zone of deformation implies the fault extends to within 1 to 2 kilometers of the surface, and perhaps into the shallow subsurface.

Rinconada Fault

The Rinconada fault is a north- to northwest-striking late Cenozoic right-slip fault (Dibblee, 1971, 1976). Based on regional stratigraphic and structural relations documented by Dibblee (1976), total right-slip displacement on the fault since early Tertiary time may be about 75 kilometers. At the latitude of Paso Robles in southern Salinas Valley, the Rinconada fault is bordered on the west by zones of folding and reverse faulting. For example, the San Antonio fault, which borders the eastern San Antonio River valley and is several kilometers west of the Rinconada fault, is an east-side-up reverse fault (Figure 2-7). The crustal block bounded on the west by the San Antonio fault and on the east by the Rinconada fault is deformed by tight, closely spaced, northwest-trending folds. Following Dibblee (1976), we interpret this folded block and the San Antonio fault to be part of a positive flower structure associated with the Rinconada fault. This interpretation is illustrated in regional geologic cross section A-A' (Figure 2-11) and is further discussed in Section 4.1.2.

Nacimiento Fault Zone

The northwest-striking Nacimiento fault zone is located in the eastern Santa Lucia Range east of the Oceanic fault zone. As defined by Hall (1991), the Nacimiento fault zone is a subvertical to steeply east dipping normal fault that displaces Cretaceous and Tertiary marine strata down on the east against equivalent rocks and the Franciscan complex on the west. Prior to Hall's study (1991), many workers correlated the Nacimiento fault zone with the Sur fault, an east-dipping, low-angle fault that places granitic rocks of Mesozoic Salinian block and depositionally overlying Cretaceous strata up on the east over the Franciscan complex on the west. For example, in the Adelaida 15' Quadrangle, the structure Dibblee (1971) maps as the Nacimiento fault is located east of the structural contact between the Franciscan rock and the Cretaceous marine sediment (the "Sur" fault of Hall, 1991), characterized by east-side-down displacement and thickening of the Monterey Formation to the east.

Hall (1991) made a distinction between the Sur and Nacimiento faults, stating that the Nacimiento fault is a "multi-phase Cenozoic fault zone," which "formed along or near the older Sur thrust zone, or as a reactivated strand of the Sur thrust zone." In several geologic cross sections through the southern Coast Ranges, Hall (1991) depicts the Nacimiento fault zone as a subvertical structure that cuts and displaces the Sur fault down to the east. We have followed Hall's interpretation that the Nacimiento fault zone is clearly distinct from the Sur fault in developing geologic cross sections of the Santa Lucia Range (Figures 2-11 and 2-12). We show the Sur fault at depth separating the Salinian basement rock (inferred to underlie the Cretaceous marine sediments) from the Franciscan complex.

In the Bryson 15' Quadrangle to the southeast, the structure mapped as the Nacimiento fault by Dibblee (1971) is part of a zone of faulting that juxtaposes northeast-dipping Late Cretaceous to Paleogene marine deposits on the east against the Franciscan complex on the west (Figure 2-12). The trace of this fault is distinct and is not connected to the structure mapped to the northwest in the Adelaida 15' Quadrangle as the Nacimiento fault. These relations are consistent with Hall's observation (1991) that the Nacimiento fault zone is distinct from the Sur fault, but locally "formed along or near the older Sur thrust zone."

Bryson Anticline

In the Bryson 15' Quadrangle, bedding dips within the Monterey Formation define a southwest-vergent anticline between the Nacimiento fault and the Rinconada fault (Dibblee, 1971). The axis of the anticline is about 2 kilometers west of the town of Bryson; for convenience, we refer to this fold as the "Bryson" anticline. The axis of the Bryson anticline trends about N50°W, which is about 25 degrees more westerly than the strike of the Rinconada fault at this latitude (Dibblee, 1971). The wavelength of the fold is about 12 to 14 kilometers, and the back limb of the fold dips about 30°NE. Erosional windows through the Monterey Formation near the axis of the fold expose underlying Late Cretaceous to Paleogene marine deposits. Based on construction of geologic cross section A-A' across the Bryson anticline (Figure 2-11), we estimate about 4 kilometers of structural relief on the Monterey Formation across the fold. The Bryson anticline is interpreted to be a fault-propagation fold above a non-emergent, northeast-dipping reverse fault (the inferred "Bryson" fault). We assume this fault extends to the base of the seismogenic crust (Figure 2-11).

During field reconnaissance, we observed that the Bryson anticline is not associated with a topographically distinct mountain or range of hills. The axial region of the fold, however, is associated with an old, low-relief landscape surface that is presently several hundred feet above the modern stream base level (Photo 2-7). This probably is one of the old upland surfaces in the southern Coast Ranges discussed by Page and others (1988) that has been uplifted during late Cenozoic time. This relict landscape may have been uplifted due to growth of the Bryson anticline.

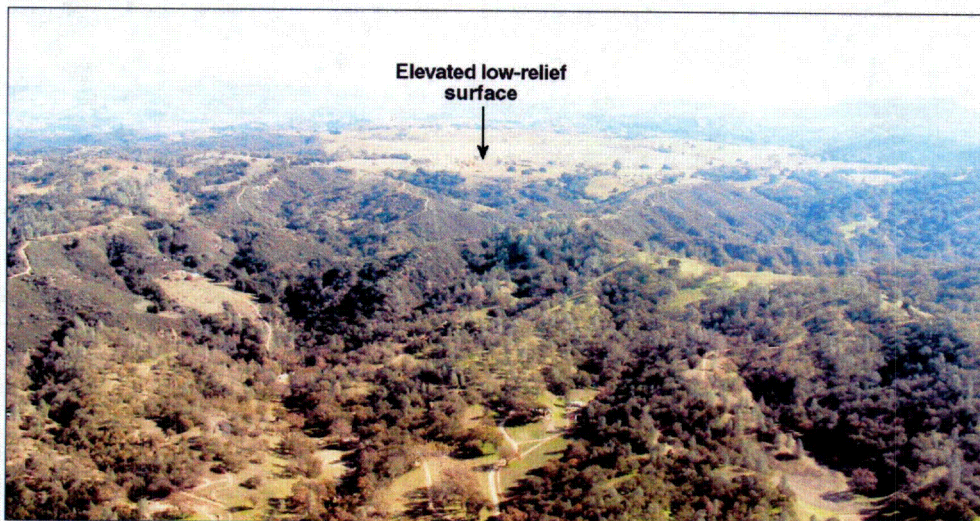


Photo 2-7. Aerial view to southeast of the Bryson anticline crestal region, northwest of Lake Nacimiento (Figure 2-7). Photo was taken about 3 kilometers west of cross-section line A-A' (Figure 2-11).

Chimney Rock Anticline

In the Adelaida 15' Quadrangle, bedding dips in the Monterey Formation and underlying Late Cretaceous to Paleogene marine deposits define a northeast-vergent anticline between the Nacimiento and Rinconada faults (Dibblee, 1971). For convenience, we refer to this fold as the "Chimney Rock" anticline because the fold axis passes close to Chimney Rock along San Marcos Creek (Photo 2-8). The axis of the Chimney Rock anticline trends about N68°W (in contrast, the Rinconada fault directly to the east strikes about N40°W). The wavelength of the Chimney Rock anticline is about 12 kilometers; the back limb of the fold dips about 30°SW. From construction of cross section B-B' (Figure 2-12), we estimate about 2.5 to 3.0 kilometers of structural relief on the folded Monterey Formation across the anticline axis. The Chimney Rock anticline is interpreted to be a fault-propagation fold above a non-emergent, southwest-dipping reverse fault ("Chimney Rock" inferred fault, Figure 2-12).

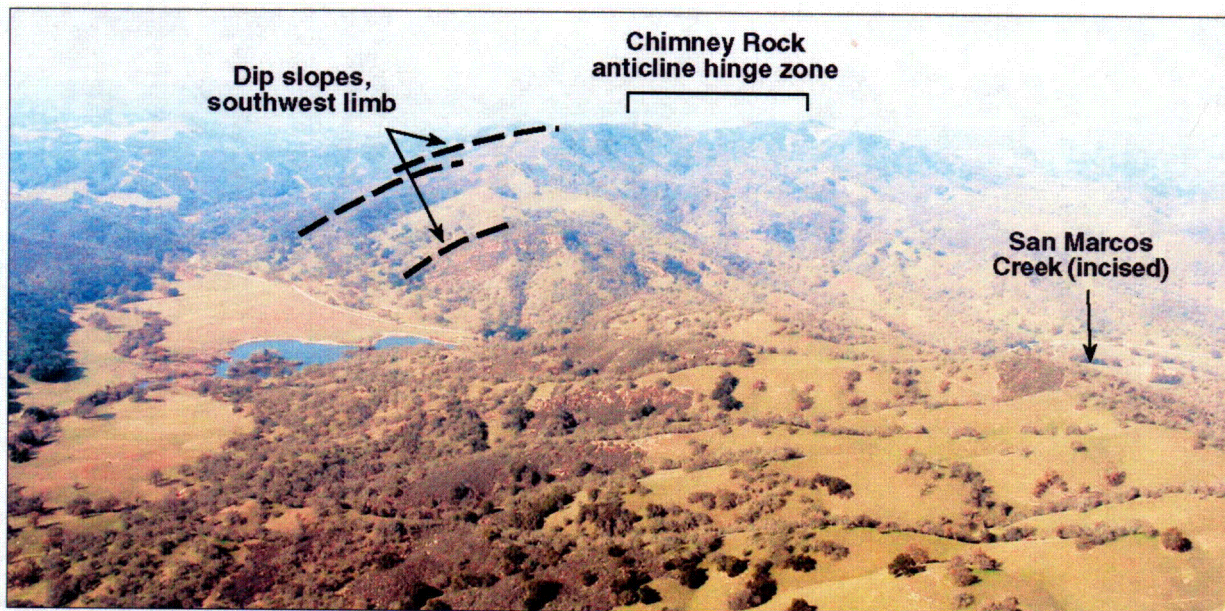


Photo 2-8. Aerial view to northwest of the Chimney Rock anticline across San Marcos Creek. Dip slopes along the southwest fold limb, the topographically high crestal region of the anticline, and the incision of San Marcos Creek into a graded, low-relief landscape in the right side of the photo all indicate active fold growth. Photo was taken about 1 kilometer south of Chimney Rock Road and cross section line B-B' (Figures 2-7 and 2-11).

During field reconnaissance, we observed geomorphic features consistent with Quaternary uplift of the Chimney Rock anticline. San Marcos Creek, which drains across the southeast-plunging nose of the fold, has deeply incised its channel and cut a series of terraces that are probably of Pleistocene age. A tributary stream to San Marcos creek is incised below an older, relict Pleistocene valley floor, also producing multiple terraces. We attribute incision of San Marcos Creek and its tributary to progressive uplift of the fold. Also, the modern morphology of the Chimney Rock anticline reflects the structure: the fold is a distinct mountain having well-defined dip slopes along the east and west limbs (Photos 2-8, 2-9).

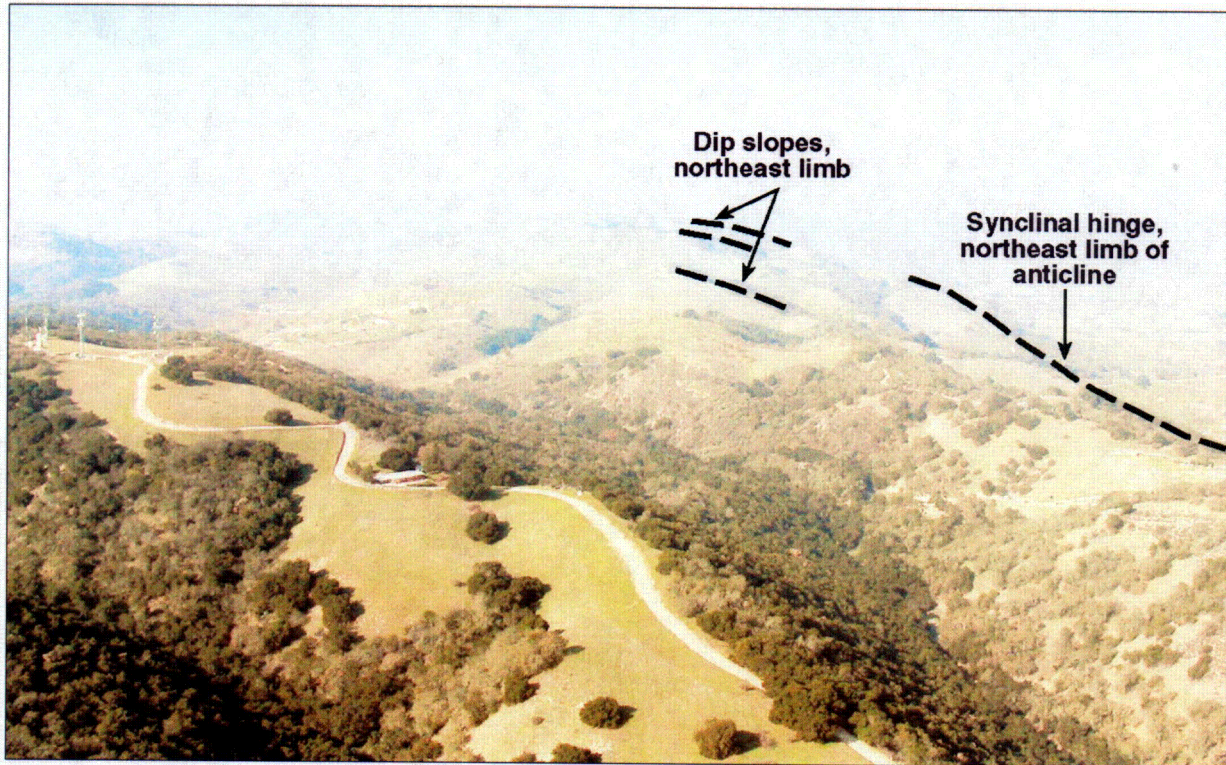


Photo 2-9. Aerial view to northwest of the Chimney Rock anticline, northeast limb. Photo was taken 4 kilometers west of Paso Robles and about 1 kilometer south of Adelaida Road (Figure 2-7). Dip slopes on the northeast fold limb and the prominent topographic break along the synclinal hinge line farther east suggest active fold growth of the Chimney Rock anticline.

3.0 SEISMICITY

The M_w 6.5 San Simeon earthquake of 22 December 2003 initiated a prolific and ongoing aftershock sequence. As of November 16, 2004, the USGS online database (USGS, 2004) reported over 8000 aftershocks greater than about magnitude 0.5, including 6000 aftershocks of magnitude <2 , 2000 of magnitude ≥ 2 , 200 of magnitude ≥ 3 , and 19 of magnitude ≥ 4 . To date, there has not been a magnitude 5 aftershock. The graph on Figure 3-1 shows the rate of aftershocks having magnitude greater than or equal to 3.0, based on the USGS online database (USGS, 2004). The rate of aftershocks has been diminishing with time, consistent with an Omori relation. At smaller magnitudes, the catalog is incomplete prior to March 2004. Since March, the USGS has improved its ability to keep up with the smaller-magnitude data because the sequence had started to quiet down (D. Oppenheimer, USGS, personal communication).

We estimate the location of the main shock to be $35^\circ\text{N}41.88$, $121^\circ\text{W}6.21$, at a depth of 11.3 kilometers. This is an absolute depth estimate using a linear velocity model, station corrections, and the Hypoinverse 2000 location program. Our focal mechanism shows nearly pure reverse motion with a strike of 297 degrees ($\text{N}63^\circ\text{W}$), dip of 61 degrees to the northeast, and rake of 96 degrees (Figure 5-4 in PG&E, 2004b). Our epicenter and focal mechanism are in good agreement with Hardebeck and others (2004); we agree this was a reverse event that

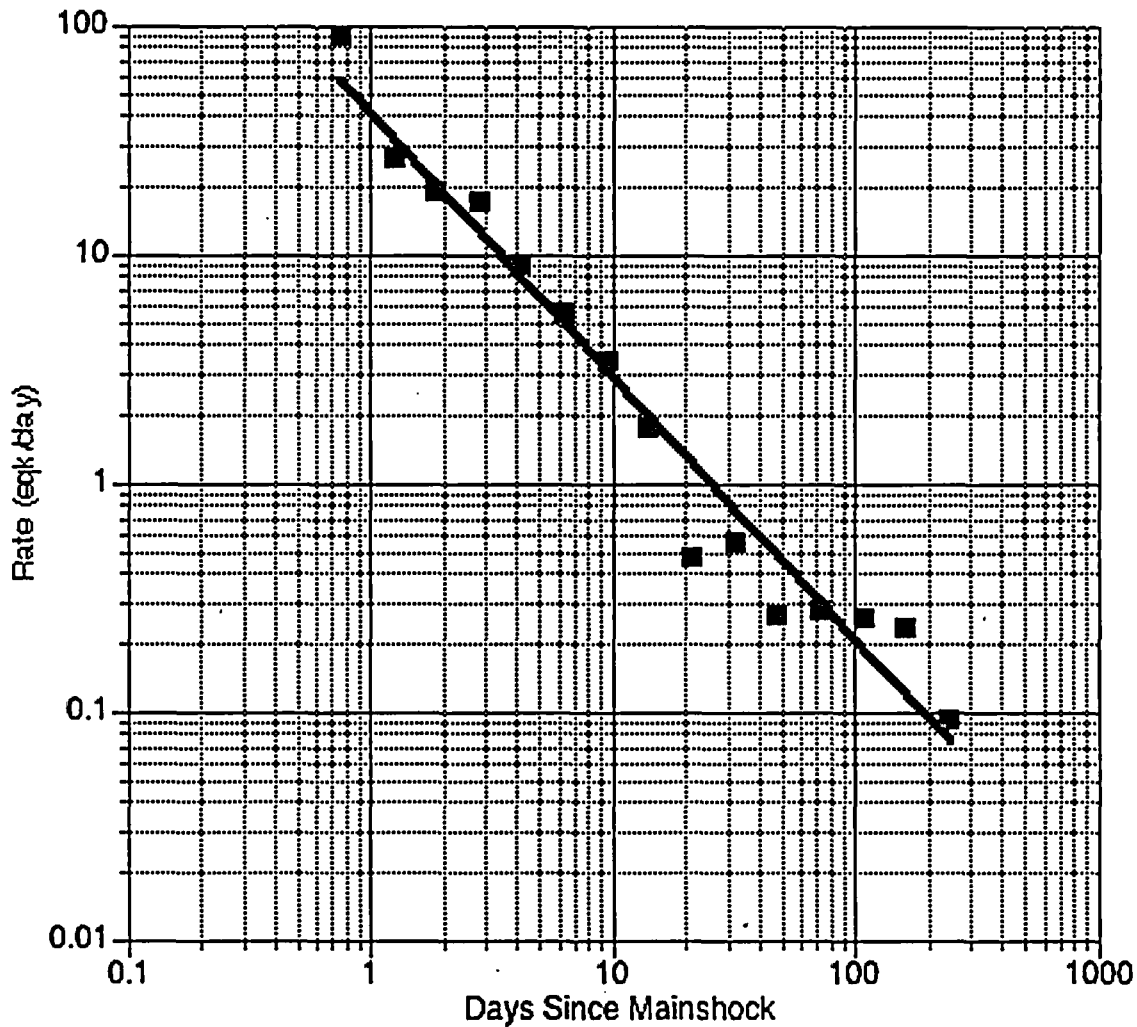


Figure 3-1. Decay rate of aftershocks having $M \geq 3.0$. The line shows the fit to an Omori relation resulting in a p-value of 1.15.

occurred between the mapped surface traces of the Oceanic and Nacimiento fault zones, and that it ruptured unilaterally to the southeast. However, our depth is about 4 kilometers deeper than the Hardebeck 7.1 kilometer-depth, which is a relative depth estimated using the double-difference method of Waldhauser and Ellsworth (2000).

The locations of the PG&E and USGS short-period seismographic stations are shown on Figure 3-2. The PG&E network was installed in 1987 and consists of 20 analog stations, including five 3-component stations. The purpose of the network is to provide PG&E with immediate access to earthquake data for monitoring the seismic activity in the Diablo Canyon Power Plant region. The station locations were chosen to infill the USGS stations; Figure 3-2 shows that the PG&E network improves the USGS seismographic coverage in the region, particularly southeast of the main shock for about 100 kilometers. The closer station spacing, within about 20 to 50 kilometers of the main shock and aftershocks, and the on-scale S-wave

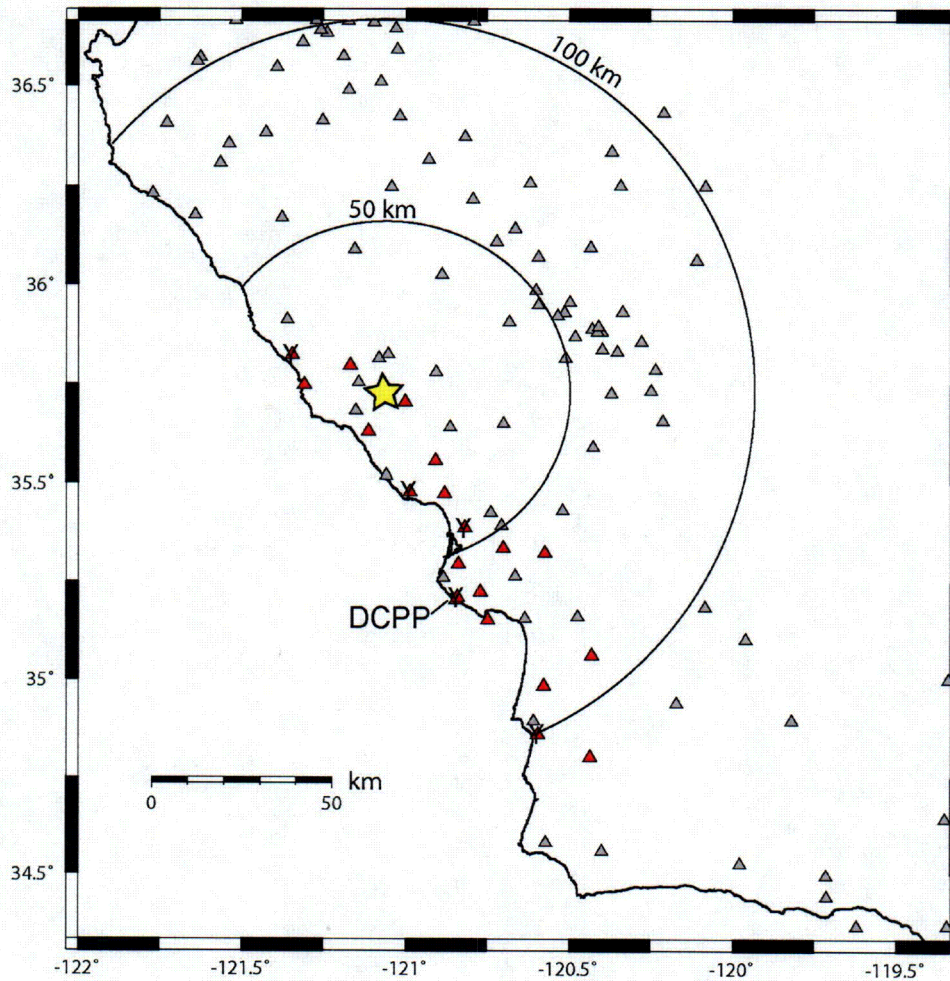


Figure 3-2. Map showing the seismographic station coverage in the region. Triangles are seismographic stations; gray are USGS stations, red are PG&E stations. The yellow star marks the location of the San Simeon earthquake. The 50- and 100-kilometer radii represent the approximate start and end of distance weighting used to locate the mainshock.

data from the five 3-component PG&E stations (generally for $M < 3$ earthquakes) adds valuable control for estimating hypocenter depth.

3.1 Data Processing

We have relocated the October 1987 through January 1997 seismicity data from McLaren and Savage (2001) discussed in our June report to the NRC (PG&E, 2004b), and have added data from February 1997 through September 2004. As described in our earlier report (PG&E, 2004b), we used a linearized version of the McLaren and Savage (2001) P-wave velocity model and Hypoinverse (Klein, 1989) to locate the earthquakes.

We merged the data from events recorded by both PG&E and USGS seismic networks to achieve optimum locations. Events recorded by only one of the networks are included in the catalog, although the majority of the events were recorded by both networks. All the PG&E arrival-time readings are hand picked; the USGS data include hand- and machine-picked readings. The updated earthquake catalog contains 5038 events: 2777 events before the San Simeon earthquake and 2261 events after, including the main shock.

Duration magnitudes (M_D) routinely were estimated for the events. Local (M_L) and moment (M_W) magnitudes from the USGS online catalog (USGS, 2004) are reported for events greater than magnitude 3 when available. The magnitude range of the pre-San Simeon earthquake data is 0.8 to 5.1; the post-San Simeon magnitude range is 2.0 to 6.5. The post-San Simeon cut-off at magnitude 2 was due to the difficulty of processing the more than 6000 smaller events.

A histogram showing the number of events per month from October 1987 to the 2003 San Simeon earthquake is shown on Figure 3-3a. We removed extraneous aftershocks using the Cluster2000 program by Reasenber (1985) to reduce their effect on the seismicity rate (for example, aftershocks from the 1991 M_L 5.1 Ragged Point earthquake). The largest number of events occurred in September 2003, 2 months before the main shock. The distribution of these events is shown in Figure 3-3b. The earthquakes are evenly scattered across the region and the largest events are in the magnitude 2 range. Most of the magnitude 2 events locate between the mapped traces of the Oceanic and Nacimiento fault zones, in the general region of the San Simeon earthquake aftershocks.

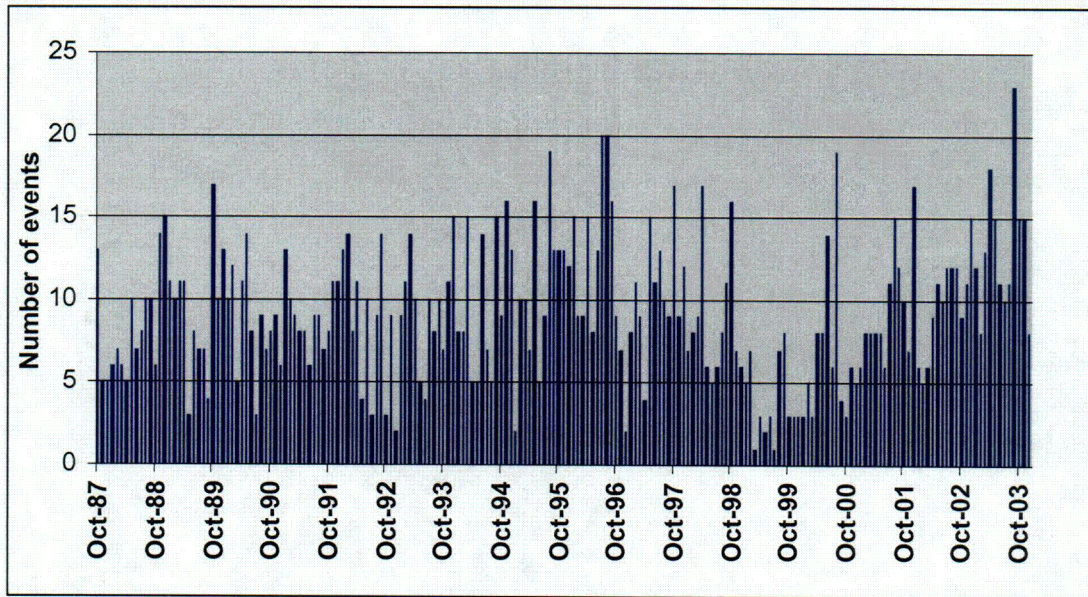
To obtain a final catalog of the most accurately located events, we applied location parameter filters to the data. Accurately located events were defined by horizontal errors of less than 2 kilometers and vertical errors of less than 5 kilometers. In addition, only events having a minimum of six P-wave readings were used, and only locations that converged to a solution (a statistically best solution was found) were included. The final catalog contains 4294 events: 2275 pre-San Simeon events and 2019 post-San Simeon events, including any aftershocks that survived the filters.

Focal mechanisms were estimated from the Hypoinverse output using FPFIT2 by Reasenber and Oppenheimer (1985). The mechanisms were compiled for events having misfit values less than 0.20, a station distribution ratio greater than 0.5, at least 20 P-wave first motions, and that converged. We also visually inspected the mechanisms and removed those having poor station distribution across the focal sphere. Multiple solutions generally were not included unless they were similar and a single representative solution could be chosen. The final dataset of focal mechanisms contains 373 mechanisms from events before the San Simeon earthquake and 808 from events after the earthquake, including the main shock.

3.2 Seismicity Patterns

Pre-San Simeon earthquakes in the region are shown in map view in Figure 3-4 (a). Diffuse activity is evident offshore west of the San Simeon fault zone, and along and to the east of the Hosgri fault zone, primarily within the San Luis/Pismo block, a main structural element in the

(a)



(b)

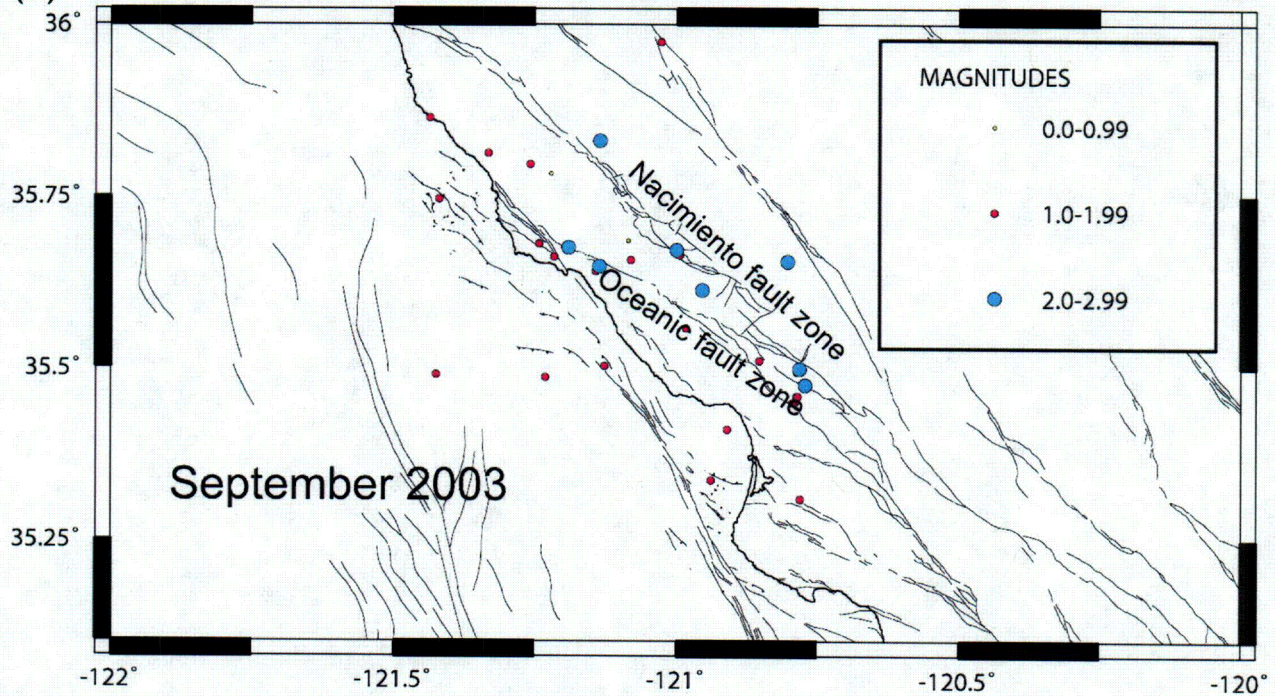


Figure 3-3. (a) Histogram of the integrated PG&E/USGS earthquake catalog for the period October 1987 to 22 December 2003 prior to the San Simeon earthquake. The data have been filtered to exclude extraneous aftershocks to reduce their effect on the seismicity rate. (b) Map shows the earthquakes that occurred in September 2003, the month having the most activity.

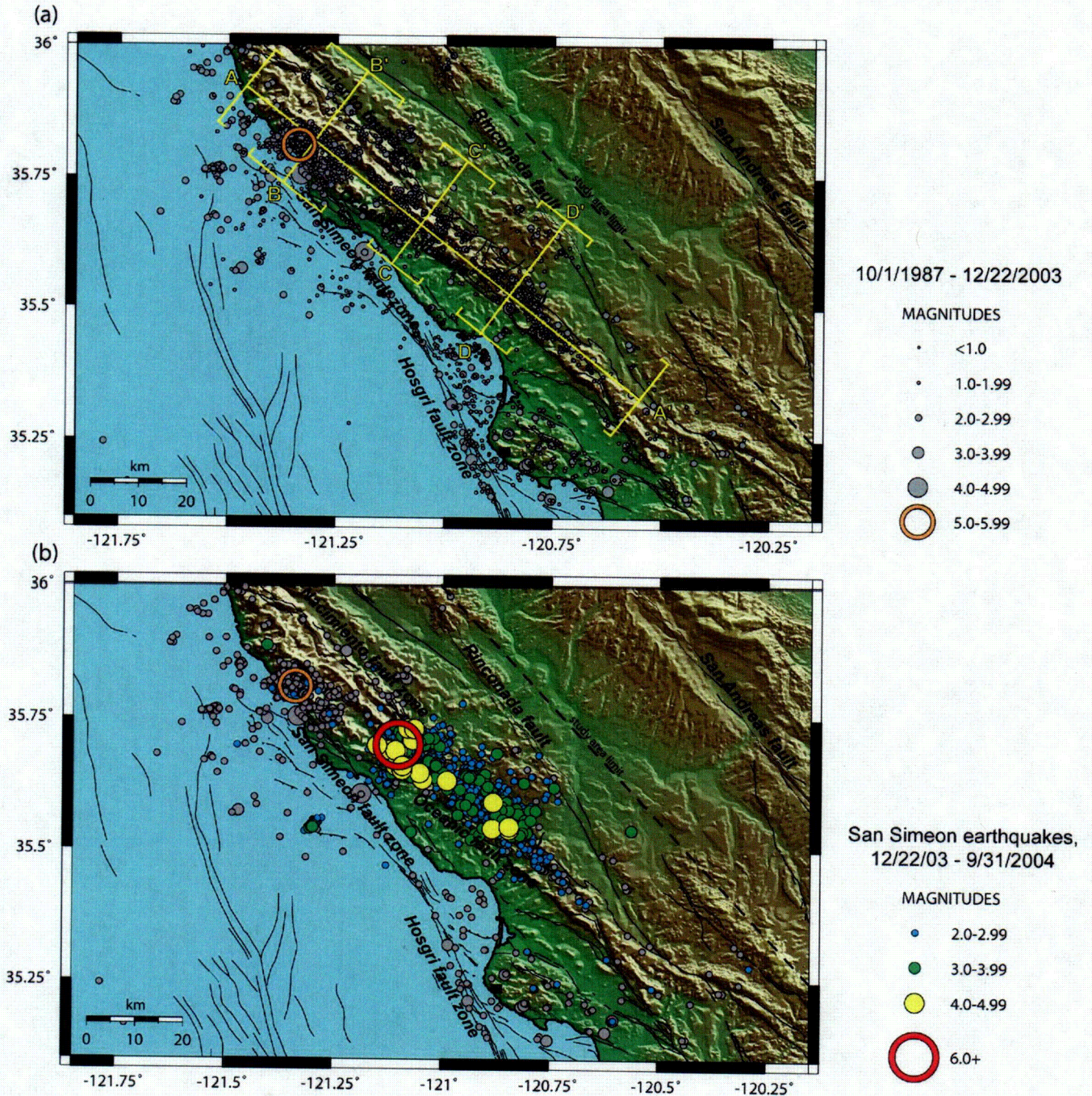


Figure 3-4. Maps showing Quaternary faults (Jennings, 1994) and regional seismicity of (a) the PG&E catalog data from October 1987 to 22 December 2003 before the San Simeon earthquake, including the M_L 5.1 Ragged Point earthquake of 17 September 1991 (orange circle), and (b) magnitude 2 and larger PG&E catalog data (gray circles), from 22 December 2003 after the San Simeon earthquake (red circle) to 30 September 2004. Aftershocks are colored according to magnitude. Regional seismicity cross section A-A' on map (a) is shown on Figure 3-5; cross sections B-B', C-C', and D-D' are shown on Figure 3-6.

Los Osos domain (Figure 2-3) (Lettis and others, 1994). Except for three small events, there is no seismicity evident west of this part of the Hosgri fault zone.

The highest concentration of activity in the region is along the northwest-trending Santa Lucia Range, between the San Simeon, Oceanic, and Nacimiento fault zones, where there are three spatial clusters. The largest cluster is near the location of the 1991 M_L 5.1 Ragged Point earthquake (orange circle). Figures 3-5 (a) and 3-6 show the clusters in cross section view. Cross section A-A' along the Santa Lucia Range shows seismicity deepening from less than 10 kilometers to the southeast to about 15 kilometers to the northwest, near the Ragged Point earthquake. Cross sections B-B' through D-D' across the Santa Lucia Range (Figure 3-6) generally show diffuse activity, except for the northeast-dipping aftershocks above the Ragged Point earthquake.

As shown in Figure 3-4 (b) the San Simeon earthquake and aftershock epicenters are nearly coincident with the middle and southeastern clusters. The main shock locates at the northwestern edge of the aftershock zone and the middle pre-San Simeon cluster. As can be seen on the regional cross section on Figure 3-5 (b), the fit of the two datasets is remarkably close, including the slightly shallower aftershock activity between the two clusters, between distance markers 50 and 60 kilometers.

As reported by PG&E (2004) an epicentral pattern of three main clusters formed nearly immediately after the San Simeon earthquake; two dense clusters northeast and south of the main shock, and one diffuse cluster to the southeast. As shown on Figure 3-7, the aftershocks through September 2004 continue this clustering. The southeast cluster ends abruptly at its southeastern end, along a northeast-southwest trend, particularly at the magnitude 3 level (Figure 3-7). Magnitude 2 aftershocks extend farther to the southeast (Figure 3-4 (b)).

On Figure 3-8, cross section E-E' is an along-strike view of the main shock and clusters and the space between the clusters. The space between the clusters near the main shock and the southeast cluster is a location of large coseismic slip modeled by Hardebeck and others (2004) and Ichinose and others (Appendix A). At distance marker 20 kilometers, the aftershock patterns and the Oceanic fault zone change strike. The large slip occurred near this change in strike.

Cross section F-F' on Figure 3-8 shows the main shock occurred at the base of a diffuse northeast-dipping aftershock pattern, near the intersection with a southwest-dipping aftershock pattern northeast of the main shock. We interpret the southwest-dipping aftershock pattern to reflect minor slip on a back thrust fault. Cross section G-G' at the northwestern end of the southeast cluster shows diffuse activity and possibly vertical faulting in the zone between distance markers at 10 and 15 kilometers. Activity is also diffuse on cross section H-H', with concentrations of activity near distance markers 10 and about 12 kilometers, between 5 and 10 kilometers depth. Cross section I-I' shows concentrated aftershock activity between about 7 and 10 kilometers depth, and a possible vertical alignment of magnitude 3 aftershocks between distance markers 5 and 10 kilometers.

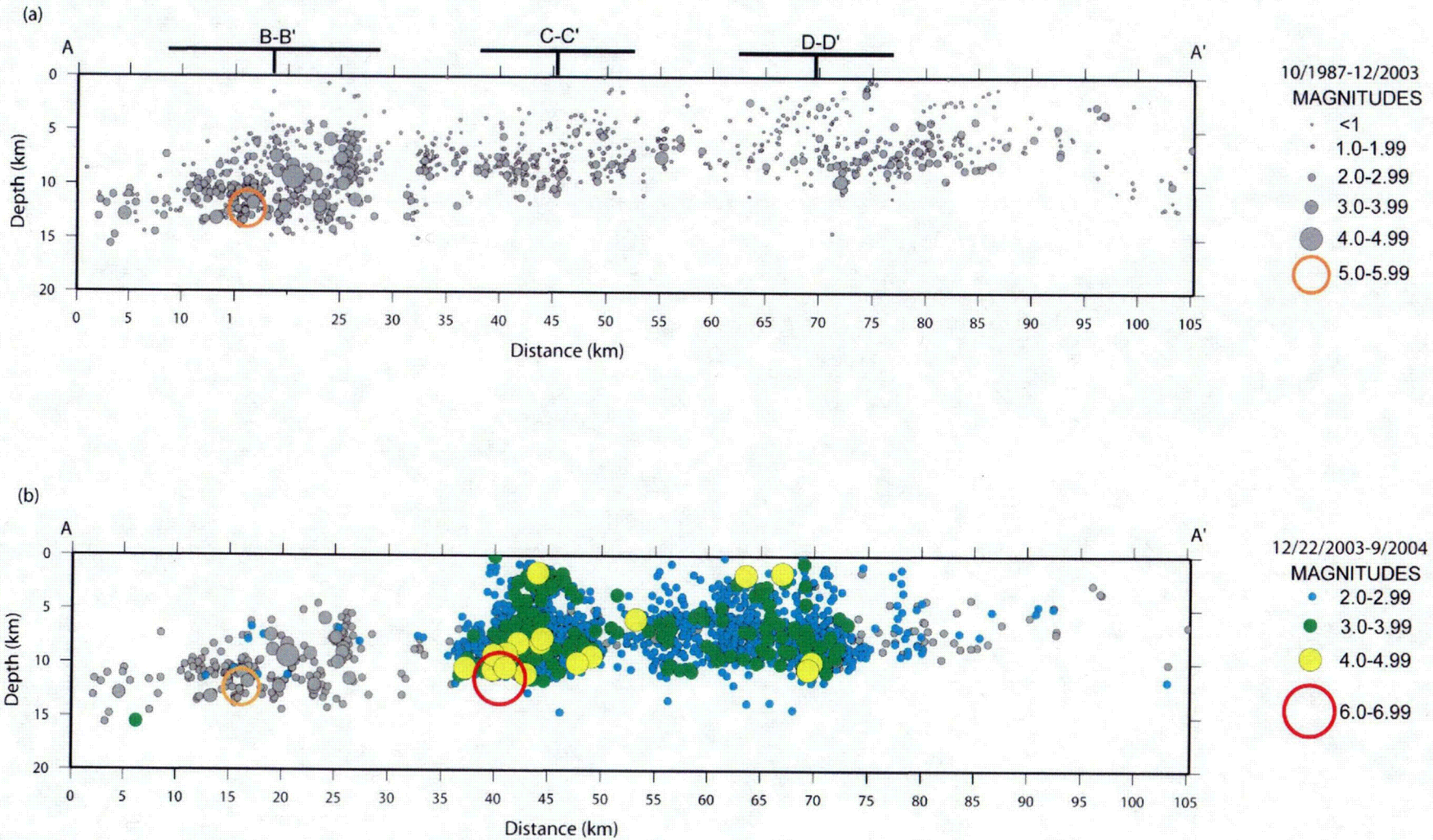


Figure 3-5. Two projections of cross section A-A' shown on Figure 3-4 (a): (a) earthquakes mapped on Figure 3-4 (a). Orange circle is the ML 5.1 Ragged Point earthquake of 17 September 1991. (b) $M \geq 2$ pre- and post-San Simeon earthquakes mapped on Figure 3-4 (b). Red circle is the 2003 San Simeon earthquake.

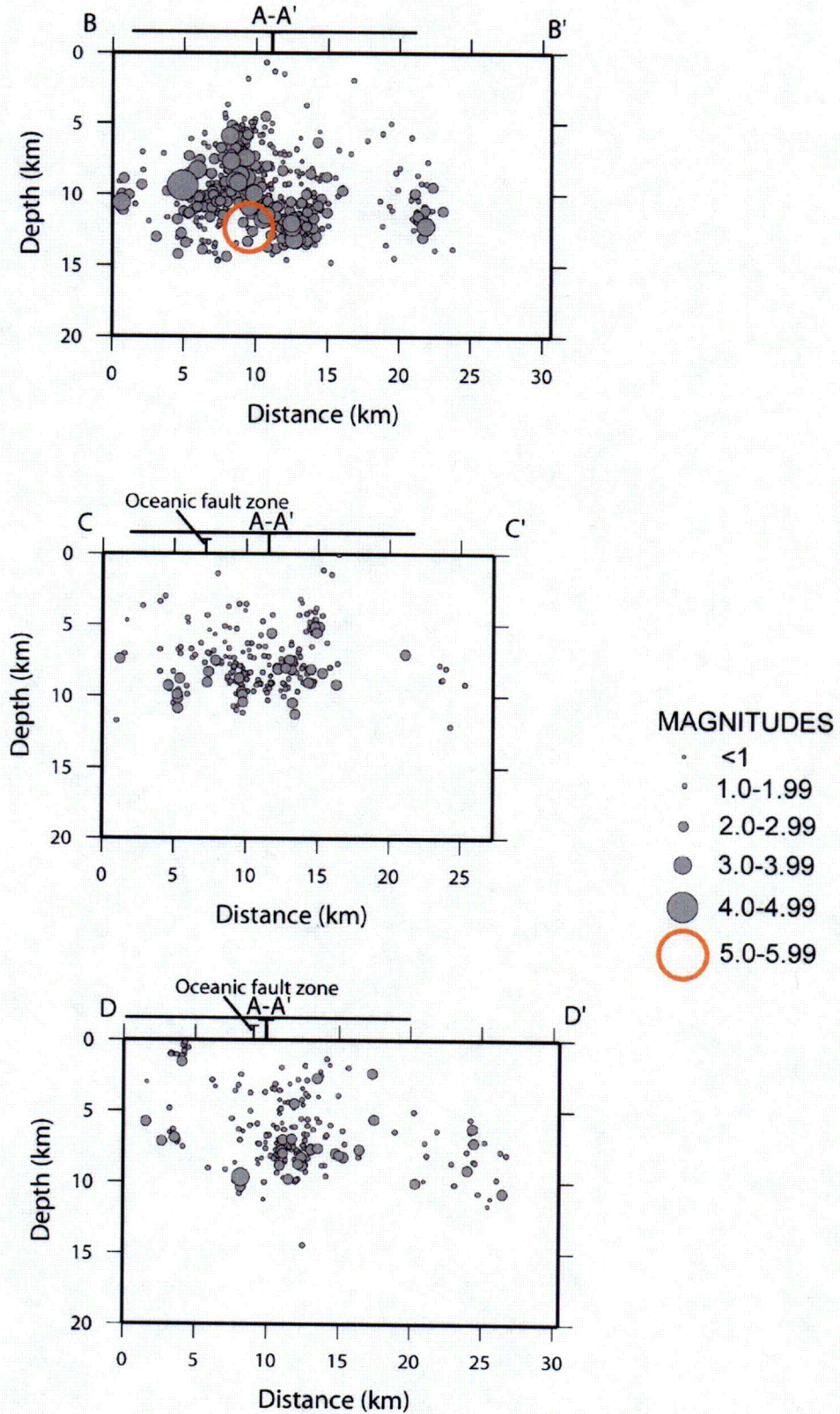


Figure 3-6. Regional seismicity cross sections B-B', C-C', and D-D'. The locations of the cross sections are shown on Figure 3-4 (a).

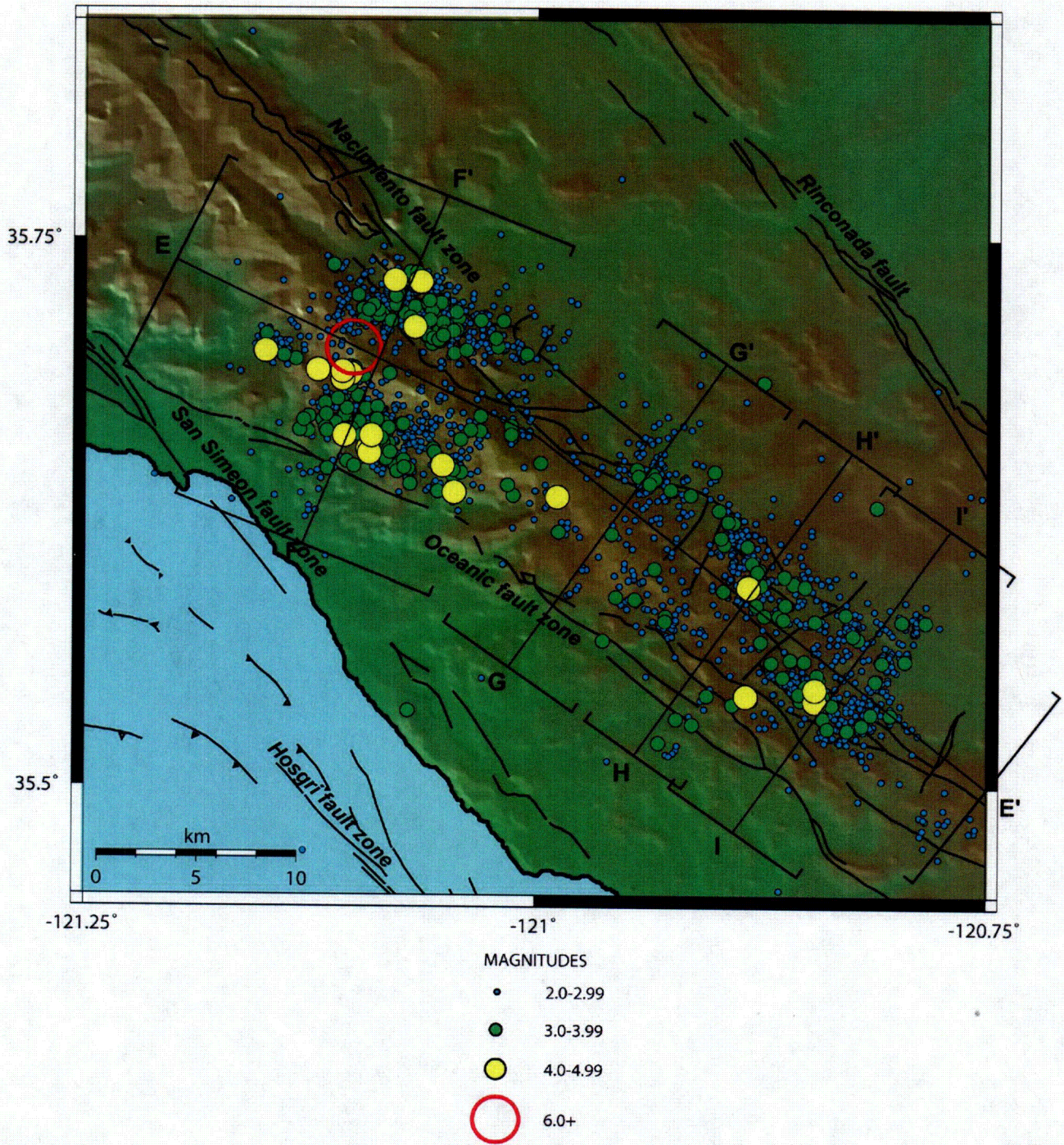


Figure 3-7. Map showing Quaternary faults (Jennings, 1994) and the San Simeon main shock and $M \geq 2$ aftershocks recorded through 30 September 2004. Cross sections E-E' through I-I' are shown on Figure 3-8.

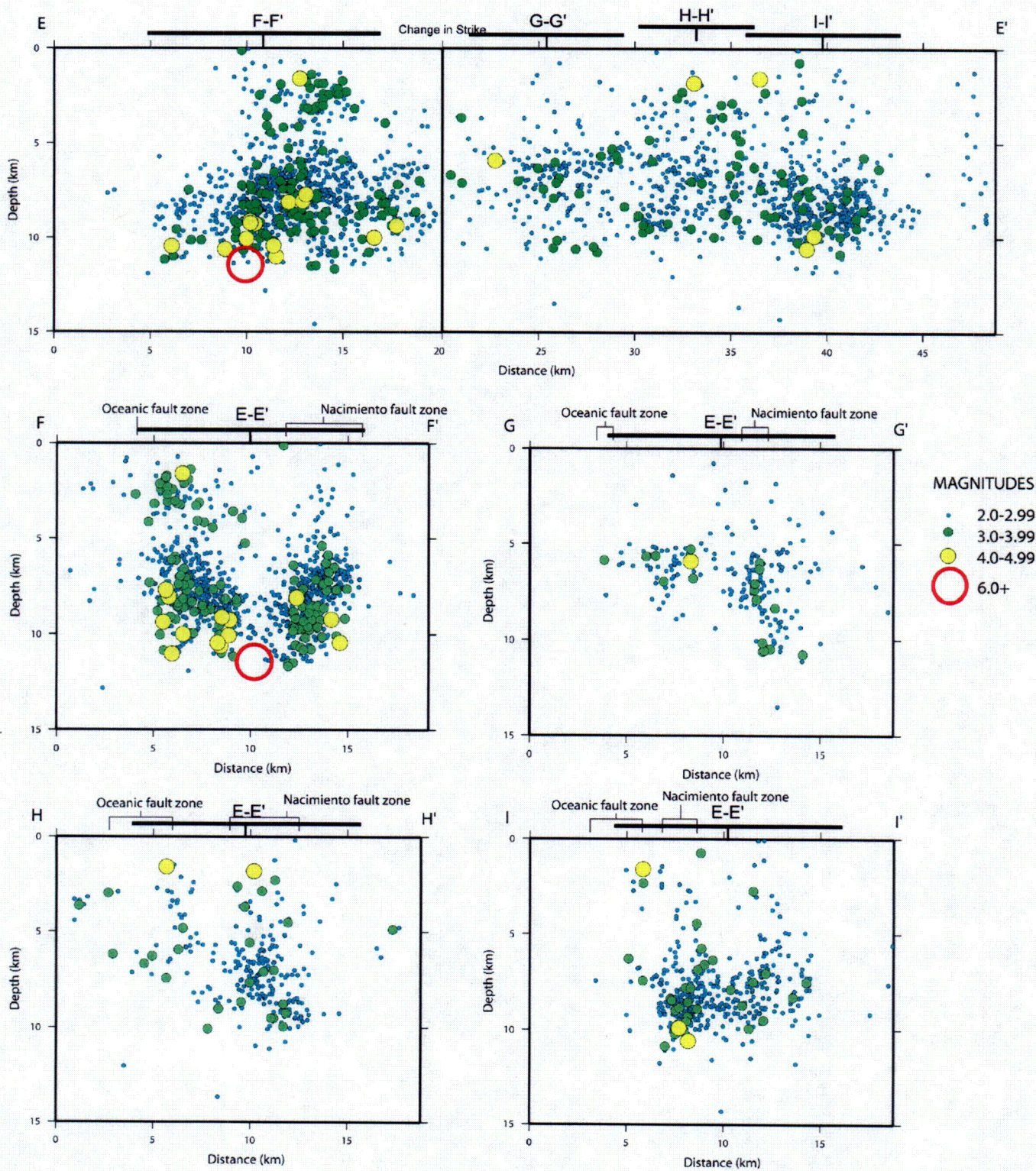


Figure 3-8. Seismicity cross sections E-E' through I-I'. The locations of the cross sections are shown on Figure 3-7.

3.3 Focal Mechanism Patterns

Regional, pre-San Simeon focal mechanisms show predominantly reverse and reverse-oblique motion along the Santa Lucia Range north of San Simeon and within the San Luis/Pismo block (Figure 3-9). Events in Estero Bay and along the Hosgri fault zone are predominantly strike slip. This is consistent with McLaren and Savage (2001).

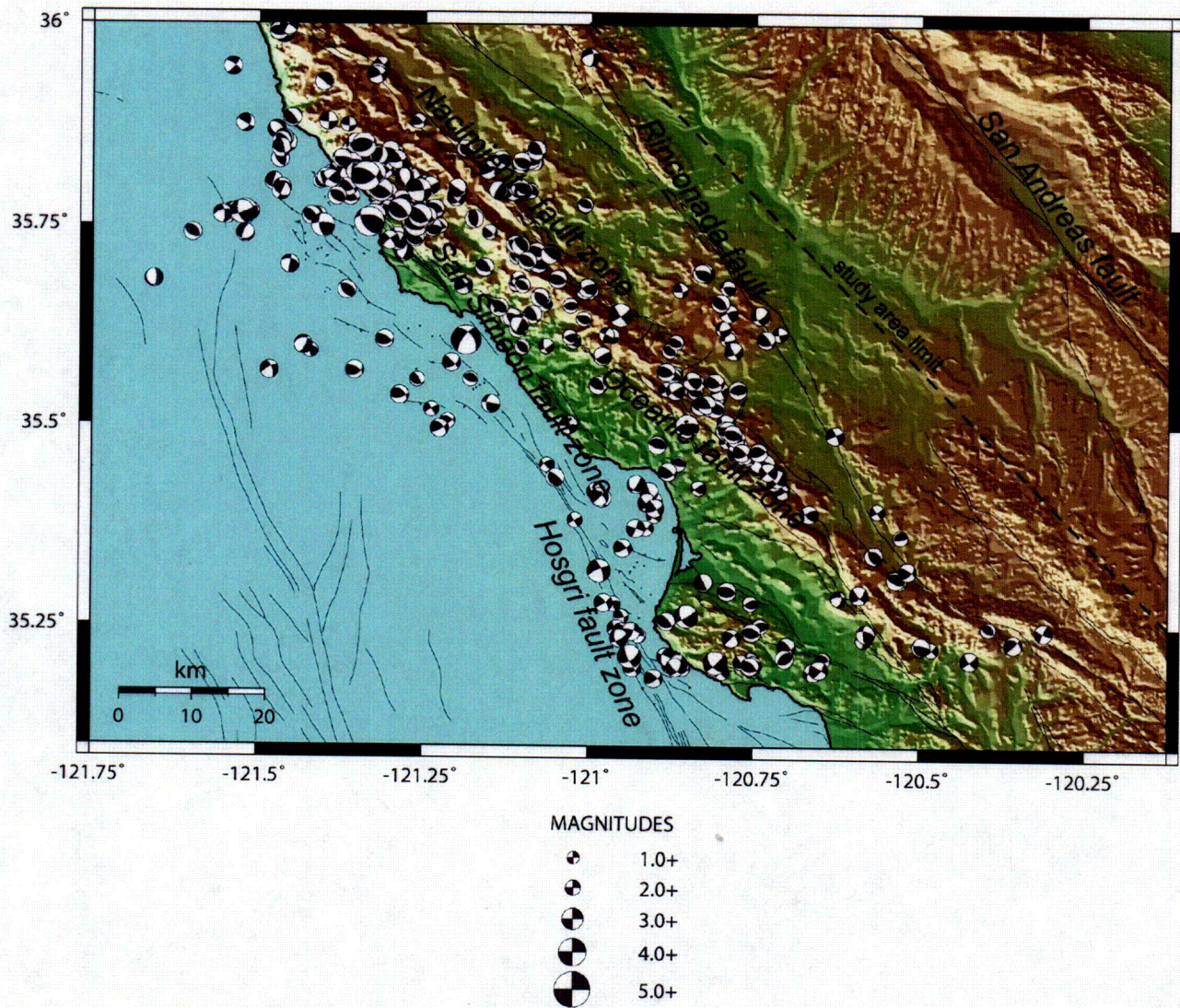


Figure 3-9. Map showing lower-hemisphere P-wave first-motion focal mechanisms of regional seismicity for the period October 1987 to 22 December 2003.

San Simeon aftershock focal mechanisms (Figure 3-10) also show generally reverse motion along the Santa Lucia Range. Mechanisms of the events in the two clusters near the main shock are predominantly reverse along northwest-trending fault planes, similar to the mechanism of the main shock. Mechanisms in the southeast cluster have considerably more variation of fault motion and fault strike. Near the locations of cross sections G-G', H-H' and the northeastern half

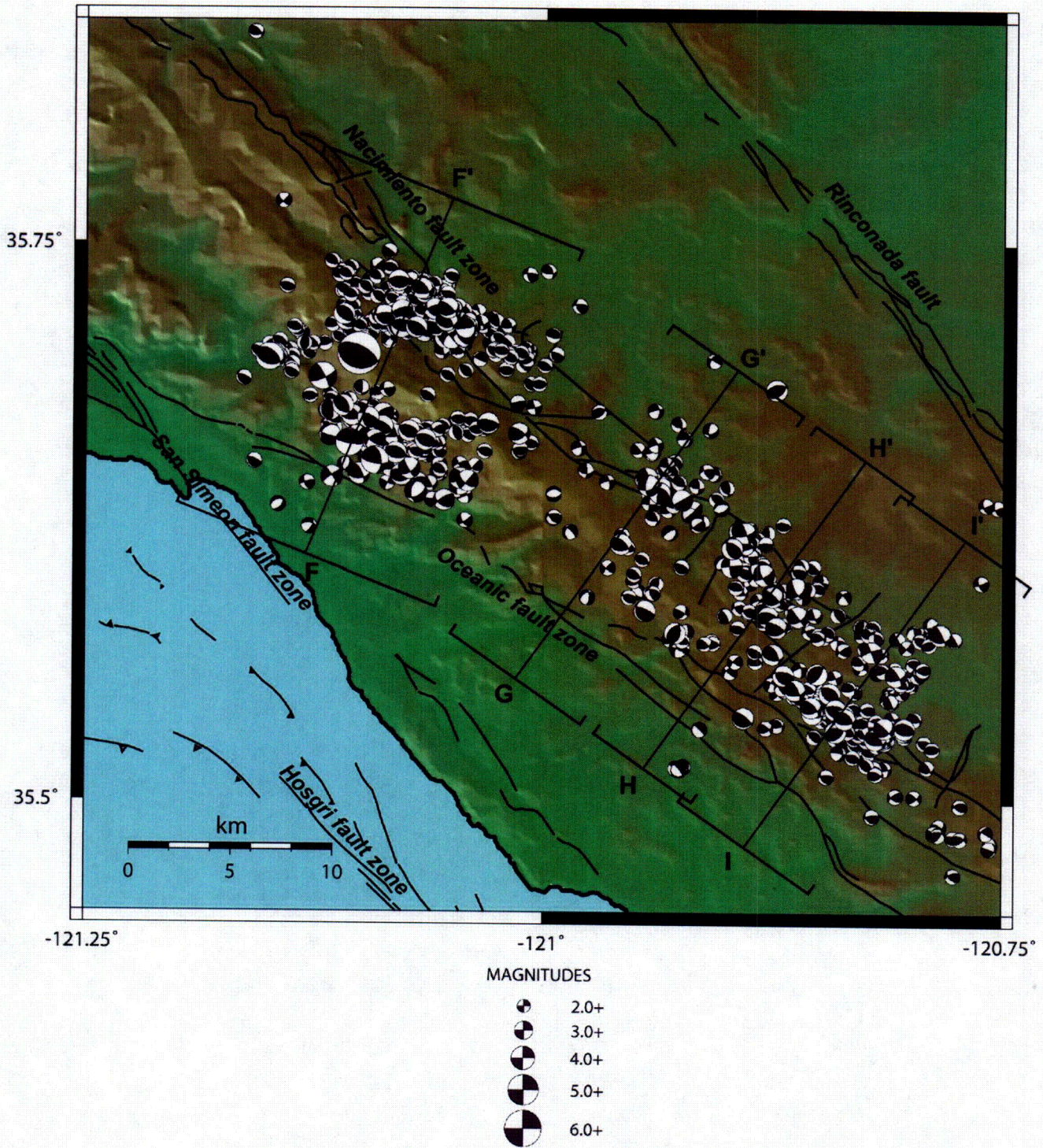


Figure 3-10. Map showing lower-hemisphere P-wave first-motion focal mechanisms of the San Simeon earthquake and aftershocks. Cross sections F-F' through I-I' are shown on Figure 3-11.

of I-I', focal mechanisms are reverse, reverse-oblique and normal. Mechanisms near the southwestern half of I-I' are part of a dense northwest-trending cluster that has predominantly reverse motion.

Figure 3-11 shows the focal mechanisms in cross section. Mechanisms projected onto cross section F-F' show the main shock and most of the aftershocks have dip-slip motion, particularly the events deeper than 5 kilometers. Several of the shallower events to the southeast have vertical motion oblique to the cross section. A variety of fault motions is seen in cross sections G-G' and H-H'. The dense cluster in cross section I-I' between distance markers 5 and 10 kilometers is similar to those in cross section F-F'.

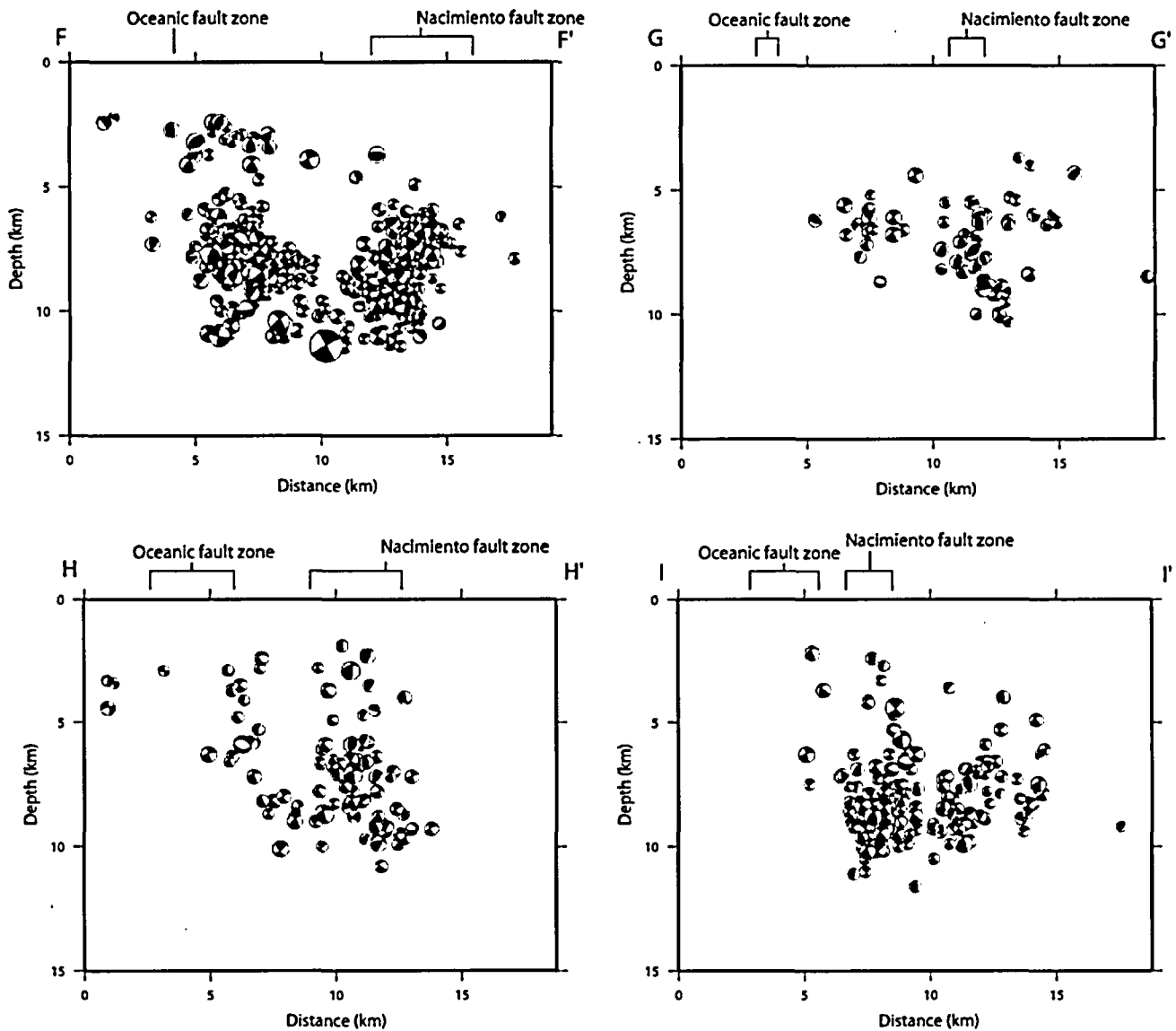


Figure 3-11. Cross sections F-F' through I-I' showing projected focal mechanisms of the San Simeon earthquake and aftershocks. The locations of the cross sections are shown on Figure 3-10.

3.4 Depth of San Simeon Earthquake

Accurate earthquake locations, which include the hypocentral depth, are important when studying the seismicity of an area because they provide valuable information for interpreting the seismotectonic environment. There are two primary methods for estimating earthquake hypocenters; one estimates an absolute location, the other a relative location. An absolute location commonly is estimated by inverting P- and S-wave arrival-time data from local stations for each earthquake using one of three types of velocity models: one-dimensional flat layer, one-dimensional linear gradient, or three-dimensional flat layer using earthquake location models such as Hypoinverse (Klein, 1989). Another absolute method is to invert waveform data from regional and teleseismic data. Relative depths can be estimated using the master event technique or a new method called double-difference (Waldhauser, 2001). The double-difference method uses an iterative linearized inversion of differences between same-phase travel-time residuals for multiple events (Michelini and Lomax, 2004).

The use of different methods by various investigators has resulted in different depth estimates, ranging from about 7 kilometers to 12 kilometers, for the San Simeon main shock. Hardebeck and others (2004) estimated a relative depth of 7.1 kilometers using the double-difference method; McLaren and Stanton (2004) calculated an absolute depth of 11.3 kilometers using Hypoinverse (Klein, 1989), and Hauksson and others (2004) estimated an absolute depth of 9.6 ± 1.0 kilometers using a three-dimensional velocity model. Ichinose and others (Appendix A) independently obtained a depth of 12 ± 2 kilometers using teleseismic data. The depth used can have an effect on the seismotectonic interpretations relating to the San Simeon earthquake (for example, the Hardebeck depth of 7.1 kilometers was used as their starting depth for subsequent slip modeling).

The different hypocentral depth estimates obtained by these investigators reflects not only the different methods employed, but also the different earthquake data sets used in the models. We believe there is a significant difference between the data used by the USGS (Hardebeck and others, 2004) and the data used by PG&E (McLaren and Stanton, 2004). The USGS uses only USGS data, includes no local S-wave readings, and machine-picks many of the P-wave arrival-times. The PG&E data incorporate both USGS and PG&E hand-picked arrival-time data and on-scale S-wave readings from the five 3-component stations when available, which is usually for aftershocks of magnitude 3 or greater. Because the PG&E data are more robust, we ran the double-difference program to compare our relative depth estimate with Hardebeck and others (2004). We also asked Dr. Hardebeck to run the PG&E data in the double-difference program using her independent solution parameters. The results of our double-difference analysis were then compared with our absolute depth estimate of the San Simeon earthquake and magnitude 2 and greater aftershocks using Hypoinverse. We also compared these results with the independent absolute depth estimate by Ichinose and others (Appendix A) using teleseism and regional waveforms and GPS data.

3.4.1 Double-Difference Method

For our double-difference run, we used the final catalog of post-San Simeon aftershock dataset of 2019 events that extends through September 2004 and includes $M \geq 2$ events. We did not include pre-San Simeon data. Only P- and S-wave arrivals from events that converge to a solution were used in the inversion. We used the five-layer one-dimensional velocity model of McLaren and Savage (2001). The San Simeon aftershock zone was inverted to a single cluster with a maximum separation of 10 kilometers between linked pairs of hypocenters. At least eight paired observations were required for an event to be linked. Using 15 iterations and damping values proceeding from 160 to 120, condition numbers between 40 and 80 were obtained (as suggested by the documentation as indicative of a “good” solution). The cluster was relocated within the error range of the initial cluster location.

Dr. Hardebeck (2004a) also ran double-difference using our data set and independently chosen parameters, and produced virtually identical results for the main shock (10.3 kilometers depth vs our 10.2 kilometers). Our inversion parameters differed only slightly in that she used slightly higher damping, a few less iterations, and a tighter separation cutoff in the final iterations (4 kilometers vs our 20 kilometers). Because the events are densely packed and strongly linked, lowering the distance cutoff to 4 kilometers for the last set of iterations results in a negligible difference in linking.

Features generally observable in the catalog were sharpened in map and cross section views after applying double-difference. In map view, (Figure 3-12) the features that are most sharpened are the two clusters near the main shock and the distinct northwest-trending cluster near the southwestern end of the southeast cluster. The cluster northeast of the main shock is resolved into three possible subparallel west-trending patterns.

Cross section E-E' along strike (Figure 3-13) shows concentrated activity updip and southeast of the main shock, between distance markers 10 and 15 kilometers. The northwest-trending concentration of events seen in map view near the location of cross section I-I' concentrate near the base of the aftershock zone at about 9 kilometers depth. A diffuse horizontal linear feature at about 4 kilometers depth appears to be enhanced. This horizontal feature may be an artifact of the velocity model (the shallowest layer is at 4-kilometers depth). Further sensitivity testing that arbitrarily increased the layers from 5 to 12 had the effect of smoothing out this horizontal feature. It is interesting that a similar layer can be seen on Figure 3b of Hauksson and others (2004). In their study, they used USGS catalog data located initially with their three-dimensional model and then double-difference. Michelini and Lomax's (2004) study using synthetic data and double-difference demonstrated that using a relative location technique such as double-difference and an erroneous velocity model could lead to an incorrect alignment of events (streaks). Presumably, Hauksson's initial locations were robust, so it is not clear if this feature is real or a velocity artifact.

Aftershocks projected onto cross section F-F' (Figure 3-14) near the main shock show diffuse activity along northeast- and southwest-dipping clusters that appear to reflect fault planes. Cross section G-G' (Figure 3-14), near the northeastern end of the southeast cluster, shows a cluster

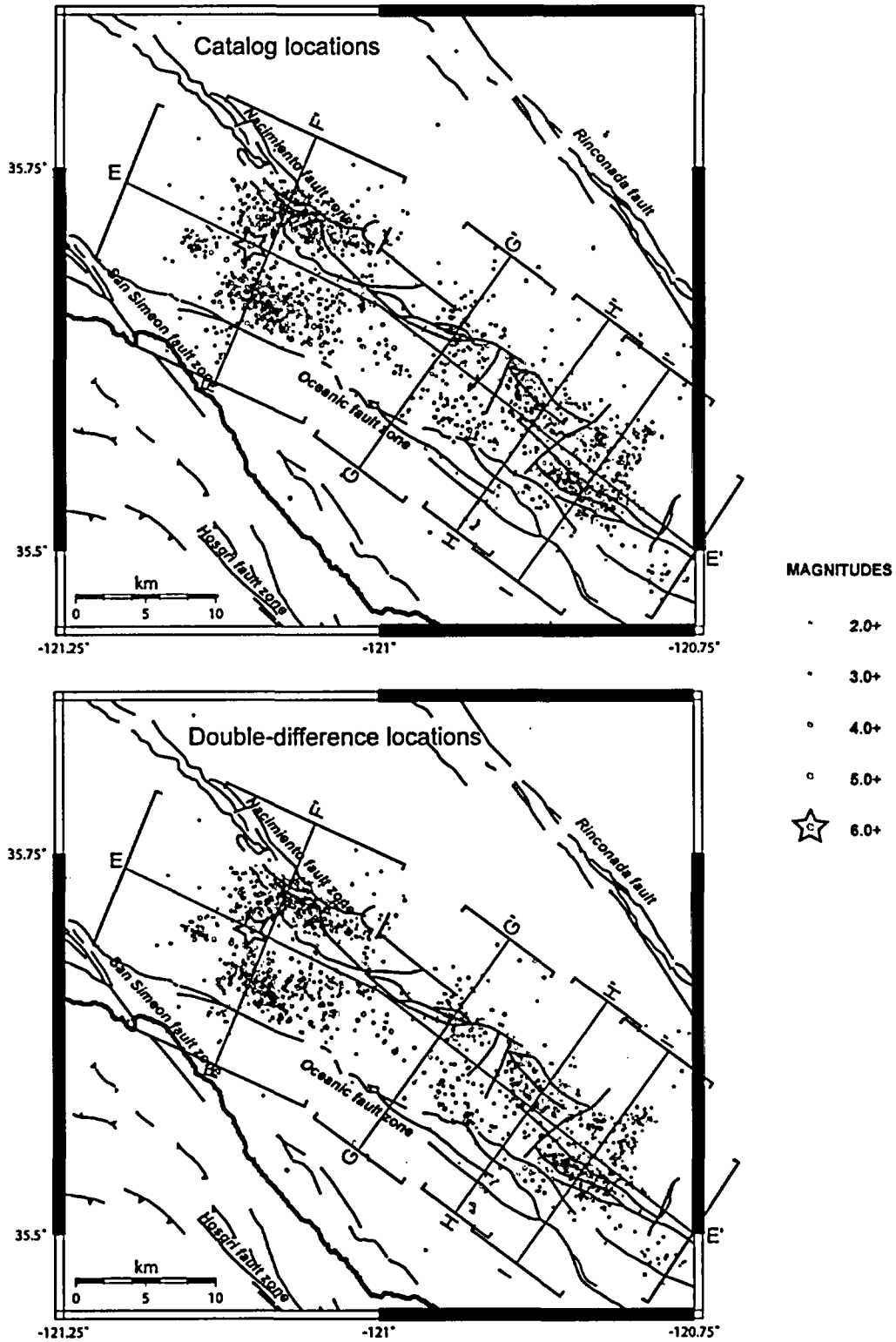


Figure 3-12. Maps of the San Simeon earthquake (star) and aftershocks showing (top) the locations from the PG&E catalog and (bottom) the corresponding double-difference (Waldheiser, 2001) locations. Cross section E-E' is shown on Figure 3-13, F-F' and G-G' on Figure 3-14, and H-H' and I-I' on Figure 3-15.

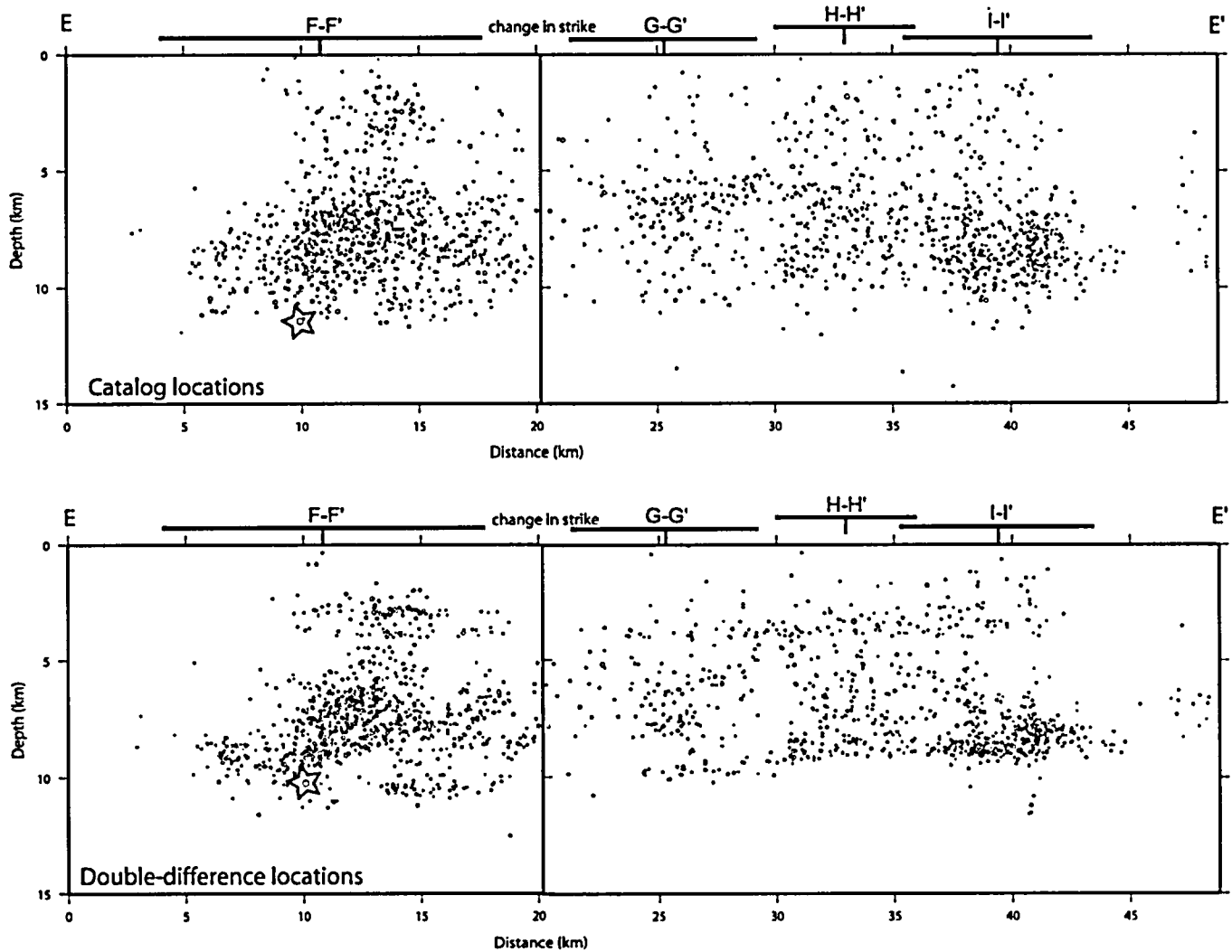


Figure 3-13. Seismicity cross section E-E' showing (top) PG&E catalog locations and (bottom) the corresponding double-difference locations. The location of the cross section is shown on Figure 3-12.

that possibly reflects a southwest-dipping fault plane in the double-difference view. Cross section H-H' (Figure 3-15) shows possible complex fault interaction, as seen in the abrupt change from vertical to low-angle, northeast-dipping seismicity patterns between distance markers 10 and about 13 kilometers. Cross section I-I' on Figure 3-13 shows a possible low-angle southwest-dipping pattern between about 7 and 9 kilometers depth, between distance markers 7 to 15 kilometers, including a concentration of activity at about 8 kilometers depth. Hauksson and others (2004, Figure 3c) show this same cross section, but with more smaller events from the USGS catalog. Their data show a much steeper southwest dip.

The double-difference method appears to be effective in improving the resolution of the seismicity patterns of our San Simeon aftershock data ($M \geq 2$). However, depths estimated using the double-difference method are relative locations and may be biased by a poorly constrained

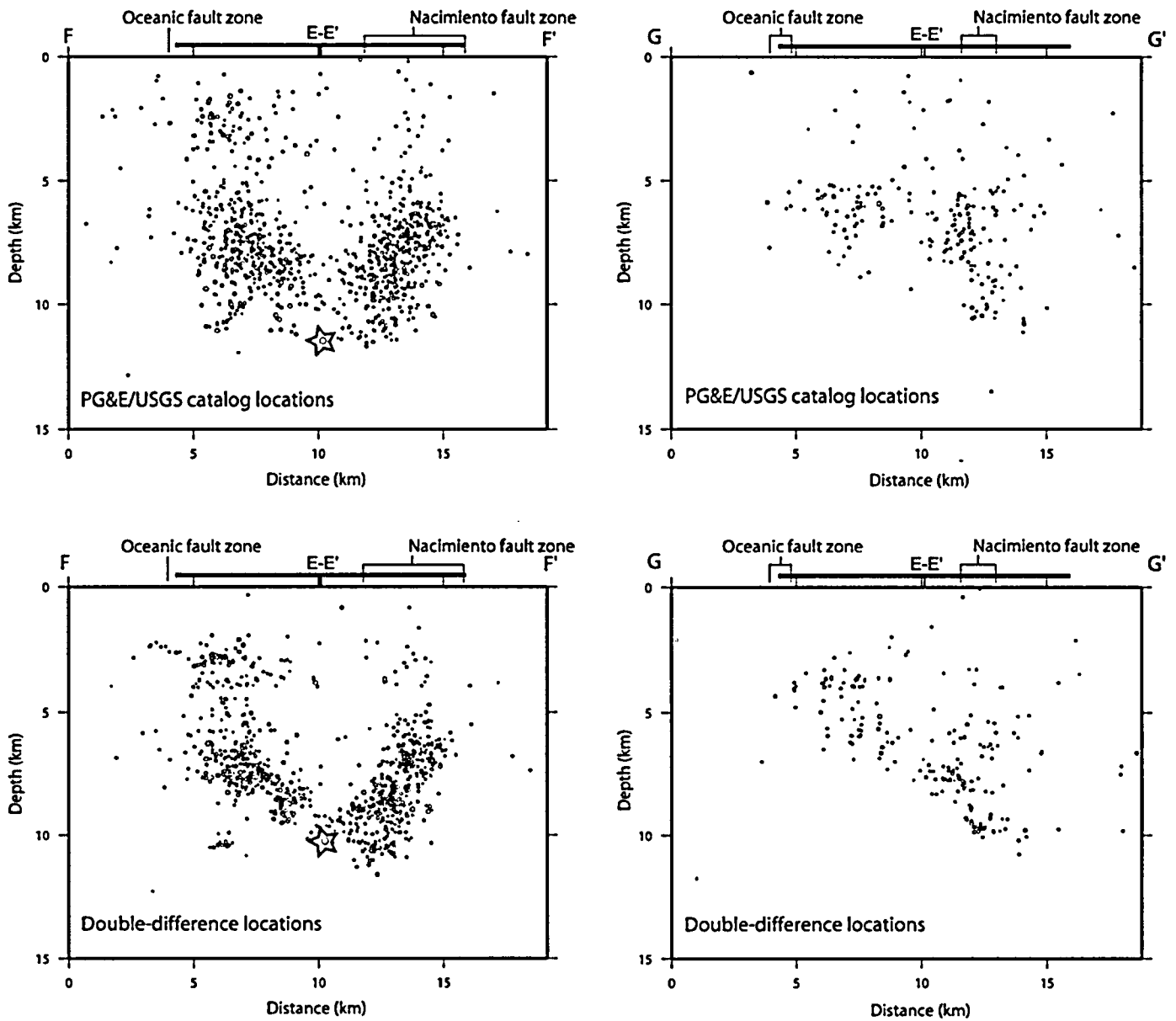


Figure 3-14. Seismicity cross sections F-F' and G-G' showing (top) PG&E catalog locations and (bottom) the corresponding double-difference locations. The locations of the cross sections are shown on Figure 3-12.

one-dimensional flat layer velocity model and a sensitivity to the linking parameters, such as the maximum number of links per event (Hardebeck, 2004b). Dr. Hardebeck agrees that our double-difference locations, including the mainshock depth, are probably better than those derived by Hardebeck and others (2004) due to the inclusion of the PG&E data (more close-in stations better constrain the depths) (Hardebeck, 2004b). We believe there is no significant difference between our absolute depth of 11.3 kilometers and the double-difference relative depth of 10.2 kilometers.

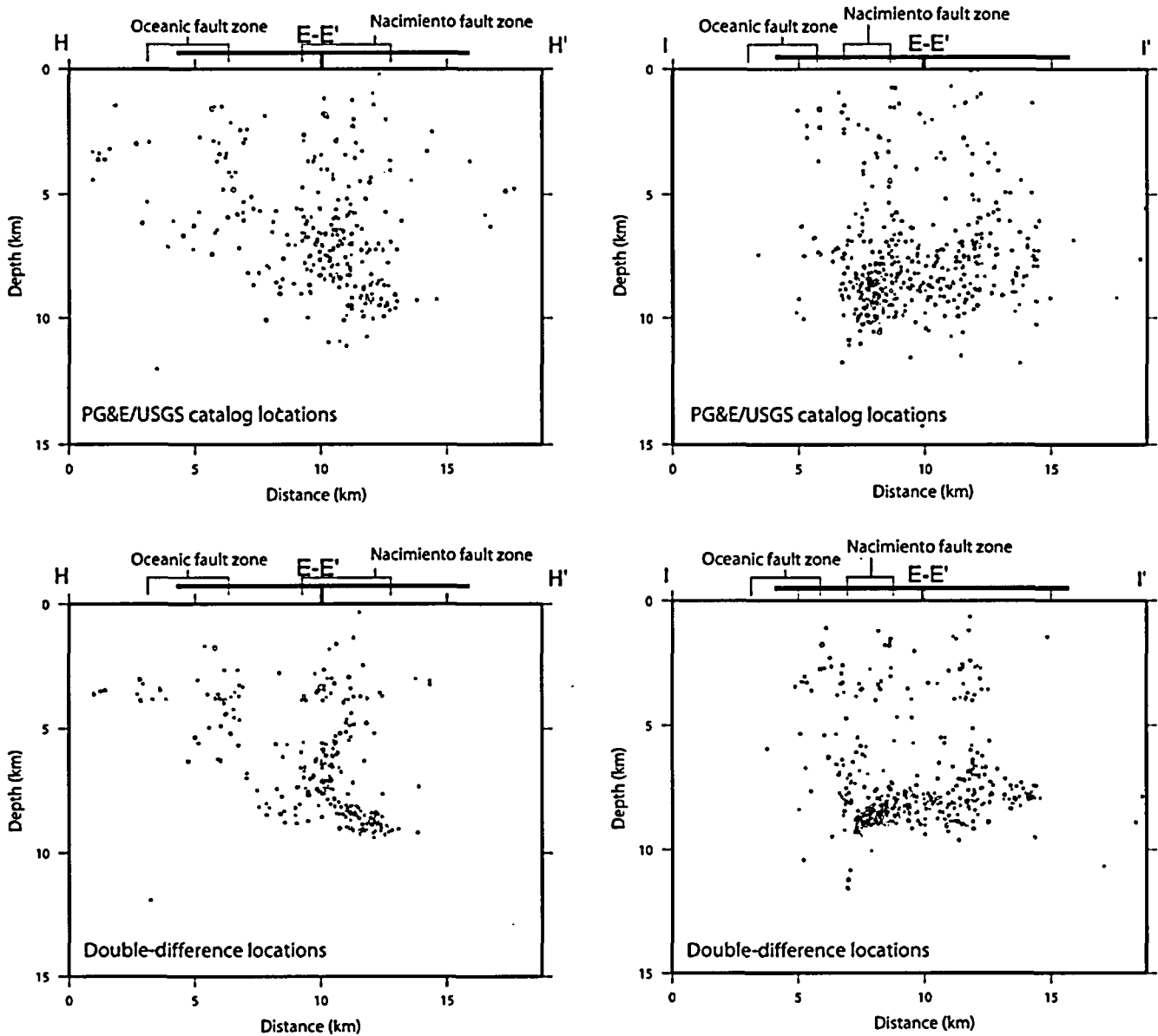


Figure 3-15. Seismicity cross sections H-H' and I-I' showing (top) PG&E catalog locations and (bottom) the corresponding double-difference locations. The locations of the cross sections are shown on Figure 3-12.

3.4.2 Independent Analysis of the Main Shock Depth and Rupture Model

Drs. Gene Ichinose, Paul Somerville, and Robert Graves (URS Corp) were asked by PG&E to independently analyze the source depth and rupture process of the San Simeon earthquake. Their study, included as Appendix A, used strong motion data, regional and global teleseismic waveforms, and geodetic data.

The primary purpose of their report was to develop a rupture model of the San Simeon earthquake and assess rupture directivity effects on the earthquake ground motions. A key source parameter, one of the first parameters derived, was the centroid depth of the main shock (initial subevent) of 12 ± 2 kilometers, estimated from teleseismic body waves and surface waves. This depth compares favorably with our 11.3 kilometers depth estimated using P-wave arrival times from local short-period seismic stations.

Strong directivity effects were seen in the teleseismic P-waves, manifested by systematic azimuthal variation in the separation in time of two main shock subevents that are prominent in the waveforms. The Cambria strong-motion recording also indicates there were two major releases of seismic energy visible in the acceleration, velocity, and displacement records. The first subevent was located near the hypocenter at 12 kilometers depth, the second occurred about 15 kilometers to the southeast at an azimuth of 110 degrees at 10 kilometers depth, 3.2 seconds after the initiation of rupture. The moment release of the second event was about 50 percent larger than the first event. The main shock first and second subevents have seismic moments of 1.61 and 2.42×10^{25} respectively.

The focal mechanism of the first subevent has a strike of 298 degrees, northeast dip of 57 degrees, and rake of 79 degrees. These parameters are very similar to ours, which show a strike of 297 degrees, dip of 61 degrees, and rake of 96 degrees, and similar to the strike of the northern segment the Oceanic fault zone. The second subevent focal mechanism has a more northerly strike and more shallowly northeast-dipping fault plane, 320 degrees strike, 47 degrees dip, and 108 degrees rake. The strike is consistent with the change in strike of the central segment of the Oceanic fault zone.

Teleseismic recordings were used to develop a representation of the source process in the form of two point sources. Regional body wave and surface waveforms from the larger aftershocks recorded at six broadband stations were used to derive regional one-dimensional seismic velocity models. These velocity models were then used in the inversion of the source rupture process of the main shock. The finite fault rupture geometry was developed using a two-fault model based on the lines of evidence that (1) the multiple-point source model derived from teleseismic data indicates the presence of two subevents having different strike angles, (2) there is a change in the strike of the aftershock zone, and (3) there is a change in the strike of the mapped surface faults in this region.

Rupture of the first subevent was mostly downdip of the hypocenter in the depth range of 12 to 15 kilometers. Rupture of the second fault segment was largest on an asperity located about 15 kilometers east-southeast of the hypocenter, at a depth of about 10 kilometers. The second fault segment had more uniform slip than the first. This is consistent with conclusions by Hardebeck and others (2004).

The rupture model has a rupture velocity of 3.5 kilometers/second, roughly equal to the shear-wave velocity of the crust. This is physically plausible for along-strike rupture propagation of dip-slip faulting. The high rupture velocity contributed to relatively strong rupture directivity effects.

4.0 DISCUSSION

4.1 Relation of the 2003 San Simeon Earthquake and Aftershock Activity to the Oceanic Fault Zone and Other Structures in the Santa Lucia Range

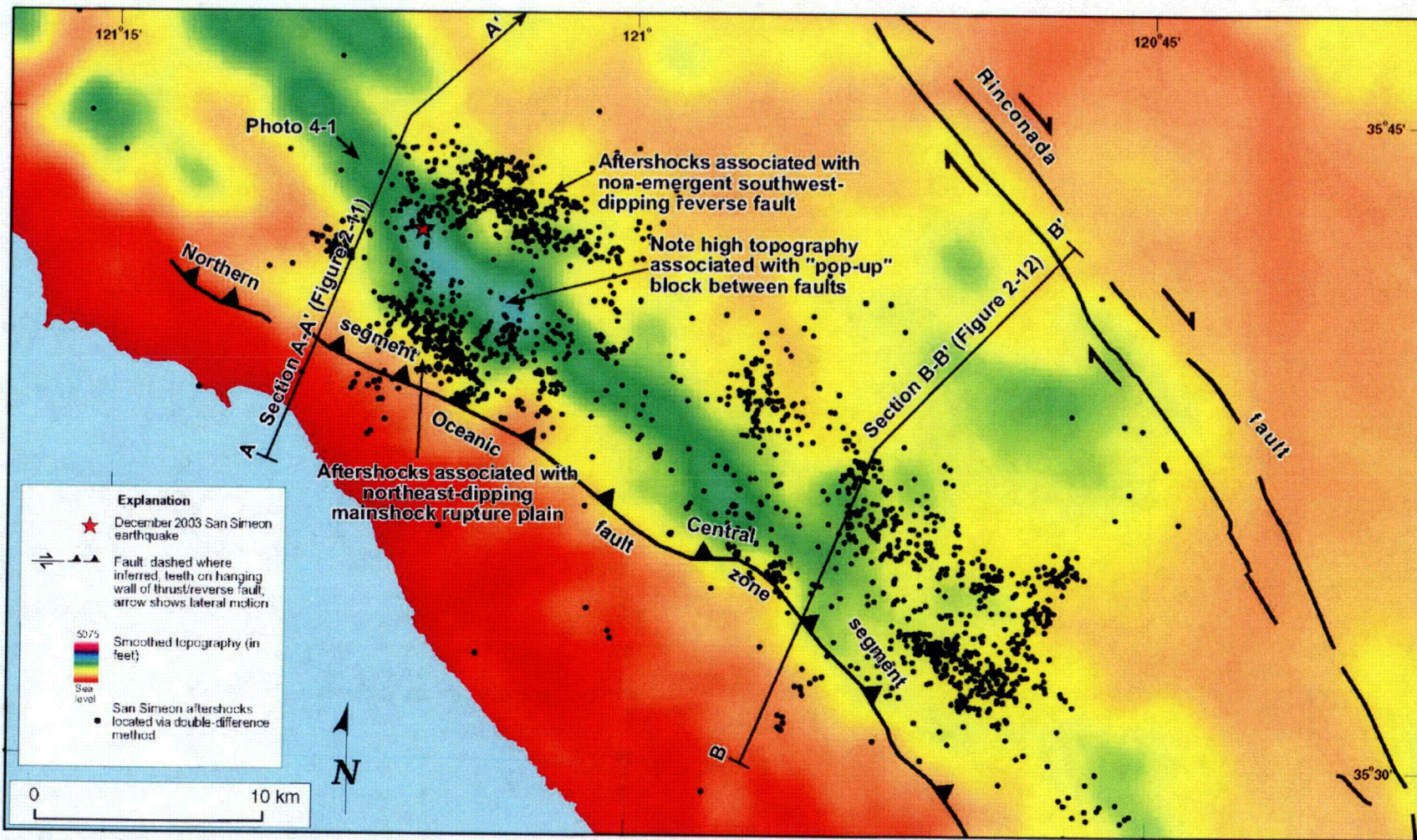
Analyses of the focal mechanism for the main event and the distribution of aftershocks indicate the 2003 San Simeon earthquake occurred on a northeast-dipping reverse fault that generally projects updip toward the northern segment of the Oceanic fault zone (Figure 2-11). The rupture propagated southward into the area of the central segment (Section 3.4.2). Detailed three-dimensional analysis of the aftershocks using visualization software confirms that the strike of the seismogenic fault rotates clockwise from north to south, similar to the change in strike of the Hall trace of the Oceanic fault zone at the surface and to the change in trend of the range front of the Santa Lucia Range. Ichinose and others (Appendix A) observed a similar change in fault strike in their finite rupture model of the San Simeon earthquake. Surface rupture was not observed on the Hall trace following the earthquake, and the geometry of the seismogenic fault (or faults) differs from that of the Hall trace, suggesting the relationship between the two is complex.

4.1.1 Northern Segment of the Oceanic Fault Zone

The main December 2003 event occurred at a depth of 11.3 kilometers, at the base of a V-shaped aftershock pattern (Figure 2-11). Three-dimensional visualization of the aftershocks reveals that the V-shaped pattern is created by two distinct, oppositely dipping reverse faults. The main shock occurred on the northeast-dipping fault, which strikes about N70°W, dips about 55°NE, and generally projects updip toward the western Santa Lucia Range front. The antithetic fault strikes about N86°W and dips about 70°SW. These reverse faults bound a northwest-trending ridge of the Santa Lucia Range that is associated with the northern segment of the Oceanic fault zone, and which stands distinctly higher than adjoining parts of the range (Figure 4-1). We interpret that the high-standing ridge is a “pop-up” block between the two reverse faults (Figure 2-11), and that the higher elevation of the ridge reflects localized uplift (Photo 2-4).

The updip projection of the northeast-dipping seismogenic fault intersects the ground surface coincident with or up to 1 kilometer west of the Hall trace of the Oceanic fault zone (Figure 2-11). There was no evidence of surface rupture along the Hall trace associated with the San Simeon earthquake (Hardebeck and others, 2004; PG&E, 2004b); however, as discussed in Section 2.2.2, surface deformation in this region may be characterized by uplift, tilting, and folding in a zone along the range front that encompasses and extends west of the Hall trace (Photo 4-1). These relations suggest the seismogenic fault is a non-emergent structure, and at the latitude of cross section A-A' (Figure 2-11), is only locally associated with the Hall trace of the Oceanic fault zone.

The cross section also reveals possible evidence for uplift and tilting above the non-emergent, southwest-dipping reverse fault. There is a syncline expressed in folded Cretaceous strata west of the axis of the Bryson anticline that lies approximately updip of the non-emergent, southwest-dipping fault (Figure 2-11). The syncline was mapped at 1:62,500 scale by Dibblee (1971), and



Note: The smoothed elevation was generated using a focalmean function. Grid cells were averaged using a nearest neighbor filter (low-pass). The new grids have a 500x500 meter resolution. Faults from Jennings (1994). Red star shows location of the December 2003 San Simeon earthquake.

Figure 4-1. Smoothed digital elevation model of the December 2003 main shock and aftershock region along the Oceanic fault zone. Double-difference aftershock relocations define a northeast-dipping main shock rupture plane and a non-emergent, southwest-dipping reverse fault along the northern segment that bound a “pop-up” block associated with a region of high topography (Figure 2-11). Elevations decrease along the central segment of the Oceanic fault zone, where the back thrust appears absent (Figure 2-12).

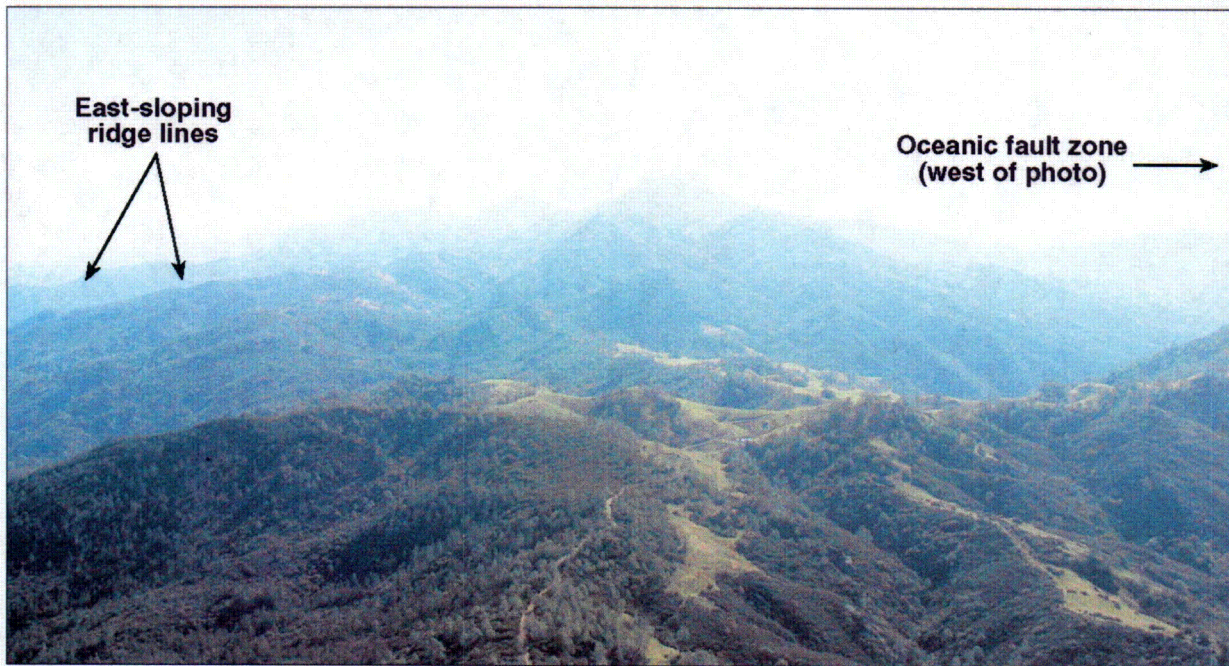


Photo 4-1. Aerial view to southeast of the broad region of high topography associated with the "pop-up" block bounded by the east-dipping Oceanic fault zone and a west-dipping back thrust identified by the distribution of aftershocks following the December 2003 earthquake. A smoothed digital-elevation model of this region and the location of this photo are shown on Figure 4-1. Photo was taken about 3 kilometers south of cross section A-A' (Figure 2-11).

in greater detail in the region just northwest of cross section A-A' by Seiders (1986), who named it the "Oak Flat" syncline. Seiders (1986) observed that rocks of the Miocene Vaqueros Formation are deformed by the Oak Flat syncline, and he interpreted that the fold is "very young...probably part of the (regional) Pliocene or Pleistocene deformation" that has produced the modern southern Coast Ranges.

At the latitude of cross section A-A', Cretaceous marine strata on the west limb of the Oak Flat syncline underlie a prominent northwest-trending ridge that forms the east flank of the Santa Lucia Range. The axis of the syncline generally follows the eastern topographic margin of the "pop-up" block. We tentatively interpret that the Oak Flat syncline represents the locus of uplift, tilting, and folding above the non-emergent, southwest-dipping reverse fault below the eastern margin of the "pop-up" block.

The Bryson anticline east of the epicentral region also is interpreted to be a fault-propagation fold above another non-emergent, northeast-dipping reverse fault (the "Bryson" fault; Figure 2-11). We assume this fault dips about 60°NE , similar to the Oceanic fault, and that it also extends to the base of the seismogenic crust. The east-dipping San Antonio fault at the northeastern end of cross section A-A' is interpreted to be part of a positive flower structure rooted in the right-lateral Rinconada fault. Short-wavelength folds in the hanging wall of the San Antonio fault (Figure 2-11) are interpreted to represent transpressional, wrench-style shortening of the downward tapering, wedge-shaped crustal block bounded by the San Antonio and Rinconada faults.

4.1.2 Central Segment of the Oceanic Fault Zone

The aftershock patterns in the area of the central segment of Oceanic fault zone are more diffuse than those in the area around the main shock, but nonetheless define a seismogenic reverse fault that strikes about N45°W and dips moderately to steeply toward the northeast (Figure 2-12). The updip projection of this fault intersects the ground surface several kilometers west of the Hall trace of the Oceanic fault zone, but generally is coincident with the zone of active range front deformation (Figure 2-12). Three-dimensional visualization of the aftershock sequence confirms that the seismogenic fault beneath the central segment of the Oceanic fault zone strikes about 25 degrees more toward the north than the seismogenic fault in the vicinity of the main shock to the north, comparable to the change in strike of the Hall trace between the northern and central segments and to the change in trend of the range front.

At the latitude of the central segment, the Hall trace is the easternmost of several faults that comprise the bedrock Oceanic fault zone and which displace middle Miocene strata in a reverse sense. In cross section B-B' (Figure 2-12), we interpret that the individual traces of the Oceanic fault zone mapped at the surface by Hall (1974) and Hall and Prior (1976) splay upward from the seismogenic fault at depth. Note that the easternmost "Hall trace" in the fault zone dips more steeply than the seismogenic fault at depth. The westernmost trace shown on Figure 2-12 is approximately coincident with the range front. The Chimney Rock anticline east of the epicentral region is interpreted to be a northeast-vergent fault-propagation fold above a non-emergent, southwest-dipping reverse fault (the "Chimney Rock" fault; Figure 2-12). We infer that the reverse fault beneath the Chimney Rock anticline dips about 60 degrees and extends to the base of the seismogenic crust.

4.1.3 Uplift of the Southern Coastal Ranges

As discussed in Section 2.2, late Cenozoic uplift of the southern Coast Ranges is the result of several interrelated processes, including northeast-southwest crustal shortening imparted to the southern Coast Ranges from the bordering Los Osos and offshore Santa Maria domains (Figure 2-4), progressive left-restraining transfer of right shear across the southern Coast Ranges from the San Gregorio-San Simeon-Hosgri fault system on the west to the southern Rinconada fault on the east (Figure 2-5), and a large left-restraining bend within the San Gregorio-San Simeon-Hosgri fault system centered on the San Simeon fault zone (Figure 2-6). These three processes combine to produce uplift and northeast-southwest crustal shortening within the Santa Lucia Range portion of the Southern Coast Ranges domain.

In the San Simeon region, a large component of crustal shortening and uplift appears to be accommodated by reverse and reverse-oblique slip along the Oceanic-West Huasna fault zone. The northern segment of the fault zone strikes about N65°W, which is 30 degrees more toward the west than the strike of the right-slip San Simeon and Rinconada faults at this latitude (Figure 2-7), and thus is in a restraining geometry relative to the direction of northwest right shear. The highest elevations in the Santa Lucia Range at this latitude are associated with the "pop-up" block east of the northern segment of the Oceanic fault zone (Figure 4-1); relief diminishes southward along the central segment, which strikes more parallel to the San Simeon

and Rinconada faults, and thus is more parallel to regional shear. Similarly, the Quaternary-active Bryson and Chimney Rock anticlines east of the Santa Lucia Range trend more toward the west than the Rinconada fault, and thus are oriented in a restraining geometry relative to regional shear. These relations are consistent with uplift and shortening driven primarily by distributed transpressional right-slip plate motion.

Uplift of the modern Santa Lucia Range likely commenced in late Neogene time (about 3.5 million years ago; Page and others, 1998). Using topographic relief as a proxy for late Cenozoic uplift and structural relief, the minimum long-term average uplift rate of the Santa Lucia Range in the epicentral region is about 0.2 millimeter per year. As discussed in Section 2.2.2, uplift rates measured from analyzing a flight of Quaternary marine terraces at the Hearst Ranch north and east of San Simeon show a change in uplift rate from 0.16 millimeter per year west of the range front to as much as 0.26 to 0.37 millimeter per year at or east of the range front. The net Quaternary uplift rate across the range front (about 0.1 to 0.2 millimeter per year) is comparable to the long-term average late Cenozoic rate estimated from topography.

4.2 Comparison with the Namson and Davis Tectonic Model

Namson and Davis (2004) presented a tectonic interpretation associating the 2003 San Simeon earthquake with a “blind thrust” fault beneath the Santa Lucia Range. This interpretation appears to be based on their 1990 structural analysis of the Santa Maria region (Namson and Davis, 1990), in which they used the theories and techniques of fault-bend folding and fault-propagation folding (Suppe, 1983) to evaluate the upper crustal geologic structure. Namson and Davis (1990) interpret the regional structure as a system of active southwest-vergent “blind thrust” faults above a basal detachment at a depth of 11 to 14 kilometers. They postulate that the Santa Lucia Mountains structural block is an anticlinorium underlain by one of these thrust faults. One of the balanced cross sections in their 1990 study (Cross Section #1, available for download as *USGS Cross Section & Recon 01.pdf* from <http://www.davisnamson.com/downloads/index.htm>) extends northwest across the Santa Lucia Range, Los Osos Valley, and San Luis Range. On this cross section, Namson and Davis project the hypocenter of the 2003 San Simeon earthquake about 60 kilometers “along structural strike” of the Santa Lucia anticlinorium. They place the earthquake at 7.6 kilometers depth (using the depth estimate in Hardebeck and others, 2004) on a thrust fault depicted as dipping about 26°NE beneath the Santa Lucia Range.

The Namson and Davis (1990) model calls upon plate-boundary-normal crustal shortening and, thus, the assumption of plane strain deformation in their structural analysis. In contrast, the PG&E (1988, 1991; McLaren and Savage, 2001; Lettis and others, 2004) model calls upon transpressional deformation along the plate margin, with the crustal shortening caused by “wrench”-style folds and thrust/reverse faults oblique to the orientation of the principal strike-slip faults of the region (for example, the Hosgri-San Simeon fault zone, Rinconada fault, San Andreas fault). In both models, crustal shortening is associated with active, seismogenic reverse and thrust faults and associated uplift and folding of the hanging wall, such as along the Oceanic-West Huasna fault zone, the Los Osos fault zone and the Southwest Boundary fault zone (PG&E, 1991).

The Namson and Davis (2004) interpretation of the 2003 San Simeon earthquake and aftershock sequence, however, is not correct as currently depicted on their Cross Section #1. As discussed above, detailed analysis of the hypocentral depth shows that the earthquake occurred at a depth of about 11 kilometers, near the base of the seismogenic zone, and significantly below the inferred low-angle “blind thrust” postulated by Namson and Davis. The main shock rupture plane dips about 60°NE, not 26 degrees, as shown on their cross section. Dynamic rupture models by Ichinose and others (Appendix A) and the distribution of aftershocks show that the rupture occurred on two distinct fault segments, with the northern segment trending more westerly than the southern segment. Given the observed change in strike of the seismogenic fault along the length of the aftershock zone, simple projection of the earthquake hypocenter from the northern segment 60 kilometers along strike to the south is at best highly uncertain. The fact that the seismogenic fault has a much steeper dip than the low-angle reverse fault in Cross Section #1 indicates the Namson and Davis interpretation does not reflect the known physical and structural reality of the earthquake rupture.

In addition, as pointed out by PG&E (Response to NRC Question GSG 10, 1990; 1991) the structural model developed by Namson and Davis violates many of the assumptions inherent in the modeling technique developed by Suppe (1983), and is not consistent with the known stratigraphic and structural relationships in the region. Their model does not portray the late Cenozoic style of deformation occurring in south-central coastal California, and their interpretation of crustal structure and rates of deformation are not appropriate for assessing seismic hazards in the contemporary tectonic setting.

4.3 Implications to Diablo Canyon Power Plant

The 2003 San Simeon earthquake provides valuable new information and insights for interpreting the style of tectonic deformation in south-central coastal California. The earthquake occurred on a reverse-right-oblique-slip fault along the northwest-trending structural boundary between the Los Osos domain and Southern Coast Ranges domain. We interpret this seismogenic fault to be associated with the Oceanic fault zone. In the context of the tectonic model developed by PG&E (1988; 1991), the Oceanic fault zone is a reverse-right-oblique-slip fault zone along the active range front of the Santa Lucia Mountains. PG&E (1988; 1991) estimated the fault zone as having a slip rate of approximately 0.5 millimeter per year, based on the uplifted marine terraces north of the Oceanic-San Simeon fault zone intersection. These terraces have been elevated at a rate of about 0.5 millimeter per year relative to the marine terraces along the San Simeon fault zone south of the intersection, suggesting that most if not all this vertical separation is occurring along the Oceanic fault zone. The magnitude, location, and sense of slip of the San Simeon earthquake are consistent with this tectonic model; therefore, the occurrence of the San Simeon earthquake does not necessitate a review of the PG&E tectonic model.

Additional studies performed following the San Simeon earthquake confirm that the Oceanic fault zone is an active range-front structure at its northern end near San Simeon, but that the bedrock trace of the Oceanic fault deviates from the active range front to the south-southeast. In the context of the PG&E (1988) tectonic model, this zone of range-front deformation is the reflection of the “Oceanic” fault, whereas the bedrock trace of the fault occurs within the

hanging wall of the currently active structure. The zone of active range-front deformation clearly deforms a flight of Pleistocene marine terraces that have an estimated rate of vertical separation of about 0.1 to 0.2 millimeter per year, somewhat less than that estimated in PG&E (1988). Our field investigations did not identify a clear surface expression of active faulting. Rather, the zone of active range-front deformation commonly is expressed by warping and/or monoclinical folding over a zone as wide as 1 to 2 kilometers, suggesting the currently active Oceanic fault zone is a non-emergent fault along the base of the range (Figures 2-7, 4-1).

Comparison of the Oceanic Fault Zone with the Los Osos Fault

The Oceanic fault zone is similar to the Los Osos fault in terms of sense of slip, slip rate, and fault segment length. Both faults are late Cenozoic range-bounding reverse faults that have strikes parallel to their respective mountain fronts. The active Los Osos fault forms the northeastern boundary of the San Luis Range and the active Oceanic fault zone forms the southwestern boundary of the Santa Lucia Range. Both faults strike more westerly than the right-slip Hosgri-San Simeon fault zone and they have a similar restraining geometry in the current tectonic regime. The original mapped bedrock trace of both the Oceanic fault (Hall, 1974; 1976) and the Los Osos fault (Hall and Prior, 1975) are steeply dipping reverse faults several hundred meters to more than 1 kilometer from the base of the range front within the hanging wall of the active fault.

The main difference between the Oceanic and Los Osos faults is that the Oceanic fault zone appears to be non-emergent and has only local geomorphic evidence for near-surface deformation (Photos 2-1, 2-3, 2-6), whereas the Los Osos fault has geomorphic evidence of activity and Holocene surface rupture along the base of the San Luis Range (Photo 4-2). The Los Osos fault is associated with scarps, lineaments, and Holocene fault traces that have been documented in trench excavations (PG&E, 1988; 1991), whereas the Oceanic fault zone is associated with apparent warping and tilting of surfaces in the hanging wall of a non-emergent fault.

The Santa Lucia Range has greater relief and higher general elevation than the San Luis Range. The difference in relief and elevation of the ranges may be a function of the relative ages of the ranges, different rates of slip on the bordering faults, or to other faults or folds within or bordering the Santa Lucia Range that contribute to uplift. The slip rate on the Los Osos fault is estimated to be 0.2 to 0.8 millimeter per year (PG&E, 1988; Lettis and Hall, 1994), whereas slip rate on the Oceanic fault zone is approximately 0.1 to 0.2 millimeter per year, based on the deformed marine terraces described above. The similarity in slip rate suggests the greater height of the Santa Lucia Range is due either to the greater age of the range or to other faults and folds within the range.

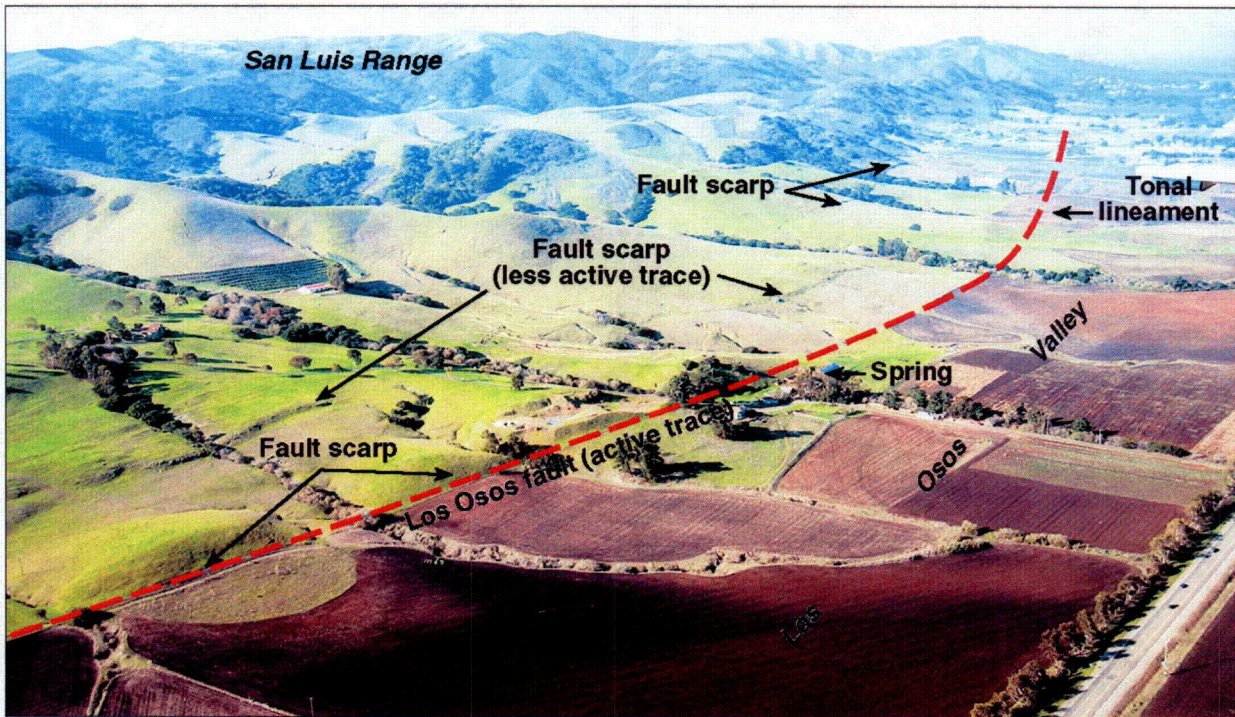


Photo 4-2. Aerial view to northwest of the Los Osos fault and deformation front of the San Luis Range. Fault scarp, tonal lineaments, and aligned springs show clear geomorphic expression of recent surface fault rupture along the Los Osos fault, and contrast with the lack of geomorphic expression associated with both the topographic range front of the Santa Lucia Range and the bedrock Oceanic fault zone mapped by Hall (1974, 1976) and Hall and Prior (1975). The town of Los Osos is visible in the upper right corner of the photo.

5.0 GROUND MOTIONS

The peak accelerations recorded at distances less than 100 kilometers, including those recorded at the Diablo Canyon Power Plant, were discussed in detail in our March report to the NRC (PG&E, 2004a). Overall, the peak accelerations recorded during the earthquake were consistent with the ground motion models used during the Long Term Seismic Program (PG&E, 1988). The free-field ground motions recorded at the Diablo Canyon Power Plant were significantly lower than the median peak acceleration expected for this magnitude earthquake and distance from the site. A likely reason they were lower is that the shear-wave velocity of the rock at the plant site is much higher than the shear-wave velocity of typical rock sites in California. A higher shear-wave velocity leads to a smaller site amplification of ground motions.

The recorded peak accelerations showed large azimuthal variability, with the largest peak accelerations recorded at stations southeast of the epicenter. This azimuthal variability has been attributed to directivity effects (for example, Hardebeck and others, 2004) because the recorded peak accelerations were larger in the direction of the rupture. However, not all azimuthal variations in ground motions are due to directivity effects. Other effects, such as the slip distribution, radiation pattern, site response, and wave propagation, can lead to strong azimuthal

variations of the ground motions and probably account for the variation in the recorded ground motions.

The term "directivity" describes the dependence of the ground motion on the location of the hypocenter on the rupture plane (Somerville and others, 1997). The increase in ground motions due to directivity is caused by constructive interference of waves generated on the parts of the rupture located between the hypocenter and the site. The amplitude of the directivity effect becomes larger as the rupture velocity approaches the shear-wave velocity.

Ichinose and others (Appendix A) evaluated the potential for directivity effects on the recorded ground motions using numerical simulation methods. First, they conducted a source inversion to determine the overall source properties, including the slip distribution and rupture velocity. Their inversion for the source properties led to a high rupture velocity of about 3.5 kilometers/second. Even using this high rupture velocity, they found that directivity effects were restricted to sites to the southeast within 25 kilometers of the epicenter. That is, they found that the observed azimuthal variation of the peak accelerations at large distances could not be explained by directivity effects. This finding is consistent with the results from previous earthquakes that found large directivity effects occur only at long spectral periods and are localized updip for reverse-slip earthquakes. This indicates that the observed azimuthal variations at larger distances is due to effects other than directivity, such as the slip distribution, radiation pattern, site response, and wave propagation.

6.0 CONCLUSIONS

Our analyses of the current data support conclusions made in our earlier reports (PG&E, 2004a; 2004b). However, some of these conclusions have been updated and modified based on the new data and analyses:

- In our current understanding of the tectonic setting of south-central coastal California (PG&E 1988; 1991), the Oceanic fault zone is recognized as a reverse-right-oblique-slip fault along the mountain front of the Santa Lucia Range that forms the boundary of the Los Osos and Southern Coast Ranges tectonic domains. The magnitude, location, and sense of slip of the 2003 San Simeon earthquake are consistent with this tectonic model; therefore, the occurrence of the San Simeon earthquake does not necessitate a review of the PG&E tectonic model.
- The crustal shortening in the San Simeon region is best explained by transpressional deformation along the plate margin, not by plate-boundary-normal deformation. Our data demonstrate the crustal shortening is caused by wrench-style folds and thrust/reverse faults, such as the Oceanic-West Huasna fault zone, that are oblique to the orientation of the principal strike-slip faults of the region, the Hosgri-San Simeon fault zone, the Rinconada fault, and the San Andreas fault.
- The San Simeon earthquake involved rupture on two segments of the Oceanic fault zone having two different strikes. This change in strike is indicated by three independent lines of evidence: (1) the multiple-point source model derived from teleseismic data indicates the presence of two events having different strike angles, (2) the change in the strike of

the aftershock zone, (3) the change in the strike of the mapped fault and range-front deformation of the Oceanic fault zone.

- The earthquake initiated a prolific aftershock sequence; over 8000 aftershocks have occurred since the main shock; to date, all the aftershocks have been less than magnitude 5. The aftershock patterns show three main clusters, two near the main shock and one large, more diffuse cluster to the southeast. These cluster patterns formed nearly immediately after the main shock and have continued to form over the past 11 months. The main shock and aftershocks occurred in a region where reverse-motion earthquakes have occurred previously.
- The main shock focal mechanism is nearly pure reverse; aftershock focal mechanisms are primarily reverse near the main shock and more varied within the southeast cluster. Centroid focal mechanisms, including mechanisms for the two main shock subevents also are reverse.
- Reverse slip on the northern segment and right-reverse slip on the central segment of the Oceanic fault zone is consistent with regional transpressional wrench tectonics across the boundary between the Pacific Plate and the Sierran microplate. As evidenced by the San Simeon earthquake on the Oceanic fault zone, and by Quaternary growth of the Bryson and Chimney Rock anticlines, crustal shortening at the latitude of San Simeon is associated with restraining bends in strike-slip faults and folds that trend more westerly than the direction of regional right shear.
- Using a combination of PG&E and USGS data, we estimate an absolute depth of the main shock of 11.3 kilometers and a relative depth of 10.2 kilometers using the double-difference relative location method. This is compatible with the 12-kilometer depth estimated using teleseismic body and surface waves (Appendix A).
- We estimate the epicentral location of the main shock at 35°N41.88, 121°W6.21. The earthquake has a reverse focal mechanism, striking 297 degrees northwest, dipping 61 degrees northeast, and having a 96-degree rake. These parameters are similar to those estimated from teleseismic body-wave data (Appendix A).
- The rupture propagated unilaterally to the southeast at a rupture velocity of about 3.5 kilometers/second, which is comparable to the shear wave velocity in the upper crust. The high rupture velocity caused large rupture directivity effects within 25 kilometers, manifested as large ground motion amplitudes to the southeast of the rupture; however, effects other than directivity are responsible for the large ground motions to the southeast at large distances.
- No surface fault rupture occurred during the 2003 San Simeon earthquake on the Oceanic fault zone or any potentially causative faults within the Santa Lucia Range. No evidence of sympathetic movement was observed on nearby regional faults, including the San Simeon, Los Osos, or Southwest Boundary zone faults. Fault rupture associated with the earthquake was not large enough to propagate to the ground surface.
- Near San Simeon, in the epicentral area of the 2003 San Simeon earthquake, deformed marine terraces indicate a rate of uplift of 0.1 to 0.2 millimeter per year along the front of the Santa Lucia Range.

- The earthquake strong ground motions recorded at the Diablo Canyon Power Plant were significantly smaller than those predicted by commonly used ground motion attenuation relations, including the ground motion models used as part of the LTSP evaluations. This is attributed to the relatively high shear-wave velocity of the rock at the Diablo Canyon Power Plant as compared with typical rock sites in California. The ground motions from the San Simeon earthquake indicate that the LTSP ground motion models may overestimate the high frequency ground motion at Diablo Canyon Power Plant.

7.0 ACKNOWLEDGMENTS

This report was prepared under the direction of Lloyd Cluff, Director, PG&E Geosciences Department (Geosciences). The tectonics and geology were investigated and assessed by William Lettis, Principal Geologist, William Lettis & Associates, Inc. (WLA), Jeffrey Unruh Principal Geologist (WLA), Steve Thompson, Project Geologist (WLA), and William D. Page, Senior Seismic Geologist (Geosciences). The seismicity was analyzed by Marcia McLaren, Seismologist (Geosciences) and Megan Stanton, Seismologist (Geosciences). Ground motions analyses were conducted by Norm Abrahamson, Seismological Engineer (Geosciences). Gene Ichinose, Paul Somerville, and Robert Graves, seismologists with the URS Corp., analyzed the source depth and rupture process of the San Simeon earthquake that is included in Appendix A. The report was peer reviewed by Stu Nishenko, Senior Seismologist (Geosciences). Janet Cluff, Word Engineering, edited the report.

We had fruitful discussions concerning the geologic and seismologic issues raised by the San Simeon earthquake with numerous geoscientists from the U.S. Geological Survey, California Geological Survey, Southern California Earthquake Center, and San Luis Obispo County.

8.0 REFERENCES

- Argus, D. F., and Gordon, R. G., 2001, Present tectonic motion across the Coast Ranges and San Andreas fault system in central California: Geological Society of America Bulletin, v. 113, p. 1580-1592.
- Cummings, D., Johnson, T. A., and Gaal, R. A., 1987, Shallow structural geology, offshore Santa Maria River to Point Arguello, central California: Geological Society of America Cordilleran Section Meeting, Abstracts with Programs, v. 19, no. 6, p. 369.
- Dibblee, T. W., Jr., 1971, Geologic maps of the Adelaida, Bryson, and Bradley 15 minute quadrangles, west-central California: U.S. Geological Survey Open-File Report 71-87. (This open-file report includes 17 geologic quadrangle maps in the greater Paso Robles-San Luis Obispo region. The three quadrangles listed above are directly relevant to the present study.)
- Dibblee, T. W., Jr., 1976, The Rinconada and related faults in the southern Coast Ranges, California, and their tectonic significance: United States Geological Survey Professional Paper 981, 55 p.

- Hall, C. A., Jr., 1974, Geologic Map of the Cambria Region, San Luis Obispo County, California: U.S. Geological Survey Miscellaneous Field Studies Map MF-599, scale 1:24,000.
- Hall, C. A., Jr., 1976, Geologic Map of the San Simeon-Piedras Blancas Region, San Luis Obispo County, California: U.S. Geological Survey Miscellaneous Field Studies Map MF-784, scale 1:24,000.
- Hall, C. A., Jr., 1991, Geology of the Point Sur-Lopez Point region, Coast Ranges, California; a part of the southern California allochthon: Geological Society of America Special Paper 266, 40 p. plus plates.
- Hall, C. A., and Prior, S. W., 1975, Geologic Map of the Cayucos-San Luis Obispo Region, San Luis Obispo County, California: U.S. Geological Survey Miscellaneous Field Studies Map MF-686, scale 1:24,000.
- Hanson, K. L., and Lettis, W. R., 1994, Estimated Pleistocene slip rate for the San Simeon fault zone, South Central California, *in* Alterman, I. B., McMullen, R. B., Cluff, L. S., and Slemmons, D. B., eds., Seismotectonics of the Central California Coast Ranges: Geological Society of America Special Paper 292, p. 133-150.
- Hanson, K. L., Wesling, J. R., Lettis, W. R., Kelson, K. I., and Mezger, L., 1994, Correlation, ages and uplift rates for Quaternary marine terraces, south-central coastal California: Geological Society of America Special Paper 292, p. 45-71.
- Hanson, K. L., Lettis, W. R., McLaren, M. K., Savage, W. U., and Hall, N. T., 2004, Style and Rate of Quaternary Deformation of the Hosgri fault zone, Offshore South-Central California: U.S. Geological Survey Bulletin 1995, Chapter BB of Evolution of Sedimentary Basins/Offshore Oil and Gas Investigations—Santa Maria Province, Keller, M. A., editor.
- Hardebeck, J. L., 2004a, Email to Nicholas Van der Elst, PG&E, from J. Hardebeck, USGS: Subject: hypoDD, November 4, 2004.
- Hardebeck, J. L., 2004b, Email to Marcia McLaren, PG&E, from J. Hardebeck, USGS: Subject: Double-Difference Analysis, December 10, 2004.
- Hardebeck, J. L., Boatwright, J., Dreger, D., Goel, R., Graizer, V., Hudnut, K., Ji, C., Jones, L., Langbain, J., Lin, J., Roeloffs, E., Simpson, R., Stark, K., Stein, R., and Tinsley, J. C., 2004, Preliminary report on the 22 December 2003, M 6.5 San Simeon, California, earthquake: Seismological Research Letters, v. 75, n. 2, p. 155-172.
- Hauksson, E., Oppenheimer, D., and Brocher, T., 2004, Imaging the source region of the 2003 San Simeon earthquake within the weak Franciscan subduction complex, central California, Geophysical Research Letters, v. 31, L20607, 4 p.
- Jennings, C. W., 1958, Geologic map of California, San Luis Obispo sheet: California Division of Mines and Geology, scale 1:250000.

- Jennings, C. W., 1994, Fault activity map of California with locations and ages of recent volcanic eruptions: California Division of Mines and Geology, Geologic Data Map 6, scale 1:750,000.
- Klein, F. W., 1989, Users guide to HYPOINVERSE, a program for VAX computers to solve for earthquake locations and magnitudes, U.S. Geological Survey Open-File Report 89-314.
- Lettis, W. R., and Hall, N. T., 1994, Los Osos fault zone, San Luis Obispo County, California; *in* Alterman, I. B., McMullen, R. B., Cluff, L. S., and Slemmons, D. B., eds., Seismotectonics of the Central California Coast Ranges: Geological Society of America Special Paper 292, p. 73-102.
- Lettis, W. R., Kelson, K. I., Wesling, J. R., Hanson, K. L., and Hall, N. T., 1994, Quaternary deformation of the San Luis Range, San Luis Obispo County, California; *in* Alterman, I. B., McMullen, R. B., Cluff, L. S., and Slemmons, D. B., eds., Seismotectonics of the Central California Coast Ranges: Geological Society of America Special Paper 292, p. 111-132.
- Lettis, W. R., Hanson, L. L., Unruh, J. R., McLaren, M., and Savage, W. U., 2004, Quaternary tectonic setting of south-central coastal California: U.S. Geological Survey Professional Paper Bulletin 1995, Chapter BB of Evolution of Sedimentary Basins/Offshore Oil and Gas Investigations—Santa Maria Province, Keller, M. A., editor.
- Lettis, W. R. and Hanson, K. L., 2004, The San Gregorio/Hosgri fault system, California: an evaluation of the style and rate of Quaternary deformation (abstr.): Seismological Research Letters, v. 74, no. 2, p. 264.
- McLaren, M. K. and W. U. Savage, 2001, Seismicity of south-central coastal California: October 1987 though January 1997, Seismological Society of America Bulletin, v. 91, no. 6, p. 1629-1658.
- McLaren, M. K. and M. Stanton, 2004, Comparison of the M_w 6.5 San Simeon, California earthquake of 22 December 2003 and early aftershocks to 1987-1997 seismicity in the region (abstr.): Seismological Research Letters, v. 74, no. 2, p. 264.
- Michelini, A., and Lomax, A., 2004, The effect of velocity structure errors on double-difference earthquake location: Geophysical Research Letters, v. 31, L09602, 4 p.
- Namson, J. S., and Davis, T. L., 2004, Tectonic model for the 22 December 2003 San Simeon earthquake (abstr.): Seismological Research Letters, v. 75, no. 2, p. 295.
- Namson, J. S., and Davis, T. L., 1990, Subsurface study of the late Cenozoic structural geology of the Santa Maria Basin, western Transverse Ranges and southern Coast Ranges, California: American Association of Petroleum Geologists, v. 74, p. 467-492

- Pacific Gas and Electric Company, 1988, Final report of the Diablo Canyon Long Term Seismic Program: U.S. Nuclear Regulatory Commission, Docket Nos. 50-275 and 50-323.
- Pacific Gas and Electric Company, 1991, Addendum to the 1988 Final Report of the Diablo Canyon Long Term Seismic Program: U.S. Nuclear Regulatory Commission, Docket Nos. 50-275 and 50-323.
- Pacific Gas & Electric Company, 2004a, Supplement to Special Report 03-04: San Simeon Earthquake of December 22, 2003: Enclosure 1 to Letter DCL-04-031, March 29, 2004, to the U.S. Nuclear Regulatory Commission, for Diablo Canyon Units 1 and 2, Docket Nos. 50-275/OL-DPR-80 and 50-323/OL DPR-82.
- Pacific Gas & Electric Company, 2004b, Update to the seismicity evaluation of the December 22, 2003 San Simeon earthquake: Enclosure 1 to Letter DCL-04-071, June 04, 2004, to the U.S. Nuclear Regulatory Commission, for Diablo Canyon Units 1 and 2, Docket Nos. 50-275/OL-DPR-80 and 50-323/OL DPR-82.
- Page, B. M., Thompson, G. A., and Coleman, R. G., 1998, Late Cenozoic tectonics of the central and southern Coast Ranges of California: Geological Society of America Bulletin, v. 110, p. 846-876.
- Reasenber, P., 1985, Second-order moment of central California seismicity, 1969-1982: Journal of Geophysical Research, v. 90. , p. 5479-5495.
- Reasenber, P. A. and Oppenheimer, D., 1985, FPFIT, FPLOT< and FPPAGE; Fortran computer programs for calculating and displaying earthquake fault plane solutions: U.S. Geological Survey Open-File Report 85-739.
- Satake, K. and Somerville, P., 1992, Location and size of the 1927 Lompoc, California earthquake from tsunami data: Bulletin of the Seismological Society of America, v. 80, p. 1118-1143.
- Seiders, V. M., 1986, Structural geology of Upper Cretaceous and lower Tertiary Rocks near the Nacimiento fault, northwest of Lake Nacimiento, California; *in* Grove, K. and Graham, S., eds, Geology of Upper Cretaceous and Lower Tertiary Rocks Near Lake Nacimiento: Society of Economic Paleontologists and Mineralogists, Pacific Section, Book 49, Los Angeles, p. 33-39.
- Somerville, P. G., Smith, N. F., Graves, R. W., and Abrahamson, N. A., 1997, Modification of empirical strong motion attenuation relations to include the amplitude and duration effects of rupture directivity: Seismological Research Letters, v. 68, no. 1, p. 199-222.
- Suppe, J., 1983, Geometry and kinematics of fault-bend folding: American Journal of Science, v. 283, p. 648-271.

U.S. Geological Survey (USGS), 2004, Northern California seismic network: On-line at <http://quake.geo.berkeley.edu/ncedc/catalog-search.html>, accessed 11/16/04.

Waldhauser F. and Ellsworth W. L., 2000, A double-difference earthquake location algorithm; Method and application to the northern Hayward Fault, California: *Seismological Society of America Bulletin*, v. 90, 1,353-1,368.

Waldhauser F., 2001, HypoDD—A program to compute double-difference hypocenter locations (hypoDD version 1.0 – 03/2001): U.S. Geological Survey Open-File Report 01-113, 25 p.

Zoback, M.L., Jachens, R.C., and Olson, J.A., 1999, Abrupt along-strike change in tectonic style, San Andreas fault zone, San Francisco Peninsula: *Journal of Geophysical Research*, v. 104, p. 10,719-10,742.